ISOTOPE EFFECTS IN VISIBLE LIGHT PHOTOLYSIS AND CHEMICAL DESTRUCTION OF OZONE

Marion Früchtl

Marion Früchtl
Institute for Marine and Atmospheric Research Utrecht (IMAU)
Atmospheric Physics and Chemistry Group

Present address:
Institute for Marine and Atmospheric Research Utrecht (IMAU)
Utrecht University
P.O. Box 80005, 3508 TA Utrecht, The Netherlands
m.fruechtl@uu.nl
fruechtl.marion@gmx.de

ISBN: 978-90-393-6418-5
Printing: Ridderprint BV, The Netherlands

ISOTOPE EFFECTS IN VISIBLE LIGHT PHOTOLYSIS AND CHEMICAL DESTRUCTION OF OZONE

ISOTOOPEFFECTEN IN DE FOTOLYSE MET ZICHTBAAR LICHT EN DE CHEMISCHE AFBRAAK VAN OZON

(met een samenvatting in het Nederlands)

ISOTOPENEFFEKTE IN DER PHOTOLYSE MIT SICHTBAREM LICHT UND DER CHEMISCHEN ZERSTÖRUNG VON OZON

(mit einer Zusammenfassung in deutscher Sprache)

Proefschrift

ter verkrijging van de graad van doctor aan de Universiteit Utrecht op gezag van de rector magnificus, prof.dr. G.J. van der Zwaan, ingevolge het besluit van het college voor promoties in het openbaar te verdedigen op

maandag 16 november 2015 des middags te 4.15 uur

door

MARION FRÜCHTL

geboren op 25 december 1983 te Schongau, Duitsland

PROMOTOR: Prof. dr. T. Röckmann
COPROMOTOR: Dr. C. Janssen

This thesis was accomplished with financial support from the Marie Curie Initial Training Network INTRAMIF (Initial Training Network on Mass-Independent Fractionation) as part of the European Community's Seventh Framework Program (FP7/2007-2013).

CONTENTS

LIST OF FIGURES

LIST OF TABLES

SUMMARY

Ozone (O_3) is a very important molecule in the Earth's atmosphere. The stratospheric O_3 layer shields the Earth from harmful solar UV radiation and the absorption of this energy produces the positive temperature gradient in the stratosphere. O_3 is also a greenhouse gas, and it plays a key role for many chemical oxidation processes in the Earth's atmosphere. In these chemical reactions ozone can transfer oxygen to other trace gases. Another characteristic of O_3 is that it has a very peculiar isotopic composition with unusually strong isotope enrichment in both rare oxygen isotopes, ^{17}O and ^{18}O, relative to the O_2 that it is formed from. This enrichment does not follow the standard mass-dependent fractionation (MDF) equation $\delta^{17}O = 0.52 \times \delta^{18}O$, but possesses significant excess ^{17}O enrichment over what is expected for MDF from the ^{18}O content. The ^{17}O excess is quantified as $\Delta^{17}O = \delta^{17}O - 0.52 \times \delta^{18}O$ and usually referred to as mass-independent fractionation (MIF). This isotope signature of O_3 is interesting both from a molecular physics and chemistry point of view. From the molecular physics perspective, it is interesting to understand its origin, and from the atmospheric chemistry point of view, because the isotope anomaly can be transferred via chemical reactions to many other atmospheric compounds.

The O_3 formation reaction is the most prominent example for a chemical reaction that leads to mass-independent fractionation. The isotope effects in O_3 formation have been studied in much detail and the magnitude of the enrichments, observed in atmospheric as well as laboratory O_3, strongly depends on temperature and pressure. In the stratosphere however, at altitudes above 25 km, it was found that the observed isotope enrichments exceed what is expected from the formation process at ambient temperature and pressure only. These findings indicated that processes other than O_3 formation might contribute to the isotopic composition of atmospheric O_3. Photolysis and chemical removal of O_3 are possible sources for the additional enrichments. To what degree these O_3 destruction reactions contribute to the isotope composition of atmospheric O_3 is not fully understood.

This thesis aims to provide further insight into the isotope effects arising from O_3 destruction reactions, in particular O_3 photolysis in the visible part of the electromagnetic spectrum (400-800 nm) and the sink reaction $O + O_3$. When the associated isotope effects in laboratory experiments are well established, also the isotope effects in O_3 formation can be reassessed.

We set up new experiments to investigate the isotope effects resulting from photo dissociation of O_3 in the Chappuis band using a broadband photolysis lamp that provides radiation between 400 and 800 nm with an emission peak at 605 nm. Initial O_3 was produced by an electric discharge. It was then photolysed to varying degree, either pure or mixed in various bath gases (CO, He, Ar). The remaining O_3 was collected in a cold trap at

the triple point temperature of nitrogen (63 K), converted to O_2 and analyzed for its isotopic composition by isotope ratio mass spectrometry (IRMS). A kinetic model was used to quantitatively interpret the results.

In previous studies, it has never been possible to separate photolysis of O_3 from chemical removal by the reaction O + O_3, which usually follows after photolysis in laboratory experiments. A major innovation of this work is that we use carbon monoxide (CO) as bath gas, because CO acts as a quencher of $O(^3P)$. This way we were able to quantify for the first time isotope fractionation effects for both photolysis in the Chappuis band and chemical removal by O + O_3 separately. A complication arises because of an unexplained loss of O_3 when exposed to a large excess of carbon monoxide. The effect of this unexplained loss has been assessed by sensitivity runs with the kinetic model. As main result of this first part of the thesis, we report fractionations of $^{18}\varepsilon_{hv} = -16.1‰$ and $^{17}\varepsilon_{hv} = -8.05‰$ for photolysis and $^{18}\varepsilon_{O+O_3} = -11.9‰$ and $^{17}\varepsilon_{O+O_3} = -5.95‰$.

Following up on these findings, we investigated the wavelength dependence of the isotope fractionations in visible light photo dissociation of O_3. O_3 was photolysed using a broadband light source with different cut-off filters (455 nm, 620 nm, 550 nm) and various LEDs with emission peaks at 660 nm, 617 nm or 530 nm. Since under these experimental conditions, the measured fractionation represents the average of fractionations in O_3 photolysis and O + O_3 of which the latter was previously determined, the photolysis-induced fractionations can be derived. The observed fractionations decrease with an increase in wavelength, but the wavelength dependence is smaller than predicted from theoretical calculations. For all experiments, the measured isotope effects lead to an enrichment of the left over O_3, which is also in contrast to calculations. The results imply that atmospheric models which use the theoretically determined fractionations in photolysis underestimate the photolytically induced isotope effects. The results also show that O_3 photolysis in the Chappuis band is associated with isotope effects that follow a pure mass-dependent fractionation pattern. Photodissociation experiments at different temperatures ranging from -90°C to +40°C demonstrate that fractionation effects in O_3 photolysis do not depend on temperature.

We then present results from photolytic recycling experiments in which O_3 is photolysed in O_2 bath gas. In these experiments the isotope effects of O_3 formation and photolysis are combined. Compared to previous experiments, slight but significant differences in the temperature dependence of the isotope enrichments are observed. Importantly, based on the careful characterization of the isotope effects in photolysis, we extract from these results the temperature dependent fractionation for O_3 formation reactions only. Using previously established results on the relative rate coefficients of some individual isotope specific ozone production channels, and their temperature dependence, we can then derive a consistent set of relative rate coefficients of isotope specific channels that lead to formation of single-substituted O_3 molecules. Since the measurements are

carried out with considerably higher precision compared to prior work, also the relative rate coefficients can be determined with improved precision. We find relatively large differences of the ^{17}O excess of O_3 in photochemical isotope equilibrium with O_2 compared to the previously accepted values. These are unlikely to be explained by real differences between the experiments, but are attributed to larger experimental errors in the isotope determination in the earlier studies.

This study presents a new experimental method to disentangle isotope effects in O_3 photolysis and the O_3 removal reaction $O + O_3$. We successfully quantify isotope effects in visible light O_3 photolysis and the simultaneous reactions $O + O_3$ and O_3 formation. However, uncertainties remain concerning the unidentified loss of O_3 in O_3 - CO gas mixtures, which requires further research. Furthermore high resolution measurements applying optical lasers would be helpful to test the trueness of theoretical calculations and the atmospheric models, especially at wavelengths where maximum fractionations are expected.

SAMENVATTING

Ozon (O_3) is een zeer belangrijk molecuul in de atmosfeer van de aarde. De ozonlaag beschermt de aarde tegen de schadelijke UV straling van de zon. De absorptie van deze UV straling door O_3 veroorzaakt de temperatuurstijging in de stratosfeer. O_3 is ook een broeikasgas en het speelt een belangrijke rol in vele chemische oxidatieprocessen in de atmosfeer van de aarde. In deze chemische reacties kan O_3 zuurstof overdragen aan andere (broeikas-) gassen**.** Een andere eigenschap van O_3 is de bijzondere samenstelling van isotopen, met uitzonderlijk sterke isotoopverrijking in beide zeldzame zuurstofisotopen, ^{17}O en ^{18}O, in relatie tot de O_2 waaruit het gevormd is. Deze verrijking volgt niet de standaard massa-afhankelijke fractionerings- (*eng.* mass-dependent fractionation, MDF) formule $\delta^{17}O = 0.52 \times \delta^{18}O$, maar heeft een significant hogere ^{17}O verrijking dan verwacht wordt aan de hand van de verrijking van ^{18}O. Dit overschot aan ^{17}O is gekwantificeerd als $\Delta^{17}O = \delta^{17}O - 0.52 \times \delta^{18}O$ en hier wordt aan gerefereerd als massa-onafhankelijke fractionering (*eng.* mass-independent fractionation, MIF). De isotoopsignatuur van O_3 is interessant uit zowel het moleculair fysisch en chemisch oogpunt. Voor de moleculaire fysica is het interessant om de oorsprong te begrijpen, en vanuit het oogpunt van de atmosferische chemie omdat de anomalieën in de isotopen via chemische reacties kunnen worden overdragen aan vele andere atmosferische moleculen.

De vormingsreactie van O_3 is het meest prominente voorbeeld van een chemische reactie die leidt tot massa-onafhankelijke fractionering. De isotoopeffecten in O_3 vorming zijn tot in detail onderzocht. De mate van de isotoopverrijking, gevonden zowel in de atmosfeer als in het laboratorium, is sterk afhankelijk van temperatuur en druk. Echter zijn er op 25 km hoogte in de stratosfeer, gelet op uitsluitend de voorwaarden van druk en temperatuur, hoger dan verwachte isotoopverrijkingen gevonden. Deze bevindingen duiden erop dat andere processen dan de ozonvorming bijdragen aan de isotoopsamenstelling van atmosferisch O_3. Fotolyse en de chemische verwijdering van O_3 zijn mogelijke oorzaken van de extra verrijkingen. In welke mate deze O_3 afbraakreacties bijdragen aan de isotoopsamenstelling van de atmosferische O_3 is tot op heden niet volledig duidelijk.

Dit proefschrift is erop gericht om verdere inzichten te verkrijgen in de isotoopeffecten die voortkomen uit de O_3 afbraakreacties, in het bijzonder de O_3 fotolyse in het zichtbare deel van het elektromagnetische spectrum (400-800 nm) en de O_3 afbraakreactie $O + O_3 \rightarrow 2O_2$. Wanneer deze isotoopeffecten in laboratoriumexperimenten vastgesteld zijn, kunnen ook de isotoopeffecten in O_3 vorming opnieuw geëvalueerd worden.

We hebben nieuwe experimenten opgezet om de isotoopeffecten van de fotolyse van O_3 in de Chappuis band te onderzoeken. De experimenten worden uitgevoerd met behulp van een breedband fotolyse lamp met een straling tussen de 400 en 800 nm en een maximum

emissiepiek van 605 nm. De initiële O_3 werd geproduceerd door een elektrische ontlading. Vervolgens werd pure O_3, of een mengsel van O_3 met verschillende badgassen (CO, He, Ar) tot verschillende gradaties gefotolyseerd. De overgebleven O_3 werd opgevangen in een koelval op de tripelpunt temperatuur van stikstof (63 K), omgevormd tot O_2 en aansluitend werd de isotoopsamenstelling geanalyseerd met een isotopen massa spectrometer (IRMS). Een kinetisch model werd gebruikt om de resultaten op kwantitatieve wijze te interpreteren.

In voorgaande studies is het nooit mogelijk geweest om de fotolyse van O_3 te scheiden van de chemische O_3 verwijderingsreactie $O + O_3$, hetgeen in laboratoriumexperimenten normale gesproken direct volgt na de fotolyse. Een belangrijke innovatie van dit werk is dat we koolstofmonoxide (CO) als bad gas gebruikten, zodat $O(^3P)$ opgevangen wordt door CO. Op deze manier waren we in staat om voor de eerste keer de isotopen fractioneringseffecten apart te kwantificeren voor de fotolyse in de Chappuis band en de chemische O_3 verwijdering $O + O_3$. Daarbij deed zich een complicatie voor vanwege een onverklaarbaar verlies van O_3 wanneer dit blootgesteld wordt aan een grote hoeveelheid koolstofmonoxide. Het effect van dit onverklaarde verlies hebben we onderzocht door een gevoeligheidsstudie met een kinetisch model. Als hoofdresultaat van het eerste deel van het proefschrift presenteren wij fractioneringen van $^{18}\varepsilon_{h\nu} = -16.1‰$ en $^{17}\varepsilon_{h\nu} -8.05‰$ voor fotolyse en $^{18}\varepsilon_{O+O_3} = -11.9‰$ en $^{17}\varepsilon_{O+O_3} = -5.95‰$ voor $O + O_3$.

Gebaseerd op deze bevindingen hebben we de golflengte-afhankelijkheid onderzocht van de isotoop fractionering in O_3 fotolyse door zichtbaar licht. O_3 werd gefotolyseerd door middel van een breedband lichtbron met verschillende optische filters (455 nm, 620 nm, 550 nm) en verschillende LEDs met emissie pieken van 660 nm, 617 nm of 530 nm. Omdat de onder deze experimentele voorwaarden gemeten fractioneringen een gemiddelde zijn van de fractioneringen O_3 fotolyse en $O + O_3$, waarvan deze laatst genoemde al eerder gekwantificeerd was, kunnen wij de door fotolyse veroorzaakte fractioneringen herleiden. De gevonden fractioneringen nemen af bij grotere golflengten, maar de golflengte-afhankelijkheid is kleiner dan voorspeld door theoretische berekeningen. Bij alle experimenten leiden de gemeten isotoopeffecten tot een verrijking van de overgebleven O_3, hetgeen ook de berekeningen tegenspreekt. De resultaten geven aan dat atmosferische modellen die gebruik maken van de theoretisch bepaalde fractioneringen in fotolyse, de door fotolyse bewerkstelligde isotoopeffecten onderschatten. Ook geven de resultaten aan dat isotoopeffecten van O_3 fotolyse in de Chappuis band een MDF patroon vertonen. Verder laten fotodissociatie-experimenten met verschillende temperaturen, variërend van -90°C tot +40°C zien dat fractioneringseffecten in O_3 fotolyse niet afhankelijk zijn van temperatuur.

Vervolgens presenteren wij resultaten van fotolytische recyclingexperimenten waarin O_3 gefotolyseerd is in O_2 bad gas. In deze experimenten zijn de isotoopeffecten van O_3 vorming en fotolyse gecombineerd. Vergeleken met voorgaande experimenten zijn er kleine maar significante verschillen in de temperatuurafhankelijkheid van

isotopenverrijking gevonden. Van belang is dat we, gebaseerd op de uitgebreide karakterisering van de isotoopeffecten in fotolyse, uit deze resultaten kunnen opmaken dat de temperatuur-afhankelijke fractionering alleen geldt voor de O_3 vormingsreacties. Gebruikmakend van resultaten uit eerdere onderzoeken van de relatieve reactiesnelheidsconstanten van sommige individuele isotopen-specifieke ozonproductiekanalen en hun temperatuur-afhankelijkheid, kunnen wij een consistente set van relatieve reactiesnelheidsconstanten van isotopen-specifieke kanalen herleiden die resulteren in de vorming van enkelvoudig vervangen O_3 moleculen. Omdat de metingen uitgevoerd zijn met aanzienlijk grotere precisie dan voorgaande studies, kunnen ook de relatieve reactiesnelheidsconstanten vastgesteld worden met verbeterde precisie. Vergeleken met voorheen geaccepteerde waarden vinden wij relatief grote verschillen in de $\Delta^{17}O$ signatuur in de vormingsreacties van O_3. Deze verschillen laten zich waarschijnlijk niet verklaren door echte verschillen tussen de experimenten, maar zijn te wijten aan vaststelling van grotere experimentele standaarddeviaties in de isotopenmetingen van eerdere studies.

Deze studie presenteert een nieuwe experimentele methode die gebruikt kan worden om de isotoopeffecten in O_3 fotolyse te kunnen scheiden van de isotoopeffecten in de O_3 afbraakreactie. Wij zijn succesvol geweest in het kwantificeren van isotoopeffecten in de fotolyse van O_3 door zichtbaar licht en de parallelle reacties $O + O_3$ en O_3 vorming. Desondanks blijven er onzekerheden bestaan over het onverklaarbare verlies van O_3 in het O_3-CO gasmengsel, hetgeen verder onderzoek behoeft. Tevens zouden hoge resolutie golflengte metingen, gebruikmakend van optische lasers, waardevol zijn in het testen van de geldigheid van theoretische berekeningen en atmosferische modellen, in het bijzonder op golflengtes waar maximale fractioneringen verwacht worden.

ZUSAMMENFASSUNG

Ozon ist ein bedeutendes Molekül in der Erdatmosphäre. Die Ozonschicht schützt die Erde vor der gefährlichen ultravioletten Strahlung der Sonne und bewirkt durch die Absorption dieser Energie einen positiven Temperaturgradienten in der Stratosphäre. Zudem ist Ozon ein Treibhausgas und spielt, dadurch dass es Sauerstoffatome an andere Treibhausgase überträgt, eine zentrale Rolle in vielen chemischen Oxidationsprozessen in der Atmosphäre. Des Weiteren besitzt Ozon eine besondere Isotopensignatur, die sich durch ungewöhnlich starke Anreicherungen in den beiden seltenen Isotopen ^{17}O und ^{18}O auszeichnet (relativ zum Anfangssauerstoff aus dem es geformt wurde). Diese Anreicherungen folgen nicht dem Prinzip der massenabhängigen Fraktionierung (*eng.* mass-dependent fractionation, MDF), definiert als $\delta^{17}O = 0.52 \times \delta^{18}O$, sondern weisen eine signifikant höhere Anreicherung in ^{17}O auf als es die Anreicherung in ^{18}O vermuten lassen würde. Dieser Überschuss in ^{17}O wird quantifiziert als $\Delta^{17}O = \delta^{17}O - 0.52 \times \delta^{18}O$ und wird normalerweise als massenunabhängige Fraktionierung (*eng.* mass-independent fractionation, MIF) bezeichnet. Die außergewöhnliche Isotopensignatur von Ozon ist sowohl innerhalb der Molekularphysik als auch innerhalb der Chemie von großem wissenschaftlichen Interesse. Molekular physikalisch betrachtet ist es interessant die Ursache der Isotopensignatur zu verstehen, wobei aus Perspektive der Atmosphärenchemie die Übertragung der Isotopenanomalie auf zahlreiche andere Spurengase interessant ist.

Die Bildung von Ozon ist die bekannteste Reaktion, die zu einer massenunabhängigen Fraktionierung führt. Die Isotopeneffekte in der Ozonbildung sind bis ins Detail untersucht und es wurde gezeigt, dass die Größe der Isotopenanreicherungen in atmosphärischem und experimentellem O_3 eine starke Temperatur- und Druckabhängigkeit aufweisen. In der Stratosphäre, oberhalb von 25 km, beobachtete man jedoch Anreicherungen welche die erwarteten Anreicherungen zu den vorherrschenden Druck- und Temperaturbedingungen übertrafen. Dies deutet darauf hin, dass die Isotopensignatur des atmosphärischen O_3 nicht nur von der Ozonbildungsreaktion herrührt, sondern auch andere Prozesse beitragen können. Prozesse, die zu solch einer zusätzlichen Isotopenanreicherung führen können sind die Photolyse und der chemische Abbau von Ozon mittels der Abbaureaktion $O + O_3$. Bis heute ist jedoch der Einfluss der Ozonabbaureaktionen auf die Isotopensignatur in atmosphärischem O_3 nicht eindeutig geklärt.

Die vorliegende Dissertation untersucht die Isotopeneffekte der Ozonabbaureaktionen, insbesondere der Ozonphotolyse im sichtbaren Licht (400 – 800 nm) und der Reaktion $O + O_3$. Durch die Quantifizierung der Isotopeneffekte in den erwähnten Reaktionen können dann auch Isotopeneffekte in der Ozonbildung neu evaluiert werden.

Wir führten neue Experimente durch, um die Isotopeneffekte in der O_3 Photolyse in den

Chappuis Banden zu bestimmen. Die Photolyse erfolgte mittels einer Breitbandlampe, charakterisiert durch ein Strahlungsspektrum von 400 bis 800 nm mit einem Maximum bei 605 nm. Das Anfangsozon wurde durch eine elektrischen Entladung hergestellt und anschließend entweder pur oder in Anwesenheit verschiedener Badgase (CO, He, Ar) für variierende Zeitdauer photolysiert. Das verbleibende O_3 wurde in einer Kühlfalle bei der Tripelpunkttemperatur von Stickstoff (63K) gesammelt, zu O_2 umgewandelt und schließlich die Isotopenzusammensetzung mit Hilfe eines Isotopenverhältnis-Massenspektrometers (isotope ratio mass spectrometer, IRMS) bestimmt. Zur quantitativen Interpretation wurde ein kinetisches Reaktionsmodel entwickelt.

In vorherigen Untersuchungen ist es nicht möglich gewesen, die Ozonphotolyse von der chemischen Abbaureaktion $O + O_3$ zu trennen, da in Laborexperimenten letztere stets nach Freisetzung eines O Atoms aus der Photolyse auftritt. Eine entscheidende Neuheit dieser Dissertation ist die Verwendung von Kohlenstoffmonoxid (CO) als Badgas, welches mit $O(^3P)$ reagiert und somit weitere Reaktionen unterdrückt. Auf diese Weise gelang es uns erstmals, die Isotopeneffekte in der O_3 Photolyse und $O + O_3$ Reaktion getrennt voneinander zu quantifizieren. Schwierigkeiten ergaben sich durch einen bisher ungeklärten Abbau von O_3 in O_3 + CO Gasgemischen. Der Effekt dieses Abbaus wurde durch Sensitivitätstests mit Hilfe eines kinetischen Models abgeschätzt. Als Hauptresultate präsentieren wir im ersten Teil dieser Dissertation Fraktionierungsfaktoren von $^{18}\varepsilon_{hv}$ = −16.1‰ und $^{17}\varepsilon_{hv}$ −8.05‰ für die Photolyse und $^{18}\varepsilon_{O+O_3} = -11.9‰$ and $^{17}\varepsilon_{O+O_3} = -5.95‰$ für die $O + O_3$ Reaktion.

Basierend auf den vorhergehenden Ergebnissen untersuchten wir die Wellenlängenabhängigkeit der Isotopenfraktionierungen in der Photolyse von Ozon im sichtbaren Licht. In diesen Experimenten wurde Ozon mittels einer Breitbandlampe, ausgestattet mit einzelnen optischen Filtern (455 nm, 620 nm, 550 nm), oder mit verschiedenen LEDs (Strahlungsmaximum jeweils bei 660 nm, 617 nm oder 530 nm) unterschiedlich lange photolysiert. Unter den gegebenen experimentellen Bedingungen stellt die gemessene Fraktionierung einen Mittelwert der Fraktionierungen in der O_3 Photolyse und der $O + O_3$ Ozonabbaureaktion dar. Da die Isotopenfraktionierung bei der $O + O_3$ Reaktion bereits in den vorherigen Experimenten bestimmt wurde, konnte die Fraktionierung in der Ozonphotolyse hergeleitet werden. Mit steigender Wellenlänge nehmen die ermittelten Fraktionierungen zwar zu, die Intensität der Wellenlängenabhängigkeit ist jedoch kleiner als bislang von theoretischen Berechnungen vorhergesagt wurde. Im Widerspruch zu den theoretisch berechneten Effekten zeigen die gemessenen Isotopeneffekte aller Experimente eine Anreicherung des verbleibenden O_3. Diese Ergebnisse deuten darauf hin, dass Atmosphärenmodelle, die auf den theoretisch berechneten Fraktionierungen beruhen, die Isotopeneffekte in der O_3 Photolyse unterschätzen. Photolyseexperimente bei unterschiedlichen Temperaturen (-90°C bis +40°C) zeigten, dass die Fraktionierungseffekte in der O_3 Photolyse keine

Temperaturabhängigkeit aufweisen. Ein wichtiges Ergebnis unserer Experimente ist, dass Isotopeneffekte bei der O_3 Photolyse im Chappuis Band einem massenabhängigen Fraktionierungsmuster folgen.

Des Weiteren führten wir photolytische Recycling Experimente durch, in denen O_3 in Anwesenheit von O_2 photolysiert wurde und sich ein Isotopengleichgewicht zwischen Ozonbildung und Ozonzerstörung einstellte. In diesen Experimenten wurden die Isotopeneffekte bei der O_3 Bildung und O_3 Photolyse gemeinsam untersucht. Verglichen mit früheren Experimenten beobachteten wir kleine aber signifikante Unterschiede in der Temperaturabhängigkeit der Isotopenanreicherungen. Basierend auf der genauen Charakterisierung der Isotopeneffekte in der Photolyse konnten wir aus diesen Ergebnissen die Temperaturabhängigkeit der Isotopenfraktionierung in der O_3 Bildungsreaktion bestimmen. Dies ermöglichte es uns einen konsistenten Datensatz von relativen Ratenkoeffizienten für die Isotop-spezifischen Teilreaktionen, die zur Bildung von einzel-substituierten O_3 Molekülen führen, herzuleiten. Da die Messungen, im Vergleich zu früheren Untersuchungen, mit einer sehr hohen Präzision durchgeführt wurden, konnten wir auch die Ratenkoeffizienten mit einer erhöhten Genauigkeit bestimmen. Des Weiteren beobachteten wir relativ große Unterschiede in $\Delta^{17}O$ von O_3 im photochemischen Gleichgewicht mit O_2 verglichen mit früheren angenommenen Werten. Es ist unwahrscheinlich, dass dieser Effekt auf Unterschiede in der experimentellen Durchführung zurück geführt werden kann. Wahrscheinlicher sind größere experimentelle Fehler in der Isotopenanalyse früherer Studien.

Diese Dissertation beschreibt eine neue Methode zur Trennung der Isotopeneffekte bei der O_3 Photolyse und der O_3-Abbaureaktion $O + O_3$. Wir konnten die Isotopeneffekte sowohl in der O_3 Photolyse mit sichtbarem Licht, der gleichzeitig ablaufenden Reaktion $O + O_3$ als auch in der Ozonbildung erfolgreich quantifizieren. Es bleiben jedoch Unsicherheiten aufgrund des bisher nicht geklärten Abbaus von O_3 in $O_3 + CO$ Gasgemischen bestehen, was weitere Untersuchungen erforderlich macht. Zusätzlich wären Messungen mit hoher Wellenlängen-Auflösung mit Hilfe eines Lasers hilfreich, um die Validität der theoretischen Berechnungen und der atmosphärischen Modelle zu testen, vor allem in Wellenlängenbereichen mit maximal zu erwartenden Fraktionierungen.

1

INTRODUCTION

1.1 HISTORY OF OZONE

The discovery of ozone as a chemical compound dates back to the German scientist Christian Friedrich Schönbein (1799-1869), a professor of chemistry at the University of Basel. In 1839, as a researcher in the field of electric discharges in oxygen, he was the first to report the occurrence of an irritating odor during the electrolysis of water, which was usually known as a byproduct from electric arcs. In 1840, after intense study, Schönbein presented his discovery to the University of Munich and termed the gas "*ozone*", which originates from the ancient Greek word *"ozein"* (to smell). The molecular formula of ozone was determined by Jacques-Louis Soret in 1865 and was confirmed by Schönbein in 1867, only two years before his death [*Seinfeld and Pandis,* 2006; *Rubin,* 2001].

Much earlier, in 1789, the Dutch scientist, Martin van Marum (1750-1837), had already mentioned in his experimental reports a specific smell around his electrifiers, which he described as "smell of electricity", however, further investigations were missing, which left his findings unrecognized [*Rubin,* 2001].

1.2 PROPERTIES OF OZONE

Ozone with the chemical formula O_3 is a triatomic molecule and an allotrope of the chemical element oxygen. It contains three oxygen atoms which are situated at the corners of an open triangle with a bond angle of 117.47° and an interatomic distance of 1.272 Å (Figure 1.1). Ozone is a pale blue colored gas with a boiling point at 161 K below which it condenses into dark blue liquid. At its melting point of 80 K the gas solidifies in violet-black color.

Its chemical structure can be considered as a resonance hybrid and consists of several mesomeric states, which are continuously converted, in dynamic equilibrium (Figure 1.1). Ozone is extremely unstable with a dissociation energy of 106.6 $kJ \times mol^{-1}$ [*Haynes,* 2012]. As a metastable molecule, ozone easily decomposes to form molecular oxygen. The process of decomposition is exothermic and therefore care must be taken, when ozone is

used in high concentrations. The dissociation from ozone to oxygen leads to an isolated oxygen atom, which makes ozone highly reactive, and an important oxidant.

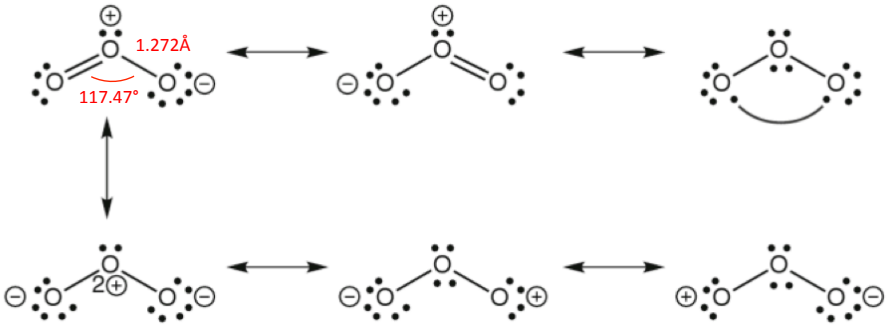

Figure 1.1. The chemical structure of the ozone molecule and its different mesomeric states. Adapted from *Kuhn and Klapötke* [2014].

It was already known in 1854, that ozone at high concentrations is noxious for living organisms [*Rubin,* 2001] and causes severe detrimental effects on the respiratory systems of humans and animals. It also inflicts cell tissue injuries of plants and damage of industrial materials such as metals, plastics and rubbers.

Under controlled conditions ozone is successfully applied for air purification in railway tunnels and assembly occupancies. It also has applications in sterilization of drinking water or preservation of meat in cold storages as well as in industry for bleaching of materials such as silk, oils and starch.

1.3 OZONE IN THE ATMOSPHERE

Due to its short lifetime, ozone is not uniformly mixed in the atmosphere and chemical and dynamical processes control its distribution. The lifetime of ozone strongly depends on removal processes, which are determined by atmospheric conditions such as temperature and humidity. This leads to an average lifetime of O_3 in the troposphere (lowest level of the atmosphere extending to about 8-18 km height) of ~23 days [*Stevenson et al.,* 2006; *Young et al.,* 2013], while the typical lifetime in the lower stratosphere (at about 20 km height) at daytime in middle latitudes is estimated at ~20 minutes [*Dessler,* 2000].

Around 90% of the atmospheric ozone is found in the stratosphere between an altitude of 20 and 30 km (Figure 1.2), commonly known as *the ozone layer*. Its concentration strongly depends on a combination of production-, destruction- and transport-processes, where the detailed distribution varies with altitude, latitude and season. The ability to absorb harmful UV radiation from the Sun makes stratospheric ozone indispensible for life

on Earth. The effective absorption of UV light and the associated exothermic dissociation of ozone cause a positive temperature gradient in the stratosphere. Between 20 and 50 km atmospheric temperature increases by almost 60 K, which is the reason for the stable stratification, thus for the existence of the stratosphere. The solar short wave heating rate of O_3 reaches a maximum of nearly 15 K/day at 50 km height, which is dominating the stratospheric heating compared to other atmospheric compounds (CO_2, O_2 and NO_2) with a maximum of < 1 K/day in the lower stratosphere (Figure 1.3).

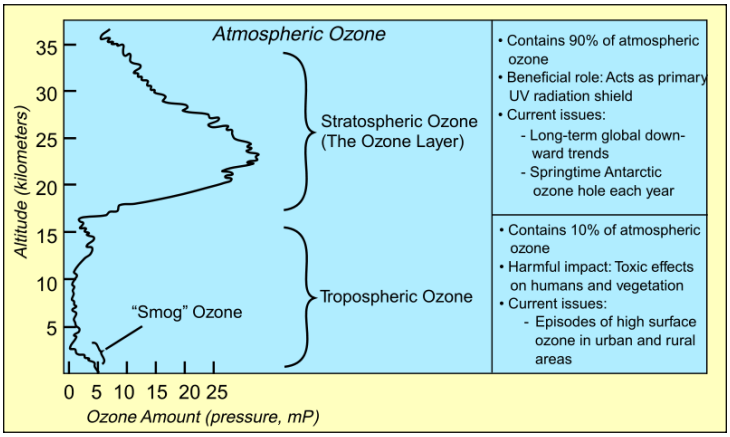

Figure 1.2. Vertical profile of ozone partial pressure in mP as a function of altitude. Including main aspects related to tropospheric and stratospheric ozone. From *Schoeberl et al*. [1999].

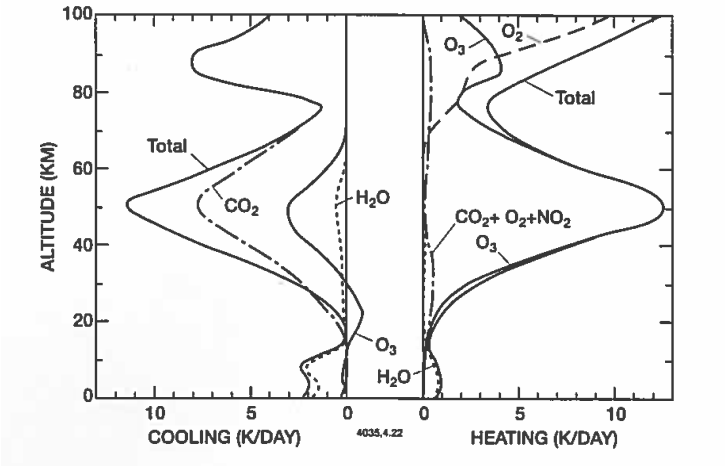

Figure 1.3. Vertical distribution of solar short wave heating rates by O_3, O_2, NO_2, H_2O, CO_2 and of terrestrial long wave cooling rates by CO_2, O_3, and H_2O. Ozone clearly dominates heating of the stratosphere and also contributes significantly to stratospheric cooling [*London,* 1980].

Only 10% of the total atmospheric ozone is found in the troposphere (0-18 km) (Figure 1.2). Although the concentrations are lower than in the stratosphere, this is the region where life is directly exposed to ozone and its adverse health effects. Because of its strong oxidative power, tropospheric ozone is a serious air pollutant.

Ozone in the troposphere is not directly emitted to the atmosphere like other pollutants such as carbon monoxide (CO), but chemically formed through various reactions of atmospheric compounds. The chemical reaction mechanisms are described in detail in chapter 1.3.3. Typical abundances for tropospheric ozone range from 10 ppb observed over the Pacific Ocean, to 100 ppb measured downwind in strongly polluted regions. Average background levels range between 30 and 40 ppb. Values are reported in parts per billion (ppb) which corresponds to the SI unit nanomol/mol [*Pyle and Shepherd,* 2005; *Seinfeld and Pandis,* 2006; *Schoeberl et al.,* 1999; *Myhre et al.,* 2013].

1.3.1 *Radiative effects of ozone*

The primary absorption of radiation by ozone takes place in three specific spectral regions, the Hartley band (200-310 nm), the highly structured Huggins bands (310-350 nm) and the Chappuis band (400-800 nm) (Figure 1.4).

The Hartley band is a strong broad continuum with a maximum absorption at 255 nm. It is characterized by a smooth shape, which is caused by the fast and direct O_3 photo-dissociation in the upper electronic band. On the low-energy flank of the Hartley band, in the Huggins bands, the absorption cross section shows significant variations with wavelength and the diffuse absorption structures in the Huggins bands show strong temperature dependence. The absorption cross-sections increase with temperature due to changes in rotational and vibrational distributions in the electronic ground state of O_3. In the visible light region, the Chappuis band extends over a broad range of the spectrum and shows small changes in absorption structure with wavelength, caused by the interaction of two excited electronic states. Compared to the Hartley bands, the temperature dependence in this spectral region is small. Peak absorption only increases by 0.5% when temperature drops from 203 to 293 K [*Chehade et al.,* 2013].

While the absorption in the Hartley and Huggins bands are dominant in the middle and higher stratosphere, the absorption of visible light in the Chappuis band plays a dominant role in the lower stratosphere as well as in the troposphere [*Andrews,* 2010].

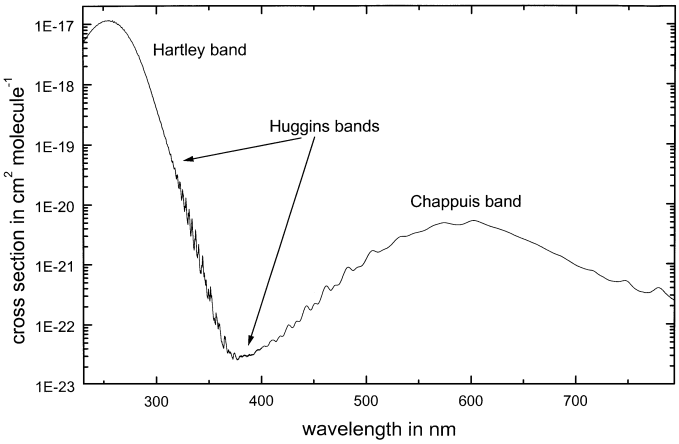

Figure 1.4. O_3 absorption cross section. From *Burrows et al.* [1999].

The ability to absorb short and long wave radiation makes O_3 a radiatively active gas and its long wave properties an important greenhouse gas. Greenhouse gases absorb and reemit thermal infrared radiation emitted from the Earth surface, and the resulting natural greenhouse effect leads to an average atmospheric temperature of 15°C at the Earth's surface. The increase of greenhouse gases associated with anthropogenic activity since the beginning of the industrial period leads to increases in these gases in the atmosphere and a corresponding anthropogenic greenhouse effect.

The predicted change in net radiative flux at a certain level in the atmosphere as a consequence of a perturbation is quantified by the *radiative forcing* (RF). In the literature *"radiative forcing"* is defined in several ways, depending on the atmospheric level at which the net flux is calculated and whether the atmosphere is allowed to adjust to the perturbation. In the following RF refers to the change in net downward radiative flux at the top of the tropopause after temperatures in the stratosphere adjusted to the radiative equilibrium. Surface and tropospheric temperature, as well as water vapor and cloud cover are assumed fixed at the values before the perturbation [*Myhre et al.,* 2013].

The effect of tropospheric O_3 on the anthropogenic warming depends on changes in temperature, water vapor and clouds. Since tropospheric O_3 is not directly emitted, but formed chemically in presence of other atmospheric compounds, tropospheric O_3 increases when the precursor compounds increase. The global mean radiative forcing associated with the increase in tropospheric ozone is estimated at +0.40 Wm^{-2}, whereas the radiative forcing for stratospheric ozone is of opposite sign with a value of −0.05 Wm^{-2}. The long wave radiative forcing is larger in the lower stratosphere and lower in the upper stratosphere where the shortwave radiative forcing dominates. Thus whether the total radiative forcing of stratospheric O_3 is positive or negative is determined by the vertical

profile of the change in stratospheric ozone due to anthropogenic emissions. Negative RF results from models assuming a decline in ozone mixing ratio close or at the tropopause. Of the total O_3 radiative forcing of 0.35 Wm^{-2}, 0.5 Wm^{-2} can be attributed to the increase in ozone production from ozone precursors and -0.15 Wm^{-2} to the decrease in ozone from depleting substances (details about chemical reactions involving ozone depleting substances can be found in chapter 1.3.2) [*Myhre et al.,* 2013].

1.3.2 *Ozone chemistry in the stratosphere*

In the stratosphere the mixing ratio of ozone is determined by photochemical formation and destruction reactions in photochemical equilibrium. In 1930, Sydney Chapman first explained the chemical processes of ozone formation and destruction reactions, which is commonly known as the *Chapman Cycle* [*Chapman,* 1930].

The production of stratospheric ozone is initiated by the dissociation of molecular oxygen (O_2) at wavelengths (λ) lower than 240 nm.

$$O_2 + h\nu \rightarrow O + O \ (\lambda < 240 \text{ nm}) \qquad \text{(R1.1)}$$

The oxygen atom (O) produced in this reaction rapidly reacts with O_2 to form ozone (R1.2) in the presence of an inert molecule M removing the excess energy of the reaction. Because the bonds of the O_3 molecule are weaker compared to the ones in O_2, ultraviolet (UV) (R1.3a) or visible light (R1.3b) photons of lower energy can photolyze O_3. The reaction product from UV photolysis, $O(^1D)$, is highly unstable and quickly stabilizes to $O(^3P)$ by collision with nitrogen (N_2) or O_2. Once ozone is photolysed, the product atomic oxygen $O(^3P)$ reforms ozone (R1.2) or undergoes a reaction with another ozone molecule to form new O_2 (R1.4), which completes the Chapman cycle.

$$O + O_2 + M \rightarrow O_3 + M \qquad \text{(R1.2)}$$
$$O_3 + h\nu \rightarrow O(^1D) + O_2\ (^1\Delta_g), \ (\lambda \leq 320 \text{ nm}) \qquad \text{(R1.3a)}$$
$$O_3 + h\nu \rightarrow O(^3P) + O_2\ \left(X^3\Sigma_g^-\right), \ (\lambda > 320 \text{ nm}) \qquad \text{(R1.3b)}$$
$$O_3 + O \rightarrow 2O_2 \qquad \text{(R1.4)}$$

However, in the stratosphere additional O_3 removal occurs due to a number of catalytic cycles involving nitrogen (N), hydrogen (H) and halogen (e.g. Cl, Br) radical species in the form of

$$XO + O \rightarrow X + O_2 \qquad \text{(R1.5)}$$
$$X + O_3 \rightarrow XO + O_2 \qquad \text{(R1.6)}$$
$$\text{Net: } O + O_3 \rightarrow 2O_2 \qquad \text{(R1.7)}$$

The most efficient catalysts (X) in the upper stratosphere are nitric oxide (NO), chlorine (Cl), hydrogen (H) and the hydroxyl radial (OH). Halogen radical species are mostly formed by photolysis of anthropogenic precursor gases, such as chlorofluorocarbons (CFCs). The long-term increase in the precursor gases consequently leads to significant long-term decrease of ozone [*Jacob,* 1999; *WMO,* 2014].

The occurrence of extremely low stratospheric ozone abundances in the polar stratosphere is referred to as stratospheric *ozone hole* and was first reported by *Farman et al.* [1985] and *Chubashi* [1985]. The pronounced thinning of the ozone layer occurs in the polar vortex regions, where polar stratospheric clouds can form at very low temperatures. On the surface of these clouds, chlorine reservoir species are converted to active ozone destructive compounds that are stable when not exposed to sunlight. At the beginning of polar spring, requiring only relatively little solar radiation, large amounts of activated chlorine initiate very effective catalytic ozone-destruction cycles (R1.8 - R1.14) [*Seinfeld and Pandis,* 2006].

$$Cl + O_3 \rightarrow ClO + O_2 \quad \text{(R1.8)}$$
$$ClO + O \rightarrow Cl + O_2 \quad \text{(R1.9)}$$
$$ClO + ClO + M \rightarrow Cl_2O_2 + M \quad \text{(R1.10)}$$
$$Cl_2O_2 + h\nu \rightarrow 2Cl + O_2 \quad \text{(R1.11)}$$

and

$$BrO + ClO + h\nu \rightarrow Br + Cl + O_2 \quad \text{(R1.12)}$$
$$Cl + O_3 \rightarrow ClO + O_2 \quad \text{(R1.13)}$$
$$Br + O_3 \rightarrow BrO + O_2 \quad \text{(R1.14)}$$

The strongest ozone depletions are observed above Antarctica. In the Arctic similar events occur, however, because of differences in topography and the resulting meteorological conditions, the polar vortex is less stable and therefore the low temperatures necessary for the formation of polar stratospheric clouds are not often reached.

In 1989, the emissions of ozone depleting substances were regulated by the implementation of the Montreal Protocol, because of the risk involved for human health. In the following years, amendments to the Montreal Protocol also prohibited the production of CFCs. As a consequence of the treaty, stratospheric ozone abundance at 42 km height increased by 5% over the period from 2000-2013. However, since CFCs have a very long lifetime, their impact on stratospheric ozone will remain decades after emissions have been reduced. Assuming continued compliance with the Montreal Protocol it is expected that by 2050 the abundance of bromine and chlorine in the stratosphere will return to levels that were measured before 1980. Low-ozone events due to cold winters or volcanic eruptions may occur until 2100 [*Hegglin et al.,* 2015].

1.3.3 *Ozone chemistry in the troposphere*

In contrast to other greenhouse gases, tropospheric ozone is not directly emitted from surface sources to the atmosphere, but chemically produced by ozone precursors such as nitrogen oxide (NO_x), carbon monoxide (CO) and non-methane hydrocarbons (NMHC). NO_x and CO emissions are mainly of anthropogenic origin and largely emitted from combustion of fossil fuel, while NMHC are mostly emitted by the biosphere, with a significant contribution from anthropogenic sources.

The photolysis of nitrous oxide (NO_2) leads to the formation of atomic oxygen that reacts with O_2 to form O_3 (R1.15-1.17). In a next step nitrous oxide (NO) reacts with O_3 and thus destroys again the O_3 molecule produced via NO_2 photolysis (R1.15). This so-called *Leighton cycle* is a null cycle for O_3 and it is well known that a photo stationary state establishes quickly in this system.

$$NO_2 + h\nu \rightarrow NO + O \quad \text{(R1.15)}$$
$$O + O_2 + M \rightarrow O_3 + M \quad \text{(R1.16)}$$
$$NO + O_3 \rightarrow NO_2 + O_2 \quad \text{(R1.17)}$$

In order to explain ozone production in the troposphere this steady state needs to be disturbed and shifted towards O_3 formation. In the atmosphere this is realized by an alternative reaction for oxidation of NO to NO_2, and the most important additional reaction is the one of NO with peroxy radicals, e.g. HO_2 (R1.21).

The O_3 formation reaction sequence starts with the reaction of an organic compound (CH_4, CO, VOC) with an OH radical (R1.18-R1.19) that leads to the formation of RO_2 or HO_2. In turn RO_2 or O_2 react with NO to form NO_2 (R1.20-R1.21). While OH is recycled, NO has been converted to NO_2 and initiates another O_3 production cycle via photolysis as shown in reactions R1.15 to R1.17.

$$VOC + OH \xrightarrow{[O_2]} RO_2 + HO_2 \quad \text{(R1.18)}$$
$$CO + OH \xrightarrow{[O_2]} HO_2 + CO_2 \quad \text{(R1.19)}$$
$$NO + RO_2 \xrightarrow{[O_2]} VOC + HO_2 + NO_2 \quad \text{(R1.20)}$$
$$NO + HO_2 \rightarrow OH + NO_2 \quad \text{(R1.21)}$$

Episodes of high concentrations of tropospheric ozone and photo oxidants mainly occur in summer and are known as *ozone smog*. The World Health Organization (WHO) defined an exposure level for humans of 60 ppb (maximum daily eight hours mean), as health safety limit [*World Health Organization,* 2000]. This 8 hours mean value entered into

legitimate force for Europe in 2010, but in contrast to the WHO guideline, it permits the exceedance of this value for 25 days average within 3 years [*European Union,* 2015]. In urban areas the ambient O_3 values frequently exceed the safety limit, especially when in hot summers the photochemical O_3 production increases. Thus in 2003, 65% of the European urban population was exposed to harmful levels of O_3 for more than 25 days, which was the highest violation of the air quality standards recorded in history. Over the last 5 years, the proportion of urban population exposed to dangerous levels of O_3 according to the EU air quality standard was not higher than 20%. However, when following the WHO guideline, which does not allow any exceedance of the given health safety limit, the proportion of the people exposed to concentrations above the guideline value (between the years 2000 and 2012) was ~96%, with no significant changes over time [*EEA,* 2014].

1.4 ISOTOPES

Atoms consist of a nucleus, which contains Z protons (p^+) and uncharged N neutrons (n) (Z and N are number of protons and neutrons, respectively). The positive charge of the nucleus is compensated by a number of negatively charged electrons (e^-). Protons and neutrons are referred to as nucleons, which define the mass number A of an atom (A = Z+N). Atoms with the same number of protons Z, but different mass number A (thus different number of neutrons) form different isotopes of the same chemical element. While different isotopes have generally the same chemical characteristics, there are differences in their physical properties such as nuclear spin and lifetime [*Bransden and Joachain,* 2003].

Isotopes can be classified as either stable isotopes or radioactive isotopes. Stable isotopes are relatively evenly distributed in nature, but small differences exist in the abundance in different reservoirs. These differences are a consequence of kinetic and equilibrium isotope fractionation processes that occur at the molecular scale and can serve as tracers for the respective processes. Radioactive isotopes can either exist since the formation of the element (primordial isotopes) or be formed through natural or anthropogenic processes. They are also called unstable isotopes, since they contain an unstable nucleus, which decays over time emitting alpha, beta or gamma radiation. The stable end product is a non-radioactive isotope of another element. Therefore under certain circumstances, radioactive isotopes can be used for dating purposes in earth system science, but also find application in other areas such as medicine and industry [*Faure and Mensing,* 2005].

The isotopic composition of an element is commonly expressed as delta value (δ) and defined as relative isotopic enrichment of a sample to a standard reference material (1.1). Since the variations are small, δ values are usually given in units of per mill (‰):

$$\delta = \left(\frac{R_{sa}}{R_{ref}} - 1 \right) \times 1000‰ \tag{1.1}$$

where R is the isotope ratio of the heavy isotope versus the light isotope of a sample (R_{sa}) and a reference material (R_{ref}). In the case of oxygen the two possible stable isotope ratios are $^{17}O/^{16}O$ and $^{18}O/^{16}O$. Primary international reference materials are Vienna Standard Mean Ocean Water (VSMOW), Vienna Pee Dee Belemnite (VPDB) and tropospheric oxygen (Air-O_2) for O_2 measurements. The use of international accepted reference materials enables an easy comparison of results from different laboratories. Positive δ-values describe an isotopic enrichment, whereas negative δ-values denote isotopic depletion relative to the reference material.

In general, the fractionation factor α is used to describe the isotope ratio (R) of an instantaneously formed reaction product (A) and the isotope ratio of the reactant (B) (1.2a). For kinetic reactions, this is equivalent to the ratio between reaction coefficients k for the isotopically substituted reactant k_h (with a **h**eavy isotope) and the reaction coefficient for the standard species k_l (with only **l**ight isotopes) (1.2b).

$$\alpha_{A,B} = \frac{R_A}{R_B} \tag{1.2a}$$

$$\alpha_k = \frac{k_h}{k_l} \tag{1.2b}$$

Since α usually is close to unity, the fractionation ε is defined as follows.

$$\varepsilon = \alpha - 1 \tag{1.3}$$

There are different processes, which lead to isotope fractionations between different reservoirs. Mechanisms that lead to isotope fractionation are for example diffusion, gravitational settling, photolysis, thermodynamic equilibrium or isotopic exchange.

1.4.1 *Stable isotopologues of ozone*

Oxygen has three stable isotopes ^{16}O, ^{17}O and ^{18}O. The average abundance of the stable isotope ^{16}O is 99.76%, followed by ^{18}O with 0.2% and ^{17}O with 0.04%. The O_3 molecule can consist of all possible isotopic combinations of ^{16}O, ^{17}O and ^{18}O. Molecules containing different isotopes, but of the same chemical composition are called *isotopologues*. Not only the combination of isotopes characterizes the O_3 molecule, the position of the different oxygen isotopes also varies. Isotopologues with the same number of the different isotopes, but with variations in their position are *isotopomers* [*International Union of Pure and*

Applied Chemistry, 2014]. A complete list of O_3 isotopologues and isotopomers is given in Table 1.1.

Table 1.1: Isotopologues and isotopomers of O_3.

Molecular masses	*Isotopologues and Isotopomers*
$^{48}O_3$	$^{16}O^{16}O^{16}O$
$^{49}O_3$	$^{17}O^{16}O^{16}O$, $^{16}O^{17}O^{16}O$
$^{50}O_3$	$^{16}O^{16}O^{18}O$, $^{16}O^{18}O^{16}O$, $^{16}O^{17}O^{17}O$, $^{17}O^{16}O^{17}O$
$^{51}O_3$	$^{17}O^{17}O^{17}O$, $^{16}O^{17}O^{18}O$, $^{18}O^{16}O^{17}O$, $^{17}O^{18}O^{16}O$
$^{52}O_3$	$^{16}O^{18}O^{18}O$, $^{18}O^{16}O^{18}O$, $^{18}O^{17}O^{17}O$, $^{17}O^{18}O^{17}O$
$^{53}O_3$	$^{17}O^{18}O^{18}O$, $^{18}O^{17}O^{18}O$
$^{54}O_3$	$^{18}O^{18}O^{18}O$

1.4.2 *Mass-dependent and mass-independent fractionation*

As described before, changes in isotope ratios occur due to various thermodynamic and kinetic phenomena. Most of these processes are dependent on mass and the isotope changes therefore follow a mass-dependent fractionation line that can be approximated in linear form as

$$\delta^{17}O = \beta \times \delta^{18}O \tag{1.4}$$

In a three-isotope plot ($\delta^{18}O/\delta^{17}O$), the slope β for all natural materials is close to 0.5 and defines the so-called terrestrial fractionation line (TFL), which describes mass-dependent fractionation processes observed in terrestrial and lunar rocks (Figure 1.5). However, dependent on the specific chemical processes and the underlying reactants, β varies between 0.501 and 0.53 [*Pack and Herwartz,* 2014; *Thiemens,* 2013].

For oxygen atoms the three isotope slope β in the high temperature limit can be calculated from the thermodynamic equilibrium composition as follows, where m_{16}, m_{17} and m_{18} are the masses of the three isotopes ^{16}O, ^{17}O and ^{18}O [*Young et al.,* 2002].

$$\beta = \left(\frac{1}{m_{16}} - \frac{1}{m_{17}}\right) / \left(\frac{1}{m_{16}} - \frac{1}{m_{18}}\right) \tag{1.5}$$

In 1973, Clayton *et al.* [1973] discovered an unexpected deviation from the terrestrial fractionation line in meteoric material. The observed isotopic enrichment fell on a slope β of ~1, and thus, deviated significantly from the TFL. This extraordinary signature was interpreted as an isotopic signature of extra-terrestrial material, which was at that time believed to arise only from nuclear processes, such as nucleosynthesis or cosmic rays.

In 1983, *Thiemens and Heidenreich* [1983] were the first to show that an unusual isotope fractionation also occurs when ozone is produced by electric discharge in pure O_2. Contradictive to the classical theories of mass-dependent isotope effects, the relative enrichments of ^{17}O and ^{18}O showed a clear offset from the mass-dependent fractionation line. This offset ($\Delta^{17}O$) describes a "mass-independent fractionation" or "non-mass-dependent" pattern and is quantified in linear form as

$$\Delta^{17}O = \delta^{17}O - \beta \times \delta^{18}O, \tag{1.6}$$

where β requires a clear specification in order to avoid confusion when comparing results from different laboratories. Another way to describe mass-independent fractionation is to report the three-isotope slope as $\beta \neq 0.5$. However, since β shows small variability, care must be taken that β significantly deviates from the standard mass-dependent fraction value [*Weston et al.,* 2012].

Figure 1.5 represents a three-isotope plot including oxygen containing species for which a mass-independent isotope effect in oxygen was observed. The mass-independent isotope effect occurs in many atmospheric trace gases, which contain oxygen. Dependent on the atmospheric compound isotope enrichments can vary by more than 100‰. The highest enrichments were found for stratospheric and tropospheric ozone, which have their origin in the O_3 formation reaction, as shown later. Since the high mass-independent isotope signature cannot be erased by normal mass-dependent processes, it is transferred to other oxygen containing atmospheric compounds via chemical reactions. Thus, the signature of mass-independent fractionation represents a sensitive marker for particular chemical reactions.

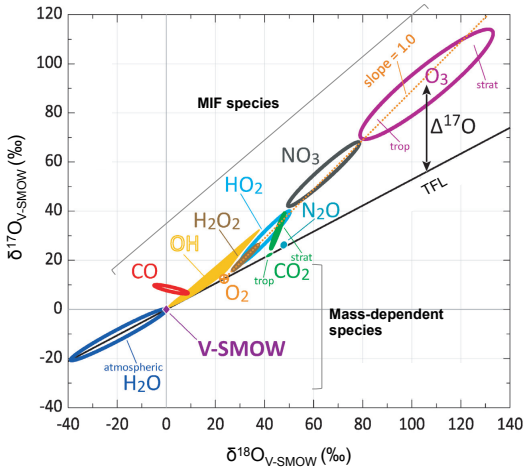

Figure 1.5. Three-isotope plot of different oxygen containing trace gases. Adapted from *Brenninkmeijer* [2009].

1.5 THE ISOTOPE ANOMALY IN OZONE

1.5.1 *Atmospheric measurements*

Mauersberger et al. [1981] reported a very high ^{18}O enrichment in stratospheric ozone, measured with a mass-spectrometer installed on a balloon. They found extremely high enrichments of 400‰ in ^{18}O measured at an altitude of 32 km. A few years later using improved equipment, *Mauersberger et al.* [1987], reported somewhat lower enrichments, which were of the same magnitude for ^{17}O and ^{18}O. This was also confirmed by *Schueler et al*. [1990] who measured enrichments of 80-100‰ for $\delta^{17}O$ and $\delta^{18}O$ at 30 km using a balloon borne cryogenic sampler. By careful laboratory studies, it was possible to track down the origin of the observed unusual enrichments to the O_3 formation reaction [*Morton et al.,* 1990] (a detailed description is given in section 1.5.2). *Krankowsky et al.* [2000] extended the available data of atmospheric measurements with further balloon flights and were able to link the measured enrichments of 70 and 110‰ in ^{17}O and ^{18}O, to atmospheric temperature and pressure. Based on balloon-borne remote sensing, *Haverd et al.* [2005] showed that, over the altitude range from 20 to 35 km, atmospheric fractionations of heavy O_3 were in agreement with already published data. However, observed fractionation values at higher altitudes increased further, which was not compatible with known isotope effects in ozone formation. This gave reason to the assumption of an additional fractionation effect in ozone photolysis. *Krankowsky et al.* [2007] drew similar conclusion from their high altitude (30 - 33 km) mass spectrometric data on ^{17}O and ^{18}O at equatorial latitudes.

The collection of tropospheric ozone is very challenging, because of the very low abundance of O_3 compared to oxygen and the difficulty to separate those gases from each other. Consequently, only a limited number of data are available. *Krankowsky et al.* [1995] conducted first measurements of tropospheric ozone and reported enrichments of 70‰ for ^{17}O and 90‰ for ^{18}O in molecular oxygen as a product from O_3 conversion. Other measurements by *Johnston and Thiemens* [1997] found similar overall isotopic enrichments for tropospheric ozone but suggested differences in different photochemical regimes. A more recent study by *Vicars and Savarino* [2014] presented $\Delta^{17}O$ of tropospheric O_3 measured with high precision using ozone collected with a nitrite-coated filter technique [*Vicars et al.,* 2012]. The isotope enrichments reported for tropospheric O_3 are in good quantitative agreement with the cryogenic measurements mentioned before. However, values for $\Delta^{17}O(O_3)_{bulk}$ are lower than what is expected following the temperature and pressure dependencies of O_3 formation. Additionally, contrary to *Johnston and Thiemens* [1997] who observed a systematic variability in their data measured at three different sites, data by *Vicars and Savarino* [2014] suggested a rather low level of natural variability in $\Delta^{17}O$.

1.5.2 *Laboratory measurements*

A few years after the anomalous enrichment in atmospheric ozone was detected, *Thiemens and Heidenreich* [1983] were the first to reproduce this effect under experimental conditions. Ozone was produced by an electric discharge and it was found that $\delta^{17}O$ and $\delta^{18}O$ were similarly enriched, which was the first demonstration of a mass-independent fractionation in a chemical reaction. These findings triggered a large number of follow-up studies, both in the atmosphere and in the laboratory, and a large scientific effort in numerous laboratories to understand the origin of the isotopic anomaly. To this end, follow up studies focused on the identification of the molecular processes behind the anomalous isotopic composition. In a first set of studies, the temperature [*Morton et al.,* 1990] and pressure dependence [*Bains-Sahota and Thiemens,* 1987; *Thiemens and Jackson,* 1988; *Thiemens and Jackson,* 1990; *Morton et al.,* 1990] of the fractionation in ozone, generated by electric discharge or photolysis, was investigated in detail.

The dependence of the isotopic enrichment in O_3 on pressure has been studied at 321 K [*Morton et al.,* 1990] and room temperature [*Thiemens and Jackson* 1988, 1990]. High enrichments of about 130 and 110‰ in ^{18}O and ^{17}O were observed at lower pressures, whereas at pressure higher than 100 Torr, the enrichments strongly decreased to 25‰ in ^{18}O and ^{17}O measured at 10000 Torr (Figure 1.6).

The temperature dependence was determined in experiments by *Morton et al.* [1990] and *Janssen et al.* [2003] in the low pressure regime, i.e. the pressure was held constant at 50 Torr [*Morton et al.,* 1990] and 45 Torr [*Janssen et al.,* 2003]. In their experiments, $\delta^{17}O$ and $\delta^{18}O$ values increased with temperature from 36 and 26‰ at 130 K to 117 and 146‰ at 361 K, respectively (Figure 1.7).

Morton *et al.* [1990] furthermore applied the technique of *photolytic recycling* and were able to successfully attribute the anomalous fractionation effect to the O_3 formation reaction. They conducted visible light photolysis of an O_3+O_2 gas mixture (O_3/O_2 = 0.1 Torr/50 Torr) for a sufficient time period and ensured that the isotopic signature of the final O_3 was independent of the isotopic composition of O_3 before photolysis. In a reaction system under the given conditions, the only sources for the observed isotopic anomaly are O_3 formation and O_3 photolysis and *Morton et al.* concluded that O_3 photolysis does not significantly contribute to the anomalous isotopic enrichment in O_3.

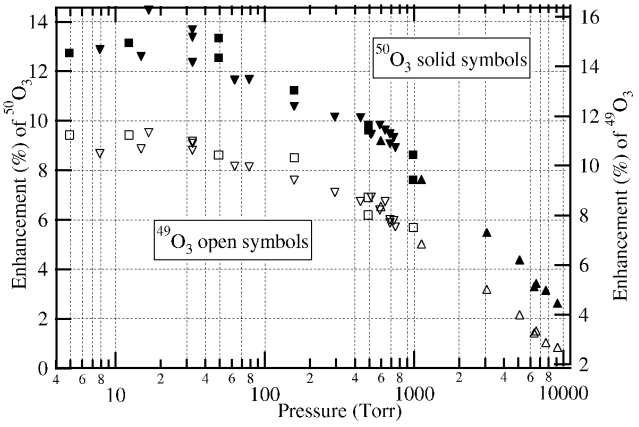

Figure 1.6. Pressure dependence of the isotope enrichment of $^{50}O_3$ (solid symbols) and $^{49}O_3$ (open symbols) measured at room temperature. Square symbols are from *Morton et al.* [1990], downside triangles and upside triangles from *Thiemens and Jackson* [1988] and [1990] respectively. From *Mauersberger et al.* [2003].

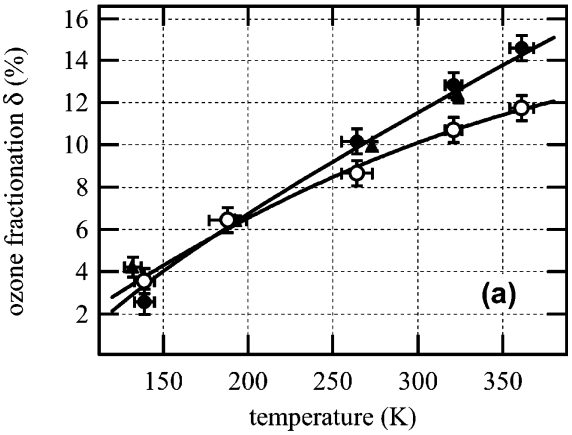

Figure 1.7. Temperature dependence of $\delta^{17}O$ (open symbols) and $\delta^{18}O$ (solid symbols) between 130 and 360 K. Circles refer to data from *Morton et al*. [1990], measured at 50 Torr, triangles represent values calculated at 45 Torr [*Janssen et al.* 2003]. From *Brenninkmeijer et al.* [2003].

To demonstrate the role of molecular symmetry effects in the fractionation effect observed in O_3, experiments with isotopically enriched oxygen mixtures were performed [*Mauersberger et al.,* 1993]. The highest enrichments were found for the totally asymmetric molecule $^{16}O^{17}O^{18}O$, whereas symmetric homonuclear O_3 molecules ($^{17}O_3$ and $^{18}O_3$) were depleted. The isotopic composition of O_3 isotopologues which can form a

symmetric or an asymmetric molecule showed enrichments that were only two-thirds of the one observed for the totally asymmetric molecule $^{16}O^{17}O^{18}O$ (Figure 1.8).

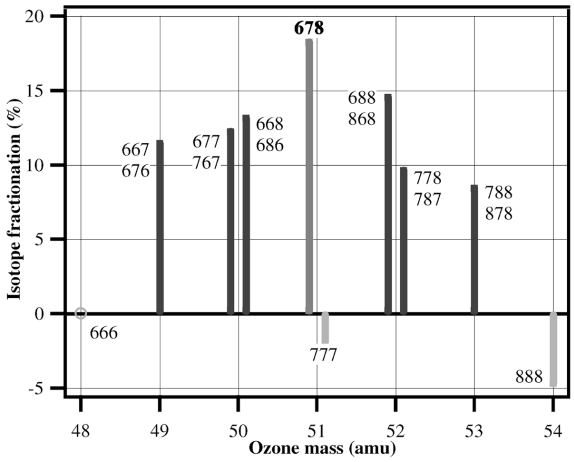

Figure 1.8. Isotope enrichments for the different ozone isotopologues. Numbers 6,7 and 8 denote ^{16}O, ^{17}O and ^{18}O. From *Mauersberger et al.* [2003].

The well established isotope exchange reactions (R1.22-R1.23), in which the O-atoms are exchanged multiple times with O_2 before O_3 is formed, would lead to a mass-dependent depletion of the heavy isotopologues of O_3 [*Kaye and Strobel,* 1983], and this is the reason for the depletion in the homonuclear isotopologues in Figure 1.8.

$$^{18}O + {}^{16}O^{16}O \leftrightarrow {}^{18}O^{16}O + {}^{16}O \quad \text{(R1.22)}$$

$$^{17}O + {}^{16}O^{16}O \leftrightarrow {}^{17}O^{16}O + {}^{16}O \quad \text{(R1.23)}$$

Because of differences in zero point energies (ZPE) of the participating O_2 molecules the exchange reactions are faster for exothermic (from left to right in R1.22-1.23) and slower for endothermic processes (from right to left in R1.22-1.23). Therefore the distribution of the heavy oxygen atoms is determined by isotopic exchange, which on its part directly influences the production of O_3 isotopologues [*Mauersberger et al.* 2003]. The deviation of isotope effects expected from isotopic exchange reactions only and the actual findings by *Mauersberger et al.* [1993] demonstrated that another effect must be present to explain the isotope anomaly. Based on their results, *Mauersberger et al.* suggested molecular symmetry effects, to be the origin of the isotope effects in O_3.

Anderson et al. [1997] who measured in their experiments the relative rate coefficients for four ozone formation channels leading to symmetric ($^{16}O+{}^{16}O^{16}O+M \rightarrow {}^{16}O^{16}O^{16}O+M$, $^{18}O+{}^{18}O^{18}O+M \rightarrow {}^{18}O^{18}O^{18}O+M$) and asymmetric ($^{18}O+{}^{16}O^{16}O+M \rightarrow {}^{18}O^{16}O^{16}O+M$,

$^{16}O+^{18}O^{18}O+M \rightarrow {}^{16}O^{18}O^{18}O+M$) ozone molecules found that symmetry effects only cannot explain the origin for the observed isotopic anomaly. If symmetry effects would dominate, rate coefficients of reactions that lead to symmetric ozone would have same values and differ from rate coefficients of reactions, which induce an asymmetric O_3 molecule. But their findings showed that rate coefficients of reactions which both lead to asymmetric O_3 formation differ by 50% and reactions in which a light molecule reacts with a heavy atom ($^{18}O + {}^{16}O^{16}O$) are slower compared to reactions in which a heavy molecule reacts with a light atom ($^{16}O + {}^{18}O^{18}O$). This also holds for relative rates of further isotope variants as shown by *Janssen et al.* [1999].

Another study by *Janssen et al.* [2001] showed that the measured isotope specific rate coefficients in O_3 formation correlate with differences in zero point energy of the oxygen molecule involved in the respective $O + O_2$ exchange reaction (Figure 1.9). An endothermic isotope exchange implies a longer lifetime of the metastable state O_3* and thus a higher chance of stabilization, whereas exothermic exchange induces the opposite. Consequently O_3 formation that involves an endothermic exchange product is increased compared to O_3 formation involving an exothermic exchange. This explains qualitatively why the difference in zero point energy of the O_2 molecule, before and after the isotope exchange, is linearly correlated with the relative rate coefficients of the asymmetric ozone molecules. However, rate coefficients for symmetric molecules ($\Delta ZPE = 0$) were about 20% lower than predicted by the linear fit line, which implies the occurrence of a symmetry effect, which favors formation of asymmetric molecules.

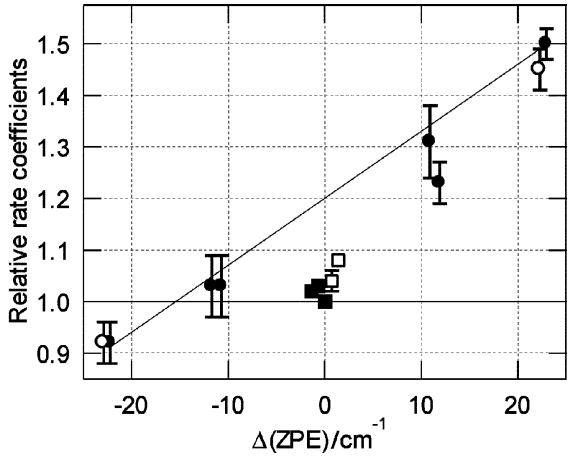

Figure 1.9. Relative rate coefficients versus differences in zero point energy in the oxygen molecules of the corresponding isotope exchange reactions. Circles represent exothermic and endothermic isotope exchange reactions. Squares illustrate energetically neutral collisions. Full symbols are reactions involving collisions with homonuclear diatoms, open symbols reactions with heteronuclear diatoms. From *Janssen et al.* [2001].

Additionally the pressure and temperature dependence of various rate coefficients has been investigated [*Günther et al*., 1999; *Janssen et al.,* 2003]. While rate coefficients for combination reactions of a heavy O_2 molecule with a light O atom (relative to $^{16}O + {}^{16}O^{16}O$) decreased with increase in pressure, rate coefficients for reactions of a heavy atom with a light molecule remained unchanged. Furthermore, low rate coefficient ratios (with a value of 0.92) decreased with an increase in temperature while high rate coefficient ratios (with a value of 1.5) showed no temperature dependence.

Further focus of research was the possible isotope effect arising from the bath gas in which ozone is formed [*Günther et al.,* 2000; *Feilberg et al.,* 2013]. It was found that the presence of different bath gases (Ar, Kr, Xe, O_2, CO_2, CH_4) has no significant effect on the isotopic composition of the formed O_3. However, *Feilberg et al.* [2013], reported for the bath gas SF_6 a total elimination of the isotope selectivity to form ozone at a pressure of 700 Torr. This influence of SF_6 compared to other gases was suggested to arise from differences in ΔE (the average amount of energy transferred per collision) which is with ~280 cm^{-1} relatively high compared to the other bath gases (Ar = 18 cm^{-1}, O_2 = 25 cm^{-1}, CO_2 = 150 cm^{-1}). The strong difference in isotopic composition between the bathgases SF_6 and CO_2 indicates that a sensitive energy barrier may be involved.

Only few attempts have been made to determine the isotope effects in O_3 photo dissociation. Measurements by *Bhattacharya and Thiemens* [1988] and *Chakraborty and Bhattacharya* [2003] in which ozone was photolysed using a UV light source concluded that photolytic O_3 decomposition in the Hartley bands leads to isotopic fractionation in a mass-independent manner with ($\delta^{18}O/\delta^{17}O \sim 1$). However, a later modeling study by *Cole and Boering* [2006] attributed the mass-independent effect in the experiments of *Chakraborty and Bhattacharya* [2003] to the known effect of mass-independent fractionation in ozone formation. Different results were obtained in different studies for photo dissociation in the Chappuis bands. While *Morton et al.* [1990] reported no significant change in the isotopic composition of ozone when photolysed with visible light, *Chakraborty and Bhattacharya* [2003] reported mass-depended enrichments for photolysis of O_3 at 520 nm and 630 nm.

Whereas the study of the anomalous isotope effect arising from the O_3 formation reaction was intensive, the investigation of the contribution of O_3 photolysis to the ozone isotope anomaly has received comparatively little attention. Furthermore in the available experimental studies on O_3 photolysis the isotope effect of the O_3 decomposition reaction $O+O_3$, which always goes along with O_3 photolysis, hinders the quantification of fractionation effects in only O_3 photolysis. A careful analysis of the isotope effects associated with visible light photolysis of O_3 is the subject of this thesis.

1.5.3 *Theoretical and modeling approach*

As shown above, the strong enrichments observed in O_3 formation result from differences (of about 50%) in the rate coefficients of the individual ozone formation channels and from the isotopic exchange reaction, which equilibrates the isotopic composition between molecules and atoms. However, different from statistical expectations, the O_3 isotopologues do not show isotopic depletion, but high enrichments for hetero-nuclear O_3 molecules [*Krankowsky and Mauersberger,* 1996; *Janssen et al.,* 2001].

Marcus and coworkers [*Gao and Marcus,* 2001; 2002] successfully presented a modified RRKM (Rice-Ramsperger-Kassel-Marcus) theory to explain these observations. From standard RRKM theory, the effect of differences in zero point energy between the different dissociation channels of the metastable state O_3* in O_3 formation is considered. The modified theory introduces two additional temperature dependent empirical parameters ΔE and η, which both need to be adjusted in order to reproduce the rate coefficient ratios of the experimental observations. Parameter ΔE, the average energy transferred per collision, was tuned to a value of 210 cm^{-1} and η, which describes the difference in statistical behavior between asymmetric and symmetric molecules was set to a value of 1.18, which was directly applied from *Janssen et al.* [2001]. By selecting these values *Gao and Marcus* were able to reproduce experimental observations of O_3 formation rate coefficients and it was shown that the isotopologue specific rate coefficients in O_3 formation depend on a) differences in ZPE, which implies mass-dependent fractionation effects and b) the non-mass-dependent symmetry selectivity. However, the parameter ΔE is much higher than the usual range (~20 cm^{-1}, Figure 1.9) and η was derived *a posteriori* from experiments.

A full quantum mechanical calculation was presented by *Babikov et al.* [2003a,b], in which they presented calculated $O + O_2$ scattering resonances for different ^{16}O -^{18}O isotope combinations and zero angular momentum. A big advancement was the application of a fully developed potential energy surface. This theory states that the mass-independent effect originates from the energy transfer mechanism when ozone metastable states are formed and stabilized. The availability of the different $O + O_2$ formation channels (metastable O_3 states) is again determined by the differences in zero point energy of isotopically substituted and non-substituted O_2 molecules. *Babikov et al.* showed that the density of metastable states is high in the small energy range represented by the zero point energy difference and much lower above it, providing an explanation for the observation that the minute zero point energy differences can lead to such large rate coefficient differences (Figure 1.10)

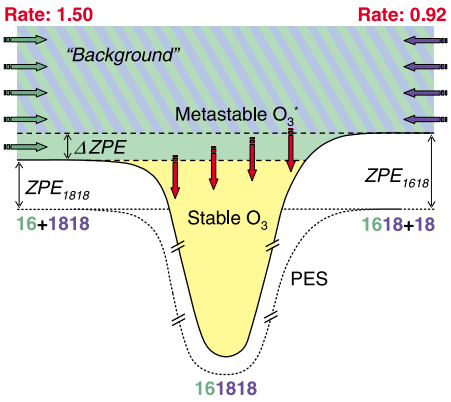

Figure 1.10. Schematic illustration of the recombination processes leading to the formation of $^{16}O^{18}O^{18}O$. Metastable states of O_3 (O_3*), formed above the stabilization well (green/green blue striped) are stabilized in the potential well (yellow). O_3* can be formed from two different entrance channels $^{16}O+^{18}O^{18}O$ (left) or $^{18}O+^{16}O^{18}O$ (right), while in the ΔZPE region (green) O_3* is only formed from the $^{16}O+^{18}O^{18}O$ entrance channel. The potential energy surface (PES, dotted line) and the zero point energy for both channels are indicated not on scale. Relative rates for O_3 formation of the individual channels are given in red. From *Babikov et al.* [2003a].

Theoretical calculations were also performed to understand fractionation processes in O_3 decomposition with UV as well as visible light. Based on differences in zero point energy, model calculations by *Miller et al.* [2005] and *Liang et al.* [2004, 2006] predicted large wavelength dependent fractions for UV as well as visible light photolysis. Fractionations vary by several hundreds of per mill depending on the wavelength at which ozone is photolysed. However, as shown later by *Ndengué et al.* [2012, 2014] and *Schmidt et al.* [2013] the application of zero point energy based models ignore changes of the width of the absorption spectra as well as changes in cross sections due to differences in transition dipole moments.

In summary, although the *Gao and Marcus* [2001, 2002] model convincingly reproduced the experimental findings, the theory involves two tuning parameters and a fundamental explanation for the large isotope effects in O_3 formation is still lacking. Furthermore, different models calculating isotope effects in O_3 photolysis show different results, but very few experiments exist to test these models.

1.6 INITIAL TRAINING NETWORK ON MASS-INDEPENDENT FRACTIONATION

This thesis is part of the Marie Curie Initial Training Network INTRAMIF (Initial Training network on mass-independent fractionation), which was initiated in 2009. Not only the oxidative capacity or the ability to absorb harmful UV radiation makes ozone a remarkable molecule. The peculiar isotopic composition of O_3 caught the interest of many scientists in

atmospheric research, because it can be used as a tracer for particular chemical reactions. INTRAMIF brought experts from atmospheric research, hydrology, oceanography and molecular physics together to advance the investigation of this powerful research tool.

Each scientific project within the INTRAMIF network focuses on a different mass-independently fractionated compound in the atmosphere (Figure 1.11). As mentioned before, ozone displays a very strong mass-independent signature, which originates from the O_3 formation reaction $O_2 + O + M$. Due to the high reactivity of the O_3 molecule, the anomaly is transferred to many other trace gases. For example, the transfer reactions to the NO_x family have been explained in detail in chapter 1.3.3, and subsequent reactions transfer the oxygen atoms to nitrate, where very strong mass-independent effects have been established (Figure 1.5). The UV photolysis product $O(^1D)$ facilitates oxygen transfer to stratospheric CO_2 and to OH (R1.3a) which may transfer the anomaly to stratospheric water. These are only few examples that illustrate the complexity of the MIF transfer reactions.

The work described in this thesis focuses on the isotopic effects occurring in the photolysis of O_3 in the wavelength region of 400-800 nm and the reactions $O + O_3$ and $O + O_2$ (R1.24-R1.26). This project is indicated as number 5 in Figure 1.11.

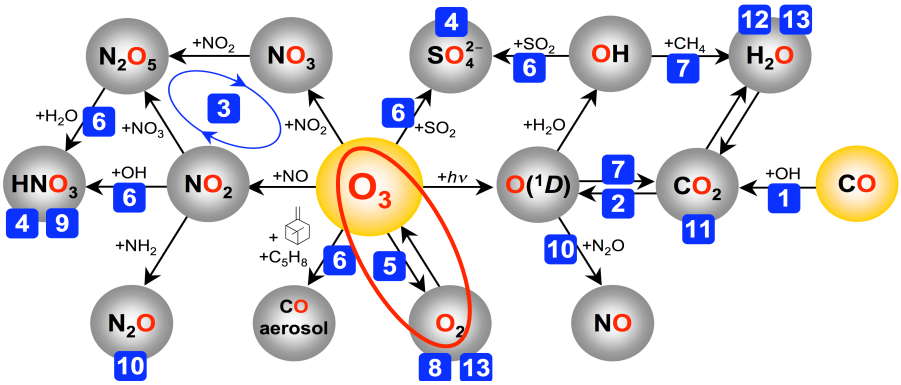

Figure 1.11. The transfer of the mass-independent fractionation signature through different chemical reactions in the atmosphere. Red marked: the research project of this work. [Adapted from INTRAMIF proposal 237890 Annex 1].

1.7 THESIS OUTLINE

As shown before, the isotope effects associated with O_3 formation have been studied in great detail, while the available data on the contribution of O_3 photolysis to the isotope anomaly in O_3 is sparse. One reason for the limited data availability is that laboratory

investigation of the fractionation effects in O_3 photolysis is difficult, because O_3 photolysis (R1.24) cannot easily be separated from O_3 decomposition in reaction with molecular oxygen (R1.26) or secondary O_3 formation (R1.25).

$$O_3 + h\nu \rightarrow O_2 + O \quad \text{(R1.24)}$$
$$O + O_2 + M \rightarrow O_3 + M \quad \text{(R1.25)}$$
$$O + O_3 \rightarrow 2O_2 \quad \text{(R1.26)}$$

When pure O_3 is photolysed, the O atom formed from O_3 photolysis (R1.24) undergoes reaction (R1.26) leading to destruction of another O_3 molecule. As the reaction proceeds, O_2 builds up and secondary O_3 formation gets increasingly more important (R1.25). As a consequence the observed isotopic fractionation observed in previous experiments of O_3 photolysis always represents a combination of fractionation effects in all three reactions R1.24 - R1.26.

The goal of this thesis is to investigate isotope effects in visible light O_3 photolysis and to provide answers to the following questions:

(i) What is the oxygen isotope fractionation associated with photolysis of O_3 in the Chappuis band? What is the isotope fractionation associated with removal of O_3 via reaction with O atoms? (Chapter 2)

(ii) What is the wavelength dependence of fractionation effects in visible light photolysis of O_3? (Chapter 3)

(iii) What is the fractionation effect arising from the O_3 formation reaction only, when separated from effects in O_3 photolysis and the O_3 decomposition $O + O_3$? What is the temperature dependence of fractionation effects in O_3 formation? What is the effect of photolysis fractionations on the calculation of the isotope specific relative rate coefficients for O_3 formation? (Chapter 4)

Chapter 2 presents key experimental results of isotope effects observed during pure O_3 photolysis and O_3 photolysis in the presence of different bath gases (He, Ar, CO). The principle idea was to add a large excess of CO as an O atom quencher to the reaction system in order to suppress the O_3 destruction reaction via $O + O_3$ as well as secondary O_3 formation. For this purpose, pure O_3 samples as well as O_3 in the different bath gases were irradiated with a broadband light source with an emission peak in the visible wavelength region (peak at 605 nm) for different time periods. Supported by kinetic modeling we were able to separately quantify the isotope effects in visible light O_3 photolysis and the $O + O_3$ reaction, which is of major interest for the interpretation of atmospheric measurements as well as model calculations.

In chapter 3, these measurements were extended to study the wavelength dependence of the isotope fraction in visible light O_3 photolysis. To reach this goal, different light sources (LEDs and a broad band light source with different optical filters) were applied for photolysis of pure O_3. Since the fractionation in $O + O_3$ was quantified in the previous investigation, the fractionation in O_3 photolysis for different photolysis wavelengths could be derived.

In chapter 4, we combine fractionation effects in O_3 formation and visible light photolysis in photolytic recycling experiments. With the experimental setup it is possible to quantify the temperature and pressure dependence of the isotope effects during photolytic recycling of O_3 in O_2 bath gas with very high precision.

Finally chapter 5 summarizes the main findings of this thesis and gives an outlook for further research in order to advance the understanding of the mass-independent isotope effect in atmospheric O_3.

2

EXPERIMENTAL STUDY ON ISOTOPE FRACTIONATION EFFECTS IN VISIBLE LIGHT PHOTOLYSIS OF O_3 AND IN THE $O+O_3$ ODD OXYGEN SINK REACTION

Abstract

Investigation of isotope effects in ozone (O_3) photolysis and its contribution to the overall ozone isotope composition is difficult since photolysis always leads to secondary O_3 formation and O_3 decomposition by reactions with $O(^3P)$. Here we use a large excess of carbon monoxide (CO) as $O(^3P)$ quencher to suppress $O(^3P) + O_3$. This allows disentangling the isotope effects in photolysis and chemical removal when the data are evaluated with a kinetic model. The largest systematic uncertainty arises from an unidentified O_3 removal reaction, which is responsible for an unaccounted-for 20% of the total removal rate. Assuming no isotope fractionation in this reaction we find ${}^{18}\varepsilon_{O_3+h\nu} = ({}^{18}J/{}^{16}J - 1) = -16.1$ (±1.4)‰ and ${}^{17}\varepsilon_{O_3+h\nu} = -8.05$ (±0.7)‰ for O_3 photolysis and ${}^{18}\varepsilon_{O+O_3} = ({}^{18}k/{}^{16}k - 1) = -11.9$ (±1.4)‰ and ${}^{17}\varepsilon_{O+O_3} = -5.95$ (±0.7)‰ for chemical removal via $O(^3P) + O_3$. Allowing for isotope fractionation in the unidentified reaction results in lower fractionation values for photolysis and higher fractionations for chemical removal. Several fractionation scenarios are examined, which constrain the fractionation in photolysis to ${}^{18}\varepsilon_{O_3+h\nu} > -9.4$‰ and ${}^{17}\varepsilon_{O_3+h\nu} > -4.7$‰ and in the chemical removal to ${}^{18}\varepsilon_{O+O_3} < -18.6$‰ and ${}^{17}\varepsilon_{O+O_3} < -9.3$‰. Both fractionations are thus significant and of similar magnitude. Because our measurements are dominated by photolysis in the peak region of the Chappuis band, isotope fractionation of atmospheric O_3 by visible photons should also be in the same range. The isotope fractionation factor for $O + O_3$ directly bears on ozone chemistry in the lower thermosphere.

This chapter has been published as:
Früchtl, M., C. Janssen, and T. Röckmann (2015), Experimental study on isotope fractionation effects in visible photolysis of O_3 and in the $O + O_3$ odd oxygen sink reaction, J. Geophys. Res. Atmos., 120, pp. 1-19, doi:10.1002/2014JD022944.

2.1 INTRODUCTION

Ozone (O_3) is of great importance for atmospheric chemistry. It is a strong oxidant that contributes significantly to the removal of many carbon-, nitrogen- and sulfur-containing species in the atmosphere. It is also the precursor of the hydroxyl (OH) radical, which is the principal "cleansing agent" of the atmosphere. Via these two pathways, O_3 determines to a large degree the oxidative capacity of the atmosphere and its ability to absorb harmful UV radiation makes it indispensable to protect life on Earth from radiation emitted from the Sun [*Jacob*, 1999].

In addition, O_3 carries a very peculiar isotopic composition, which can serve as a sensitive marker for chemical reactions involving O_3. Compared to other oxygen containing trace gases O_3 exhibits very large enrichments in the heavy isotopes of oxygen (^{17}O and ^{18}O) with respect to the oxygen from which it is formed. Isotope enrichments or depletions are reported in the traditional δ notation where $\delta^{18}O = (N(^{18}O)/N(^{16}O))_{SA}/(N(^{18}O)/N(^{16}O))_{ST} - 1$ quantifies the relative deviation of the ratio $N(^{18}O)/N(^{16}O)$ of isotope abundances (indicated by the symbol N) in a sample (SA) from the same ratio in an international standard material (ST). Since deviations are small, δ is usually given in per mill (‰). Contrary to the classical theories of mass-dependent isotope effects, the relative enrichments of ^{17}O and ^{18}O show a clear offset from the mass-dependent fractionation line. This offset is termed "mass-independent" or "non-mass-dependent" fractionation and is quantified in linear form as $\Delta^{17}O \approx \delta^{17}O - 0.52 \times \delta^{18}O$ [*Brenninkmeijer et al.,* 2003].

First evidence for an anomalous isotopic composition of O_3 came from stratospheric balloon measurements, which revealed unexpectedly strong ^{18}O enrichments [*Mauersberger*, 1981]. In the laboratory *Heidenreich and Thiemens* [1983] produced O_3 by an electric discharge, and found that the magnitude of the enrichment was similar for ^{17}O and ^{18}O. These findings triggered many laboratory and atmospheric studies and the ozone system and its isotope anomaly were investigated thoroughly [*Morton et al.,* 1990; *Mauersberger et al.,* 1993, 1999, 2001; *Anderson et al.,* 1997; *Janssen et al.,* 1999, 2001, 2003; *Johnson et al.,* 2000; *Chakraborty and Bhattacharya*, 2003; *Haverd et al*., 2005; *Krankowsky et al.*, 2007].

It has soon been established that the process of O_3 formation via the three body reaction $O(^3P) + O_2 + M$ is the driving factor behind the observed anomalies [*Morton et al.*, 1990]. Detailed information is available on the dependence of the isotopic fractionation on temperature and pressure of the gas in which O_3 is formed. At pressures above 130 hPa, the enrichment of $^{49}O_3$ (a combination of $^{16}O^{16}O^{17}O$ and $^{16}O^{17}O^{16}O$) and $^{50}O_3$ ($^{16}O^{16}O^{18}O$ and $^{16}O^{18}O^{16}O$) decreases and almost disappears at pressures near 20 atm. Furthermore, isotope enrichments decrease with decreasing temperatures. At 300 K the enrichment of $^{50}O_3$ is higher compared to $^{49}O_3$, but below 200 K the enrichments undergo a cross over [*Morton et al.*, 1990]. The systematic variation of the enrichment for certain isotopomers suggests that molecular symmetry effects might play an important role in the isotope effect found in the

O_3 formation reaction [*Mauersberger et al.*, 1993; *Anderson et al.*, 1997; *Gao and Marcus*, 2001].

A major breakthrough in the understanding of the O_3 isotope effect came with detailed studies of individual isotope specific rate coefficients. It was shown that collisions between light atoms (^{16}O) and heavy molecules ($^{17}O^{17}O$ and $^{18}O^{18}O$) have a rate coefficient advantage of about 25 and 50% relative to the formation reaction involving ^{16}O and $^{16}O^{16}O$ [*Anderson et al.*, 1997; *Mauersberger et al.*, 1999]. O_3 formation from heavy atoms and light molecules, on the other hand, is relatively slow.

Experimental results on the relative temperature dependence of individual rate coefficients showed no temperature dependence for O_3 formation channels with high relative rate coefficients (e.g. $^{16}O + {}^{18}O^{18}O$), while the rate coefficients for slow formation channels such as $^{18}O + {}^{16}O^{16}O$ decreased with decreasing temperatures [*Janssen et al.*, 2003]. In subsequent studies, rate coefficients for many possible isotopic combinations of reactants O and O_2 were measured [*Anderson et al.*, 1997; *Janssen et al.*, 1999, 2001].

A number of attempts have been made to unravel the molecular processes behind the isotopic anomaly in O_3. The mass-independent isotope enrichment observed in the laboratory could be reproduced well in the framework of RRKM (Rice-Ramsperger-Kassel-Marcus) theory when an empirical non-statistical factor η (non-RRKM effect) was applied to describe the difference in the density of active metastable states (O_3*) in symmetric and non-symmetric O_3 molecules. Differences in zero point energies of the two transition states in O_3 formation were identified as the dominant factor controlling the lifetime of the O_3* and therefore causing the differences in the relative rate coefficients [*Gao and Marcus*, 2002]. Quantum mechanical calculations showed a strong non-statistical feature of the lifetime of the metastable O_3*. The number of ozone metastable states decays through three different $O_2 + O$ channels. Many metastable states occur at energies below the zero point energy (ZPE) thresholds, while only few occurred above it. The low-lying metastable states could be stabilized faster since they have a longer lifetime. The differences in the lifetime spectrum result from differences in zero point energy of the two formation channels $^{16}O + {}^{18}O^{18}O \rightarrow {}^{16}O^{18}O^{18}O$ and $^{16}O^{18}O + {}^{18}O \rightarrow {}^{16}O^{18}O^{18}O$ [*Babikov et al.*, 2003].

Comparison of laboratory results with early vertical profile measurements in the atmosphere between 22 and 40 km using mass spectrometry [*Mauersberger et al.*, 2001] as well as balloon based far infrared thermal emission solar occultation spectra [*Johnson et al.*, 2000] supported the hypothesis that the isotopic anomaly in O_3 originates from the O_3 formation reaction only. However, later stratospheric measurements demonstrated that temperature effects in O_3 formation could explain the enrichments of the heavy isotopologues $^{49}O_3$ and $^{50}O_3$, up to 27 km only. Above that altitude, the enrichments rose faster than expected from the temperature effect only [*Krankowsky et al.*, 2007]. Very large enrichments have been reported at higher altitudes based on balloon-borne remote sensing

[*Haverd et al.*, 2005]. It was suggested that a fractionation in the removal of O_3, in particular UV photolysis could have an additional effect on its isotopic composition.

Chakraborty and Bhattacharya [2003] showed in an experimental setting different fractionation patterns for ozone photolysed with UV (184.9 and 253.6 nm) or visible light (520 and 630 nm). Dissociation in the Chappuis band showed a mass-dependent character with a three-isotope slope $\delta^{17}O/\delta^{18}O$ of 0.54, whereas dissociation in the Hartley band was mass-independent (slope 0.63). However, a later modeling study by *Cole and Boering* [2006] attributed the mass-independent effect reported by *Chakraborty and Bhattacharya* to formation of new O_3 during the UV photolysis experiments.

Nevertheless, analysis of experimental absorption spectra by *Miller et al.* [2005], suggested that O_3 photolysis is associated with a wavelength-dependent fractionation with large variations in the fractionation constants over few nanometers. Photolytic modeling results attributed up to +45‰ of the O_3 anomaly in the middle stratosphere to ozone photolysis effects [*Miller et al.*, 2005]. Additionally, the vertical profiles between 15 and 40 km altitude of *Haverd et al.* [2005] showed fractionations for $^{16}O^{16}O^{18}O$ and $^{16}O^{18}O^{16}O$ that were in good agreement with already published data of 13.5 ± 2.7% and 7.7 ± 2.2% respectively for an average of 20-35 km. However, the fractionations showed a clear increase with altitude of 3.5 ± 2.2% and 4.0 ±1.6% for $^{16}O^{16}O^{18}O$ and $^{16}O^{18}O^{16}O$ over the 20-35 km range, and therefore deviated from those expected from temperature effects only. Also a modeling study by *Liang et al.* [2006] in which the altitude variation of heavy O_3 is combined with the known formation–induced isotope effects, enrichments were systematically 1 to 1.5% higher than the observations.

Investigation of the role of O_3 photolysis and its contribution to the O_3 isotope effect is difficult [*Brenninkmeijer et al.*, 2003], because photolysis inevitably leads to the following reactions:

$$O_3 + h\nu \rightarrow O(^3P) + O_2 \quad \text{(R2.1)}$$
$$O(^3P) + O_2 + M \rightarrow O_3 + M \quad \text{(R2.2)}$$
$$O(^3P) + O_3 \rightarrow 2O_2 \quad \text{(R2.3)}$$

This implies that the photolysis reaction (R2.1) cannot easily be separated from secondary O_3 formation (R2.2) or the O_3 decomposition in reaction with $O(^3P)$ (R2.3). In particular in laboratory photolysis experiments with pure O_3 samples, (R2.1) will always occur simultaneously with reaction (R2.3), so that the observed fractionation is the average of these two removal channels. In addition, when O_2 builds up in the reactor as the experiment proceeds, (R2.2) will become progressively more important.

In this study we attempt to disentangle the isotope effects in the different reactions by using carbon monoxide (CO) as $O(^3P)$ quencher:

$$O(^3P) + CO + M \rightarrow CO_2 + M \qquad (R2.4)$$

When using a large excess of CO, it is possible to strongly suppress reactions (R2.2) and (R2.3). To exclude isotope effects related to excited electronic states of oxygen we investigate the fractionation effect in visible photolysis (455 – 800 nm) of O_3. Results are interpreted using a kinetic model.

2.2 METHODS

2.2.1 *System description*

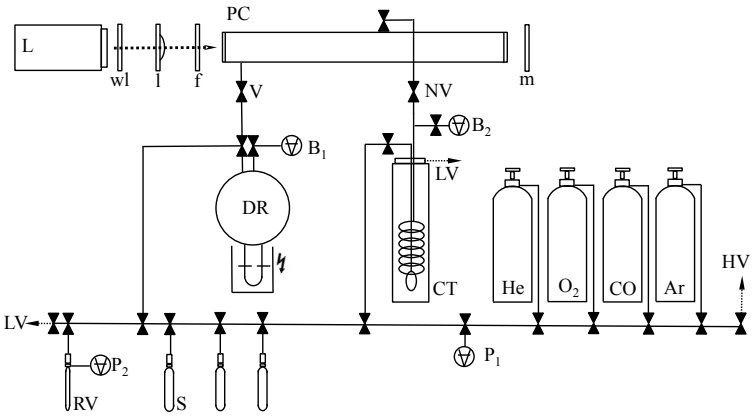

Figure 2.1. Gas handling and O_3 photolysis system. Definition of abbreviations: Discharge reactor (DR), photolytic chamber (PC), lamp (L), water lens (wl), lens (l), filter (f), mirror (m), cryogenic trap (CT), sample bottle (S), reference volume (RV), low vacuum membrane pump (LV), high vacuum pump (HV), valve (V), needle valve (NV), P_1 P_2 (pressure sensors), B_1 B_2 (Baratron pressure sensors).

The gas handling and O_3 photolysis system is mostly made out of Pyrex glass (Figure 2.1). Valves are either glass with Teflon O-rings (Glass Expansion, Australia) or Teflon only valves (Young, England). Metal parts are avoided wherever possible and remaining metal surfaces, which connect to pressure sensors (Baratron, MKS, range 10 and 100 Torr: Scientific Solutions Ltd., Institute of Geological & Nuclear Sciences Limited), the high vacuum turbo pump (HighCube, Pfeiffer, 1500Hz), the low vacuum membrane pump with end pressure of 10^{-3} hPa (KNF Neuberger) and the gas supplies can be separated from the system with additional Teflon-sealed valves. The material of the gas lines is stainless steel for He, Ar and O_2. CO is injected through a copper line. The base vacuum achieved by the system is ~ 10^{-6} hPa (measured at the pump).

The setup for the photolysis experiments consists of three major parts. A ~1.0 L discharge reactor where O_3 is created from electric discharge in pure oxygen; a photolysis chamber in which O_3 is photolysed and a cold trap which serves to collect O_3.

The spherical 12 cm diameter discharge reactor (Schott Duran®) has a 12.5 cm long and 3 cm wide cylindrical extension, which can be immersed in liquid nitrogen. It contains two electrodes that are attached to a 1500 V AC power supply. Two glass coated tungsten wires enter the reactor finger from two opposite sides and are installed at a distance of 1 cm inside the reactor volume. For fast O_3 production, the electrodes can be fully immersed in liquid nitrogen. O_3 is removed from the gas phase by condensation on the reactor walls. At the upper part two valves separate the discharge reactor from the glass line and the photolysis chamber. Additionally, in order to determine the pressure, a high accuracy pressure sensor is attached at the top of the reactor.

The cylindrical photolysis chamber (V = 630 cm^3, l = 50 cm and d = 4 cm) is placed horizontally behind the discharge reactor. The reactor walls are made out of silica glass. The quartz glass (Suprasil) windows are highly transparent from the UV to the IR wavelength region and glued to both ends of the reactor using epoxy glue (Scotch-Weld^{TM}, DP 100, 3M). The reactor is externally shielded with aluminum foil. The gas inlet of the photolysis chamber is directly connected to the discharge reactor. The gas outlet is connected to the O_3 collection trap. For precise gas handling, a Teflon needle valve is placed between these two components.

At a distance of 22 cm from the photolysis chamber, a halogen photo optic Xenophot® lamp (U = 15.9 V, I = 10.58 A, type HLX 64633) equipped with an elliptic mirror is used as light source. The spectral distribution of the lamp has been calibrated using a spectral photometer. The lamp shows a broad emission peak centered at 605 nm. However, it also emits some UV radiation, which contributes significantly to O_3 photolysis due to the high absorption cross section of O_3 in the Hartley band (Figure 2.2).We prevent UV photolysis by placing an optical filter cutting off radiation with wavelengths shorter than 455 nm directly in front of the photolysis chamber.

In order to filter out IR radiation and therefore to reduce temperature effects, a 77 cm^3 water lens that is constantly flushed with distilled water, is installed between the lamp and the photolysis chamber. An aspherical condenser lens with effective focal length of 18 mm (Edmund Optics) and a diameter of 5 cm is placed at a distance of 16 cm from the lamp to focus the light into a parallel beam. A flat surface mirror with enhanced aluminum coating (reflection >95%) is added at the end of the photolysis chamber in order to back reflect photons into the chamber and thus to increase the photolysis rate.

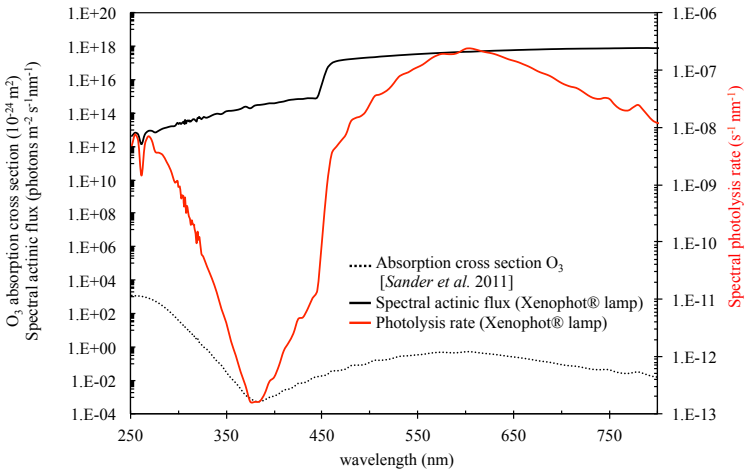

Figure 2.2. Measured spectral actinic flux spectrum of halogen photo optic Xenophot® lamp (U=15.9 V, I = 10.58 A, type HLX 64633) including band pass filter cutting off radiation at wavelength < 455 nm (solid black line) and ozone absorption cross section (dashed black line). Spectral photolysis rate (red line) is calculated (assuming quantum yield = 1) and shows a maximum at 605 nm.

After photolysis, the remaining ozone is collected in a cryogenic trap, which is connected to a vacuum pump and cooled to 63 K by pumping on the vapor when placed in liquid nitrogen. The O_3 trap contains two additional valves, which are used to separate the trap from the rest of the glass line.

For isotopic analysis, O_3 or O_2 is collected in a 44.2 cm^3 sample bottle containing approximately ten pellets of molecular sieve (13X 1.6 mm pellets, Sigma Aldrich) dipped in liquid nitrogen.

The 1.8 cm^3 reference volume used to quantify the amount of gas after an experiment has a pressure sensor attached and contains either molecular sieve (13X 1.6 mm pellets, Sigma Aldrich) or high purity nickel (Ni) foil (annealed, thickness 0.05 mm, 99.98% purity, Goodfellow, Cambridge Ltd.). Isotopic ratios are measured using a Delta^{Plus}XL (Thermo Finnigan) mass spectrometer. Typical internal uncertainties are 0.03‰ in $\delta^{18}O$ and 0.08‰ in $\delta^{17}O$ (standard deviation of 10 sequences, 15 runs each, n = 150).

For the experiments we use helium (He) of 99.9997% purity (Air products) and ultra pure plus oxygen (O_2) of 99.9998% purity (Air products) with isotopic composition of $\delta^{17}O$ = 9.5 (±0.03)‰ and $\delta^{18}O$ = 18.9 (±0.05)‰ versus V-SMOW. The CO used has a purity of 99.997% (Linde) and its isotopic composition is $\delta^{13}C$ = −54.4 (±0.2)‰ versus V-PDB and $\delta^{18}O$ = −6.0 (±0.3)‰ versus V-SMOW.

2.2.2 *Experimental procedure*

Three sets of experiments were carried out to investigate the role of O_3 dissociation processes, in particular photolysis and the $O + O_3$ reaction, in detail. In set 1, only O_3 was photolysed for different time periods (named O_3 *only*). In sets 2 and 3, O_3 was either mixed with He (O_3 + He), Ar (O_3 + Ar) or CO (O_3 + CO) bath gas before photolysis of the mixture. To test the efficiency of the extraction system and the stability of O_3 in the analytical system, runs without photolysis were carried out for the above 3 sets of experiments (i.e., the same procedure was applied, but without turning on the photolysis lamp).

For each set of experiments, O_3 was generated from 8.5 hPa pure O_2 in the discharge reactor. After filling the reactor with O_2 the cylindrical extension, including the electrodes, was immersed in liquid nitrogen. The electric discharge was turned on for about one minute during which liquid O_3 condenses on the reactor walls. After the discharge was switched off at ~ 6 hPa, the remaining O_2 was pumped away until a residual pressure of 5 Pa was reached. Thereafter the liquid nitrogen was removed and the condensed O_3 was brought to the gas phase at room temperature. After complete evaporation of O_3, different bath gases, depending on the experiment, were admitted to the discharge reactor. Gases were mixed in ratios of ~ 1: 900 (O_3 : bath gas).

The gas mixture was transferred into the photolysis chamber by opening and closing the valve between discharge reactor and photolysis chamber. In the following we call this step *expansion*. In order to assure complete mixing in the discharge reactor and its connections to the valves, a first fraction of the gas mixture was expanded into the photolysis chamber for conditioning it and then pumped away. Only the second and third expansions into the photolysis chamber were used for experiments. Standing times of the gas mixture in the discharge reactor varied between 45 minutes (2^{nd} expansion) and 4 hours (3^{rd} expansion), depending on the type of experiment. Evacuation times for experiments with CO were longer than those with He or O_3 *only*.

Irradiation times were varied between 5 and 30 minutes. For comparison of O_3 before and after photolysis, the second expansion was used for photolysis while the third expansion was sampled without photolysis in order to determine the isotopic composition of the starting O_3. This was necessary since the isotopic composition of O_3 generated by electric discharge showed small differences of 1 and 2‰ in $\delta^{17}O$ and $\delta^{18}O$ respectively, depending on small variations in discharge time.

After photolysis, the remaining O_3 was collected in the cryogenic trap at 63 K. When all O_3 was collected, the trap was isolated and the liquid nitrogen was removed. O_3 was brought to room temperature by warming the trap with a small beaker filled with room temperature water.

O_3 was then transferred to a sample bottle cooled to liquid nitrogen temperature and containing approximately ten pellets of molecular sieve. Additional heating of the sample

led to complete conversion of the O_3 sample into O_2. The O_2 was then cryogenically transferred to the reference volume using molecular sieve at liquid nitrogen temperatures. To determine the amount of molecular oxygen, the liquid nitrogen was removed and the sample bottle was warmed with room temperature water and the pressure was taken. Thereafter, the sample was frozen back at liquid nitrogen temperature on molecular sieve in the original sample bottle. As mentioned above, immediately after recovering the O_3 from the photolysis experiment, another aliquot was expanded from the discharge reactor into the photolysis reactor in order to determine the amount and isotopic composition of the starting O_3. CO_2 produced from the O + CO reaction or potentially other sources remained in the molecular sieve and therefore could not interfere with the O_2 isotopic analysis.

An additional set of experiments was performed in order to evaluate the trapping and purification procedure. In these experiments, O_3 as well as CO_2 from reaction (R2.4) were directly transferred to the reference volume using liquid nitrogen. After warming the reference volume, which contained small strips of Ni-foil, in a water bath at room temperature, the $O_3 + CO_2$ pressure was measured. Subsequent heating for three minutes at 80 °C led to catalytic conversion of O_3 to O_2. Thereafter, the reference volume was brought to room temperature again and the $O_2 + CO_2$ pressure was recorded. In a last step, the reference volume was immersed in liquid nitrogen to trap CO_2 while the molecular oxygen was transferred to a sample bottle filled with molecular sieve and held at liquid nitrogen temperature. After the CO_2 pressure was determined by warming up the reference volume, the sample was cryogenically transferred to a sample bottle. Since 1.5 moles of O_2 are formed from decomposition of one mole of O_3, the O_3 pressure in the reference volume was calculated from the two pressure measurements ($O_3 + CO_2$ and $O_2 + CO_2$) according to

$$p_{O_3} = 2 \times \left[p_{(O_2+CO_2)} - p_{(O_3+CO_2)} \right] \tag{2.1}$$

The sample bottle containing pure O_2 derived from O_3 was then attached to the sample inlet of the Dual inlet IRMS and measured relative to our O_2 laboratory standard.

In the following we refer to the O_3 sample measured after photolytic destruction as O_3*(end)*. The extraction from the expansion carried out directly after the photolysis experiment and without irradiation of the gas mixture is representative for the original O_3 produced in the electric discharge and is referred to as O_3(*start*). The ratio O_3(end)/O_3(start) (corrected for an additional volume expansion of O_3(start)) defines the remaining fraction $f(O_3)$, which quantifies the O_3 conversion for a certain photolysis period:

$$f(O_3) = O_3(end) / O_3(start) \tag{2.2}$$

2.3 MODEL DETAILS

2.3.1 *Reaction scheme*

The reaction kinetics of the gas mixture exposed to visible light only (by using a 455 nm band pass filter) was simulated using the chemical kinetics software Kintecus® [*Ianni*, 2003]. Three sets of model runs were employed to simulate the three sets of experiments: (a) O_3 *only* photolysis, (b) photolysis in the presence of He or Ar and (c) photolysis in the presence of CO. The model allows to quantitatively interpreting the experiments, because the different reaction pathways of O atoms in the different experiments can be quantified.

Four chemical reactions (R2.1-R2.4) and two isotope exchange reactions (R2.5a,b – R6) were included in our photochemical model.

$$O_3 + h\nu \rightarrow O(^3P) + O_2, \qquad J_{O_3} = 3.4 \times 10^{-4}\ s^{-1} \qquad \text{(R2.1)}$$

$$O(^3P) + O_2 + M \rightarrow O_3 + M, \qquad k_2 = 6.0 \times 10^{-34}\ (300\ K/T)^{-2.4}\ cm^6\ s^{-1} \qquad \text{(R2.2)}$$

$$O(^3P) + O_3 \rightarrow O_2 + O_2, \qquad k_3 = 8.0 \times 10^{-12} \exp(-2060\ K/T)\ cm^3 s^{-1} \qquad \text{(R2.3)}$$

$$O(^3P) + CO + M \rightarrow CO_2 + M, \qquad k_4 = 2.56 \times 10^{-36}\ cm^6 s^{-1}\ (T = 306K, p = 613\ hPa) \qquad \text{(R2.4)}$$

$$Q + OO \leftrightarrow QO + O, \qquad k_{5a} = 3.4 \times 10^{-12}(300\ K/T)^{1.1}\ cm^3 s^{-1} \qquad \text{(R2.5a)}$$

$$O + QQ \leftrightarrow OQ + Q, \qquad k_{5b} = 2.7 \times 10^{-12}(300\ K/T)^{0.9}\ cm^3 s^{-1} \qquad \text{(R2.5b)}$$

$$O + CO \leftrightarrow CO + O, \qquad k_6 = 1.65 \times 10^{-11} \exp(-2730K/T)\ cm^3\ s^{-1} \qquad \text{(R2.6)}$$

The rate coefficient applied for O_3 photolysis (R2.1) was determined experimentally as explained in detail in section 2.4.1. Rate coefficient values (R2.2, R2.3) are given based on recent recommendations [*Sander et al.*, 2011]. Values for k_{5a} and k_{5b} are adopted as given in *Fleurat-Lessard et al.* [2003]. For isotopic exchange of O and CO, rate coefficient k_6 is based on *Jaffe and Klein* [1966]. The value of k_4 is derived from studies by *Slanger et al.* [1972], *Simonaitis and Heicklen* [1972] and *DeMore* [1972] in section 2.3.3, where the bath gas dependence of k_2 is also discussed.

Most important for the interpretation of the results is the fate of the O atoms produced in (R2.1). They can either react with another O_3 molecule (R2.3), be quenched away by CO (R2.4) or form new O_3 (R2.2), with relative importance of these pathways depending on experimental conditions.

The model results shown in Figure 2.3 confirm that during photolysis of pure O_3 with visible light, virtually all of the O atoms produced within the first 30 minutes destroy another O_3 molecule via (R2.3) ($O + O_3$). Formation of new O_3 becomes significant only after 30 minutes. In sharp contrast, the presence of He bath gas strongly increases the formation process and both pathways ($O + O_3$ and O_3 formation via $O + O_2 + M$) contribute approximately equally after 25-30 min. When CO is used as bath gas, the reaction O + CO quenches away about 75-80% of the O atoms and the reaction $O + O_3$ is strongly

suppressed, which was intended by this study. Nevertheless, even at a mixing ratio of 1:900 (O_3/CO), $O + O_3$ still consumes about 25% of the O atoms at the start. O_3 formation is actually increased compared to the O_3 *only* case, because CO also serves as a third body reaction partner (M) in (R2.2), thus increasing the rate of ozone formation.

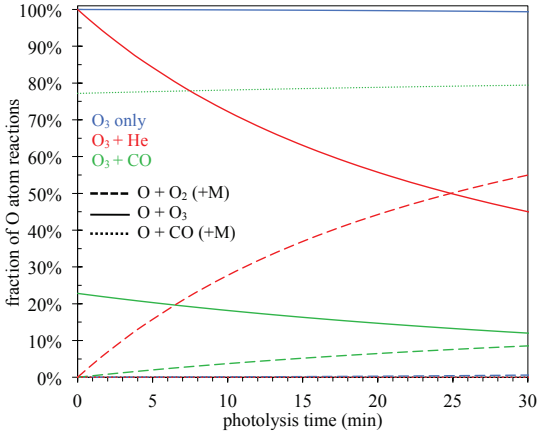

Figure 2.3. Fractions of O atoms lost via the three different reaction channels in percent. Long-dashed lines: $O + O_2$ (+M). Solid lines: $O + O_3$. Short-dashed lines: O + CO (+M). The three types of experiments are shown in different colors. Blue: O_3 *only*; red: O_3 in He bath gas; green: O_3 in CO bath gas.

2.3.2 *Isotopes*

Isotopic enrichments are calculated from modeled molecular abundances. The model explicitly calculates all possible isotopic combinations of all the above 6 reactions using the following labeling P = ^{17}O, Q = ^{18}O and O = ^{16}O. It also includes known or assumed isotope effects for the variants of reactions R2.1-R2.6. This increases the number of reactions to 159 (Table 2.1).

Table 2.1: List of main reactions in kinetic model[a]

Reaction	Number of variants	Reaction type
R2.1	27	$O_3 + h\nu \rightarrow O + O_2$
R2.2	27	$O + O_2 + M \rightarrow O_3 + M$
R2.3	72	$O + O_3 \rightarrow O_2 + O_2$
R2.4	9	$O + CO + M \rightarrow CO_2 + M$
R2.5a,b	18	$Q + OO \leftrightarrow QO + O$
R2.6	6	$Q + CO \leftrightarrow CQ + O$
(R2.7)	(81)	$(O_3 + CO \leftrightarrow CO_2 + O_2)$

[a] included are reactions with multiple substitutions. Number of variants for R2.2 increase to 270 under consideration of O_3 = M.

The model input for initial concentrations of O_3 ($^{16}O_3$) and bath gases corresponds to the experimental conditions. Initial O_3 number densities are 2.87×10^{16}, 1.52×10^{16}, 1.61×10^{16} and 1.67×10^{16} cm^{-3} for the O_3 *only*, the He, Ar and the CO experiments, respectively. Bath gas number densities are 1.34×10^{19} (547 hPa; $He/O_3 = 886.5$), 1.49×10^{19} (607 hPa; $Ar/O_3 = 925.3$), and 1.45×10^{19} cm^{-3} (591 hPa; $CO/O_3 = 868.5$) for the He, Ar and CO runs. All initial concentrations represent an average of the photolysis experiments of each data set.

For illustration purposes, we derive in the following the number density of asymmetric (OOQ) and symmetric (OQO) $^{50}O_3$, assuming a statistical distribution of isotopes. The molecule specific abundance is calculated from the atomic abundance ratio, $^{18}R_{O_3} = (N(Q) / (O))_{O_3}$ where N(O) and N(Q) stand for the absolute number of receptive O and Q atoms of ozone in a given volume, and one obtains

$$\frac{[OOQ]}{[OOO]} = 2\times(^{18}R_{O_3}) \qquad \frac{[OQO]}{[OOO]} = {}^{18}R_{O_3}. \tag{2.3}$$

Therefore the initial number density of OOQ is calculated as follows:

$$[OOQ]_{initial} = [OOO]_{initial} \times 2(^{18}R_{O_3}), \tag{2.4}$$

and initial [OQO] is correspondingly given by

$$[OQO]_{initial} = [OOO]_{initial} \times {}^{18}R_{O_3}. \tag{2.5}$$

Isotope specific enrichments are calculated from modeled molecular abundances. The definition of $\delta^{18}O$ is based on the atomic abundance ratio

$$\delta^{18}O = \frac{\left(\frac{N(^{18}O)}{N(^{16}O)}\right)_{SA}}{\left(\frac{N(^{18}O)}{N(^{16}O)}\right)_{ST}} - 1 \tag{2.6}$$

in the sample (SA) and the standard (ST), implying that all relevant species containing a heavy oxygen need to be summed up and divided by the number of species containing a light oxygen (^{16}O). For O_2 we obtain:

$${}^{18}R_{O_2} = \frac{2[Q_2] + [OQ] + [QP]}{2[O_2] + [OQ] + [OP]}. \tag{2.7}$$

Calculation of ${}^{18}R_{O_3}$ involves 18 species, if the intra-molecular isotope distribution is taken into account. This leads to

(2.8)

$$ {}^{18}R_{O_3} = \frac{[OOQ]+[OQO]+2[OQ_2]+2[QOQ]+[POQ]+[OPQ]+[OQP]+2[PQ_2]+2[QPQ]+[PPQ]+[PQP]+3[Q_3]}{3[O_3]+2[O_2Q]+2[OQO]+2[OOP]+2[OPO]+[OPP]+[POP]+[OQ_2]+[QOQ]+[POQ]+[OPQ]+[OQP]} $$

Note that similar formulas apply to the definition of $\delta^{17}O$ and to other oxygen containing molecules. For calculating ${}^{18}R_{O_3}$ our model considers all possible isotopic substitutions, while in mass spectrometric analysis, species containing two or three heavy oxygen atoms are excluded. However, model runs excluding double and triple substituted species only differ in a magnitude of 0.1‰ for ^{18}O and 0.06‰ for ^{17}O from model runs including all isotopic substitutions.

2.3.3 *Rate coefficients*

The O_3 photolysis rate coefficient has been determined experimentally (see section 2.4.1). O_3 formation rates are based on the currently recommended value for air [*Sander et al.*, 2011] using the relative third body efficiencies of 1, 0.6, 0.74, 1.06 and 2.27 for O_2, He, Ar, CO and O_3, respectively. Values for O_2, He and O_3 were taken from the recommendation of *Steinfeld et al.* [1987] while the factor used for Ar originates from a relatively recent study of *Hippler et al.* [1990]. This study has been performed at higher pressures than most of the previous work. Except for Ar, values agree very well with the older recommendation of *Steinfeld et al.* [1987] as far as the bath gas dependency is concerned. The CO efficiency is the average of two pulsed radiolysis studies performed by *Maeburn et al.* [1968] and by *Stuhl and Niki* [1971], which are the only experiments in CO that we are aware of.

The reaction coefficient for CO + O (R2.4) is not very well constrained by previous studies. After a thorough literature survey, we use low and high pressure limiting rates of $k_0 = 6.5\times10^{-33} \exp(-2184\ \mathrm{K}/T)$ $\mathrm{cm^6\ s^{-1}}$ and $k_\infty = 2.66\times10^{-14} \exp(-1460\ \mathrm{K}/T)$ $\mathrm{cm^3\ s^{-1}}$, respectively. The low pressure limiting value k_0 corresponds to the results of *Slanger et al.* [1972], which are considered to be free of contamination effects that have affected many of the earlier studies [*Baulch et al.*, 1976]. The pressure dependence of the reaction is complex and cannot simply be described using a single fall-off region and the above value of k_∞ fails to describe the high-pressure behavior [*DeMore*, 1972]. Similarly, the rate of the O + CO isotope exchange determined by *Jaffe and Klein* [1966] does not correspond to the high pressure limiting rate coefficient that would reproduce a fall-off already at about 1 atmosphere, as observed by *Simonaitis and Heicklen* [1972] and *DeMore* [1972]. Only at much higher pressures, a second fall-off consistent with the results of *Jaffe and Klein* [1966] is observed [*DeMore*, 1972]. Being concerned with pressures at and below 1 atm

only, we nevertheless adopt the value $k_\infty = 2.66\times10^{-14}\ \exp(-1460\ \mathrm{K}/T)\ \mathrm{cm^3\ s^{-1}}$ of *Simonaitis and Heicklen* [1972], which is suited to reproduce the pressure dependence in that range. The value is based on measurements at pressures of slightly above 1 atm of CO mixed with nitrous oxide (N_2O) and corresponds to a second order rate coefficient of $2.04\times10^{-16}\ \mathrm{cm^3\ s^{-1}}$ at 300 K. *DeMore* [1972] finds a similar value of $k_\infty = 1.9\times10^{-16}\ \mathrm{cm^3\ s^{-1}}$ for the pressure range below 2 atm, above which the pseudo second order rate becomes pressure dependent again. The latter value, which agrees very well with the result of *Simonaitis and Heicklen* [1972] takes into account a scaling to the actually recommended rate coefficient for the O + O_2 + M reaction using relative quenching efficiencies of 1/2.7 for $(N_2)/CO_2$, because these experiments have relied on O_3 formation in CO_2 and N_2, as a reference to determine O atom abundances.

Using the standard expression for the rate coefficient in the fall-off region [*Sander et al.*, 2011],

$$k_f([M]) = \frac{k_0}{[M]^{-1} + \frac{k_0}{k_\infty}} 0.6^{\left\{1+\left[\log_{10}\left(\frac{k_0[M]}{k_\infty}\right)\right]^2\right\}^{-1}}, \qquad (2.9)$$

the rate coefficient of (R2.4) is obtained from k_0 and k_∞. Under our conditions, at 306 K and 613 hPa of CO, we find the value of $k_4 = 3.71\times10^{-17}\ \mathrm{cm^3\ s^{-1}}$, or $k_4/[\mathrm{M}] = 2.56\times10^{-36}\ \mathrm{cm^6\ s^{-1}}$, when expressed as termolecular rate coefficient.

Rates for the isotopic exchange of O with O_2 and CO are based on available rate coefficient data [*Jaffe and Klein*, 1966; *Fleurat-Lessard et al.*, 2003] and isotope exchange equilibrium constants. For a detailed list see Appendix Table A1 and A2.

2.3.4 *Fractionation coefficients*

Fractionation coefficients for O_3 formation (R2.2) are directly adopted from *Janssen et al.* [1999] and *Mauersberger et al.* [1999] or are derived from empirical zero point energy relationship described in *Mauersberger et al.* [2002] and *Babikov et al.* [2003]. To include the pressure dependence of the O_3 formation kinetic isotope effects we apply calculations from *Wiegel et al.* [2013]. In their study the pressure dependent isotope effect is derived from the O_3 formation kinetic isotope effect at low pressure and the pressure dependence of the O_3 isotopic enrichments.

For CO_2 formation no fractionation coefficients are applied, since up to now, no values for this reaction are given in published literature. For isotopic exchange O + O_2 we use fractionation factors based on calculations by *Janssen and Tuzson* [2010]. Adopted values are 2.1563 and 2.0810 for the ^{18}O and ^{17}O isotope exchange at 306 K.

The calculation we used to determine fractionation factors for the isotopic exchange O + CO is based on the classical Urey approach [*Urey*, 1947; *Richet et al.*, 1977] and neglects nuclear spin effects in the case of ^{17}O and the fact that molecular oxygen in its ground electronic $^3\Sigma$ state is an open shell molecule, which gives rise to a fine structure beyond the coupled linear rotor - harmonic oscillator approximation. Nevertheless, the result at 300 K is reasonable close (3‰ for ^{18}O) to the results of calculations based on molecular spectroscopic data [*Fischer et al.*, 2003; *Rothman et al.*, 2013]. Since CO is a closed shell molecule, the Urey approach is directly applicable and we have obtained values of 1.1027 and 1.0530 for ^{18}O + CO and ^{17}O + CO, respectively. This is in full agreement with the tabulated results of *Richet et al.* [1977].

We derive isotopic fractionation coefficients for O_3 photolysis (R2.1) and O_3 decomposition (R2.3) by fitting the model results to the measurements. The O_3 only experiments allow deriving the combined fractionation values for O_3 photolysis and O_3 destruction via $O + O_3$.

$$\varepsilon_{O_3 only} = (\varepsilon_{O_3+h\nu} + \varepsilon_{O+O_3}) / 2 \tag{2.10}$$

By using CO as an O atom quencher, reaction $O + O_3$ is suppressed and we can separate fractionation processes in both channels, O_3 + hν and $O + O_3$. Including O_3 formation $(\varepsilon_{O_2+O+M} \times g_{O_2+O+M})$, the combination of different fractionation processes gives

$$\varepsilon_{O_3+CO} = (\varepsilon_{O_3+h\nu} \times g_{O_3+h\nu} + \varepsilon_{O+O_3} \times g_{O+O_3} + \varepsilon_{O_2+O+M} \times g_{O_2+O+M}), \tag{2.11}$$

where weights g denote the relative contributions of each channel to the overall ε_{O_3+CO}.

2.4 RESULTS

2.4.1 *Photolysis rate*

The photolysis rate is the key quantity that rules the speed of the experiment and it is determined in two independent ways. First, it is derived from the pressure increase in the reaction vessel during a typical O_3 photolysis experiment. The sum of reactions (R2.1) and (R2.3) is $2\ O_3 \rightarrow 3\ O_2$, which leads to the isothermal increase of pressure (p) during photolysis:

$$J_{O_3} = -\frac{1}{2[O_3]} \times \frac{d[O_3]}{dt} = \frac{1}{p} \times \frac{dp}{dt} \tag{2.12}$$

Note that the relative change of the O_3 number density in (2.12) has been divided by a factor of 2 (since only one half of the O_3 molecules are actually destroyed by photolysis, the other half by $O + O_3$). In practice, the observed increase in pressure during photolysis needs to be corrected for temperature effects, which were obtained from a similar experiment with pure O_2. The photolysis rate obtained in this way is $J_{O_3} = 3.2(\pm 0.1)\times 10^{-4}$ s^{-1}, which is an average of four measurements with a photolysis time of 30 minutes each.

J_{O_3} can also be determined directly from the loss of O_3 as a function of photolysis time as

$$J_{O_3} = 0.5 \ln(f) / t \tag{2.13}$$

where f is the above defined remaining O_3 fraction after t seconds of photolysis. This approach yields $J_{O_3} = 3.4\times 10^{-4}\ s^{-1}$, which is in good agreement with the result from the pressure measurements. Since the latter value is directly derived from the photolysis experiments, we use this photolysis rate in the model; the assigned uncertainty is 0.2×10^{-4} cm s^{-1}.

Some experiments that were performed at a later time showed changes in the photolysis rate due to lamp aging. The photolysis rate decreased to a value of $J_{O_3} = 2.9\times 10^{-4}$ s^{-1}. The experimental results obtained with $J_{O_3} = 2.9\times 10^{-4}$ s^{-1} have been scaled to $J_{O_3} = 3.4\times 10^{-4}$ s^{-1} by multiplying the time scale with a factor of 2.9/3.4, which allows for direct comparison with the former measurements.

2.4.2 *Measurements without photolysis and data correction*

To test the efficiency of the extraction system and the stability of O_3 during the analytical procedure, measurements without photolysis were carried out with either pure O_3 or mixtures of O_3 and the various bath gases (He, Ar, CO). The experimental procedure followed exactly the above-described procedure of the photolysis experiments, but without illuminating the reactor.

These experiments without photolysis showed a small but significant difference between the amounts of O_3 recovered between the second and third expansion, i.e. $[O_3(\text{start})] < [O_3(\text{end})]$, which implies that some O_3 was lost without photolysis (Table 2.2). This loss of 7% for O_3 *only* and 2-3% for He, Ar and CO experiments was associated with isotopic changes of 0.1-0.2‰ and 0.1-0.4‰ for $\delta^{17}O$ and $\delta^{18}O$, respectively. We correspondingly subtracted the values of the experiments without photolysis from the measured raw data of the photolysis experiments.

Table 2.2: Correction values from measurements without photolysis

	O_3	O_3 + He	O_3 + CO	O_3 + Ar
$\delta^{18}O$ (‰)	0.299	0.419	0.326	0.085
$\delta^{17}O$ (‰)	0.137	0.222	0.163	0.058
ln (f)	0.072	0.022	0.028	0.025

2.4.3 *Uncertainty estimates*

The results from the photolysis experiments ($\delta^{17}O$, $\delta^{18}O$ and ln(*f*) of O_3) and the corresponding model results are shown as a function of irradiation time in Figure 2.4a-c.

Uncertainties in $\delta^{17}O$, $\delta^{18}O$ derive from the stability of mass spectrometric measurements and the sample transfer procedure. They have been determined from repeat experiments and are between 0.1 and 0.5‰ for ^{18}O and 0.1 and 0.3‰ for ^{17}O depending on the experiment and its bath gas. The total error (σ) in $\delta^{17}O$ and $\delta^{18}O$ of the measurements includes the error arising from the correction value obtained from the experiments without photolysis and is calculated according to the standard rules of error propagation:

$$\sigma = \sqrt{(\sigma_{O_3 end})^2 + (\sigma_{O_3 start})^2 + (\sigma_{dark\,correction})^2} \tag{2.14}$$

The uncertainty in ln(*f*) has been derived from dedicated sampling runs on pure CO_2 gas, or on CO_2 admixed to various bath gases. Repeated transfers showed a > 99.5% sampling efficiency for CO_2, which allowed us to use the sampling simulations on CO_2 for establishing the uncertainty budget of the sampling procedure. A slight non-linearity in the sensor P2 (connected to the reference volume) has been found and this has been taken into account to measure the pressures of O_3(end) and O_3(start) after (p_a) and before photolysis (p_b) via the blank run. Taking small variations of temperature into account, ln(*f*) is given by

$$\ln(f) = \ln\left(\frac{p_a / T_a}{p_b / T_b}\right) = \ln\left(\frac{(1+\gamma p_1) p_1 T_b}{\alpha(1+\gamma p_2) p_2 T_a}\right), \tag{2.15}$$

where $\alpha = 0.694$ (±0.002) is an experimentally defined expansion factor which accounts for the different volumes between reactor and the aliquot for the initial O_3 (blank), $\gamma = 2.2$ (± 2.5) mPa^{-1} the non-linearity coefficient of the pressure sensor, p_1 and p_2 the pressure readings of the sample and the blank, respectively, and T_a and T_b the temperatures when the two readings were made. Pressure readings have relative standard uncertainties $u_r(p)$ of 1.8% each and the maximum temperature difference T_a-T_b was 1 K, which leads to

a relative standard uncertainty of $u_r(T_b/T_a) = 0.001$. The total uncertainty of ln(f) has been calculated from (2.14) using standard rules of uncertainty propagation from the individual components, γ, α, T and p. Uncertainties are dominated by the pressure readings and can therefore be considered statistically independent. Values depend slightly on the degree of conversion and are between 2.5 and 2.7% (1 σ).

We also have investigated the sensitivity of our derived photolysis induced fractionation values with respect to changes of reaction rates within their uncertainty limits. Generally, we assumed an uncertainty of 10%, except when rates were taken from *Sander et al.* [2011], where 1σ-uncertainty ranges are stated. It was found that uncertainties in the rate coefficient of the $O(^3P) + O_2 + M$ and the $O(^3P) + CO + M$ reactions had a small impact on the result (0.8‰ and 0.6‰, respectively), all others (R2.1, R2.3, R2.5, R2.6) changed the result by not more than 0.2‰. Altogether, the uncertainty in rate coefficients contributes 1.0 and 0.5‰ to uncertainties in $\varepsilon_{O_3+h\nu}$ of $^{50}O_3$ and $^{49}O_3$, respectively.

While the well-known symmetry dependent fractionation effects in O_3 formation are included in the kinetic model, fractionation effects in O_3 photolysis are based on assuming a statistical distribution of the heavy oxygen in O_3. In an additional sensitivity experiment, it was found that implementing different fractionation values for the symmetric and asymmetric isotopomers (e.g. $\varepsilon_{(OQO)} = 2 \times \varepsilon_{(OOQ)}$) in the model had no significant influence on the final result presented in section 2.4.

2.4.4 *O_3 photolysis: Experimental and kinetic modeling results*

As $J_{O_3} = 3.4 \times 10^{-4}\,s^{-1}$ was derived from a fit to the O_3 *only* experiments, the model reproduces ln(*f*) for these measurements very well. The isotopic composition in the O_3 *only* experiments shows an increase of $\delta^{17}O$ and $\delta^{18}O$ with time (Figures 2.4a and 2.4b). After 30 minutes, $\delta^{17}O$ reaches about 9‰ and $\delta^{18}O$ increases to 16.5‰. Also because formation of new O_3 is negligible in these experiments (Figure 2.3), the observed enrichments are caused by isotope effects in photolysis and chemical removal. The overall fractionation constant $(\varepsilon_{O_3+h\nu} + \varepsilon_{O+O_3})/2$ can be determined from a Rayleigh fractionation plot (Figure 2.5). We find mean values of −14‰ and −7‰ for ^{18}O and ^{17}O, respectively. With these values, the model reproduces the measurements for the O_3 *only* experiments very well.

In presence of He or Ar bath gas, the apparent O_3 removal rate (Figure 2.4c) decreases due to the increased importance of O_3 formation (R2.2) with He or Ar acting as a third body. Due to the large enrichments associated with the formation of this secondary O_3, δ values are higher than in the O_3 *only* experiments. As the influence of the formation reaction increases with reaction time, the isotope enrichments do not increase linearly in time anymore. In addition, the enrichments are not mass-dependent; $\delta^{17}O$ increases to 18‰ and $\delta^{18}O$ to 24‰ after 30 minutes of photolysis (Figure 2.4a and 2.4b). Similar results are

obtained for O_3 photolysis in Ar as bath gas, which results in slightly higher enrichments compared to the O_3 + He measurements. This is due to the higher quenching efficiency of Ar that increases the importance of the secondary O_3 formation pathway (Figure 2.4a and 2.4b). The good agreement between model and experiment suggests that the isotope effects in the O_3 formation reactions have been adequately assigned and that the freshly formed O_3 is responsible for the higher δ values, as expected.

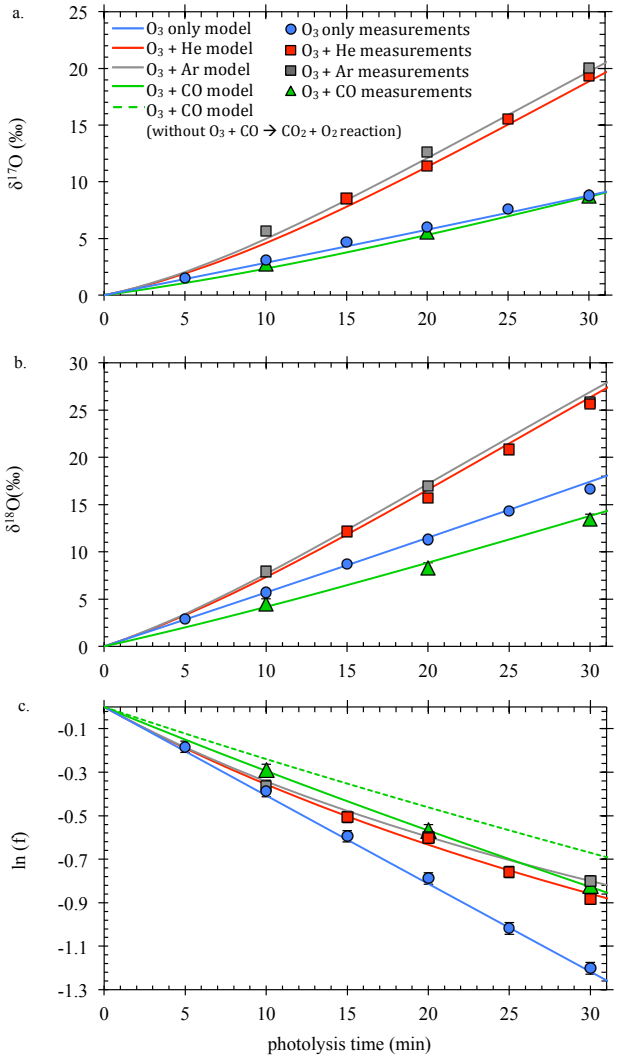

Figure 2.4. Temporal evolution of $\delta^{17}O$ (a) and $\delta^{18}O$ (b) and remaining fraction ln(f) of O_3 (c) during a photolysis experiment. Experiments in various bath gases are shown with different colors. Blue: pure O_3, red: He bath gas, grey: Ar bath gas and green: CO bath gas. Filled symbols represent measurements; solid lines model runs. Fractionations applied in the modeling are $\varepsilon_{O_3+h\nu}$ = −16.1‰ and −8.05‰ for ^{18}O and ^{17}O; for ε_{O+O_3} = −11.9‰ and −5.95‰ for ^{18}O and ^{17}O respectively. Model runs include the additional O_3 removal reaction O_3 + CO that is relevant in presence of CO. No fractionations are applied for the O_3 + CO reaction. The dashed green line represents the O_3 removal in CO bath gas, without consideration of an additional O_3 removal reaction. Error bars are 1σ.

For O_3 photolysis in CO bath gas, our model results for $f(O_3)$ differ significantly from the measurements (Figure 2.4c). The experimental data show a similar temporal evolution of $f(O_3)$ as the experiments with He or Ar as bath gas. The model, on the other hand, predicts an O_3 removal rate that is much smaller than that for O_3 + He. This is also what we expected based on the understanding of the reaction system, since O_3 destruction via O_3 + O is suppressed. When only the O_3 concentrations are evaluated, the results suggest that the O + CO reaction may be barely significant and thus much slower than assumed based on the literature values (see above). However, the isotope results in Figures 2.4a and b clearly indicate that O_3 formation is suppressed by the addition of CO. The isotopic composition attained after a certain time is much lower than that for the O_3 + He experiments; in fact it is relatively close to the O_3 *only* experiments. Also, the temporal evolution of the isotope signatures is much more linear again compared to the experiments with He and Ar, implying that the formation reaction is indeed suppressed.

The unexpected additional loss of O_3 indicates that there is a supplementary O_3 loss channel in the experiments that is not included in the kinetic model calculations. In order to reproduce the temporal evolution of $\ln(f)$ of O_3 observed in our measurements, we therefore add an additional bimolecular reaction O_3 + X to the model to account for the unidentified O_3 removal of ~20%. Since the additional decomposition of O_3 only appears in presence of CO we tentatively assign the following reaction with the value of the rate coefficient k_7 resulting from a best fit to our observations

$$O_3 + CO \rightarrow CO_2 + O_2 \qquad k_7 = 6.5\times10^{-24}\ cm^3\ s^{-1} \qquad \text{(R2.7)}$$

In addition to the rate coefficient, also the isotope effect in R2.7 influences the model results and therefore affects the data analysis. To estimate the uncertainty arising from this unknown parameter we consider three scenarios in which we assume no fractionation for ^{18}O and ^{17}O (S1), collision fractionation factors for the gas phase reaction CO + O_3 of 0.9926 and 0.9963 (S2) or fractionation factors of 0.9798 and 0.9897 based on wall collision frequencies of O_3 (S3). For further motivation and detailed description of these scenarios we refer to section 2.5.2.

2.4.5 *Fractionation in the O_3+hν and O + O_3 removal channels*

In order to quantify fractionation processes for the different channels O_3 + hν and O + O_3 we run the Kintecus model with a range of mass-dependent fractionation effects in O_3 + hν (R2.1) and O + O_3 (R2.3). The sum of both channels is kept fixed to match the results from the O_3 *only* experiments, $(^{18}\varepsilon_{O_3+h\nu} + {}^{18}\varepsilon_{O+O_3})/2 = -14‰$ and $(^{17}\varepsilon_{O_3+h\nu} + {}^{17}\varepsilon_{O+O_3})/2 = -7‰$, but the partitioning between the two channels varies. For example, one combination would be $^{18}\varepsilon_{O_3+h\nu} = -8‰$, $^{18}\varepsilon_{O+O_3} = -20‰$ and $^{17}\varepsilon_{O_3+h\nu} = -4‰$, $^{17}\varepsilon_{O+O_3} = -10‰$.

Figure 2.5a and 2.5b show the results of the model run including all reactions (R2.1-2.7). Assuming no fractionation in the unidentified reaction R2.7 (S1), fractionations in $O_3 + h\nu$ and $O + O_3$ were then adjusted in order to obtain a best fit to our experiments with CO bath gas.

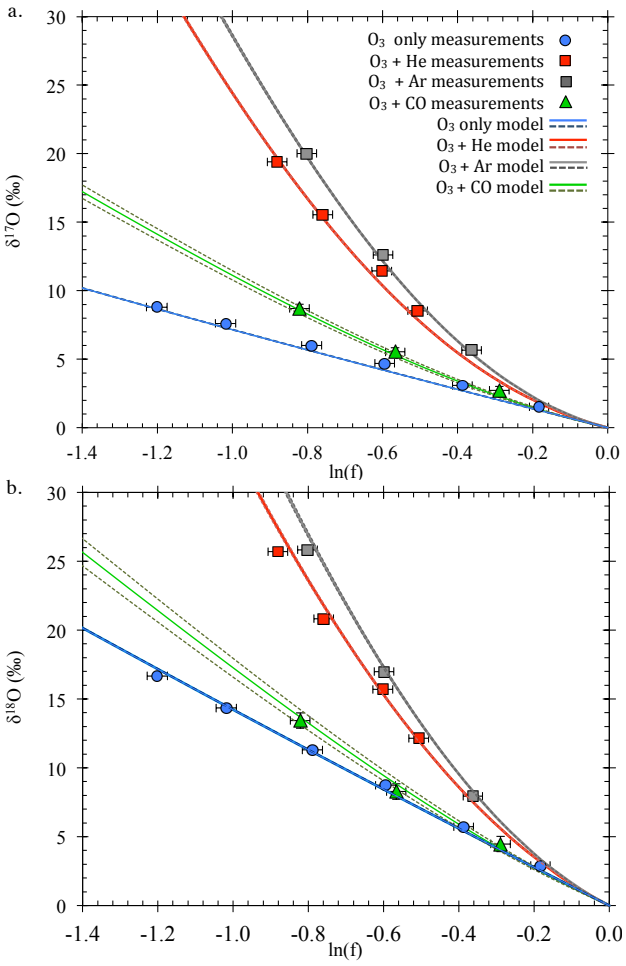

Figure 2.5. Rayleigh fractionation plots. Symbols represent measurements and lines modeled data. Red: O_3 in He, grey: O_3 in Ar, green: O_3 in CO and blue: pure O_3 experiments. Solid lines show model output with fractionation in O_3+hν of −16.1 and −8.05‰ for ^{18}O and ^{17}O respectively. Fractionations in $O + O_3$ are −11.9 and −5.95‰ for ^{18}O and ^{17}O. Dashed lines define fractionations within our experimental error of 1 σ ±1.4‰ for $^{18}\varepsilon$ and ±0.7‰ for $^{17}\varepsilon$.

Model results that agree with our experimental observations within the errors provide a range of fractionation values for the two individual channels $\varepsilon_{O_3+h\nu}$ and ε_{O+O_3}:

$^{18}\varepsilon_{O_3+h\nu} = -16.1\ (\pm 1.4)‰$, $^{17}\varepsilon_{O_3+h\nu} = -8.05\ (\pm 0.7)‰$ and

$^{18}\varepsilon_{O+O_3} = -11.9\ (\pm 1.4)‰$, $^{17}\varepsilon_{O+O_3} = -5.95\ (\pm 0.7)‰$.

Note that uncertainty values reflect measurement, fit and model errors, the latter comprising uncertainties in rate coefficients, but not differences in scenarios. Assuming strong isotope fractionations of ~20 and ~10‰ for ^{18}O and ^{17}O for R2.7 (from scenario S3), the fractionation values in O_3+hν and $O + O_3$ under our experimental conditions change to

$^{18}\varepsilon_{O_3+h\nu} = -9.4\ (\pm 1.4)‰$, $^{17}\varepsilon_{O_3+h\nu} = -4.7\ (\pm 0.7)‰$ and

$^{18}\varepsilon_{O+O_3} = -18.6\ (\pm 1.4)‰$, $^{17}\varepsilon_{O+O_3} = -9.3\ (\pm 0.7)‰$.

The best fit values for ε were obtained using total least squares regression (TLS) on the sum $\delta^{17}O + \delta^{18}O$ as a function of ln(*f*) in order to take into account uncertainties in both coordinates (δ and ln(*f*)). Taking the sum of $\delta^{17}O$ and $\delta^{18}O$ guaranteed that all measurement data were statistically independent. Monte Carlo simulations were employed to verify that our fitting procedure did not introduce a bias in the parameter estimation. Total errors in $\delta^{17}O$ and $\delta^{18}O$ of the O_3 + CO experiments are 0.3‰ and 0.5‰ respectively, leading to an uncertainty of 0.6‰ for the sum signal.

Whereas the fractionation during visible light photolysis is expected to depend on wavelength (see below) and can thus be different for different photolysis lamps, the fractionation in the $O + O_3$ reaction is independent of the light source and should be a fundamental quantity at the pressure and temperature of the experiment.

2.4.6 *Three-isotope plot*

Figure 2.6 illustrates the experimental data in a three-isotope plot. The slopes for the three distinct experiments are different. The data from the O_3 *only* experiment show a mass-dependent slope (~0.53), in good agreement with the results of *Chakraborty and Bhattacharya* [2003]. As fractionations represent averages of the fractionation constants in O_3 photolysis (R2.1) and O_3 destruction via $O + O_3$ (R2.3), we consider it extremely unlikely that the individual reactions follow non-mass-dependent fractionation manner and coincidentally sum up to produce a mass-dependent signature again. This is why the model scenarios in the O_3 + CO experiments presented above were carried out assuming a mass-dependent fractionation in both channels. Experiments in the presence of He or Ar result in clearly mass-independently fractionated O_3 (slope ~ 0.74). The model allows to clearly attributing it to the influence of O_3 formation (R2.2), because these are the only (necessary) mass-independently fractionating reactions in the model.

In our experiments with CO as bath gas, the three-isotope slope is lower than for the O_3 + He/Ar experiments (slope ~0.62). As shown in Figure 2.3, under these conditions the O_3 formation reaction (R2.2) is strongly diminished but still responsible for about 10% of the O removal in the first 30 minutes of photolysis. The fact that the model fits the

experimental results well without any other source of non-mass-dependent fractionation again shows that O_3 formation is most likely the only underlying cause of the observed departure from the mass-dependent three-isotope slope.

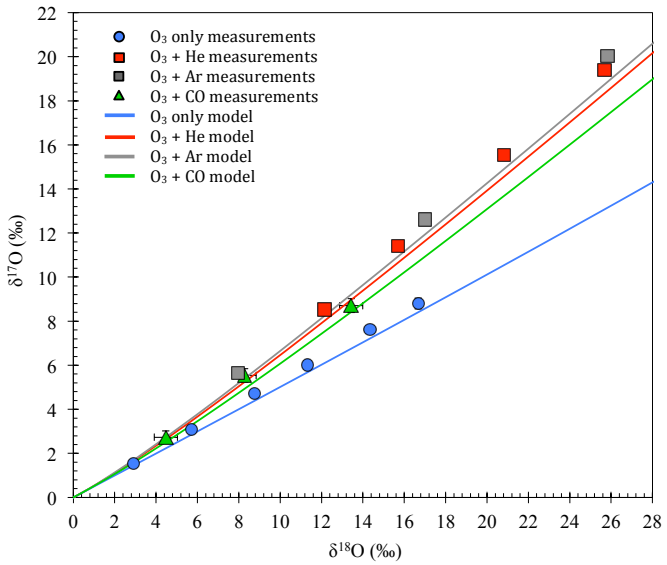

Figure 2.6. Three-isotope plot. Symbols represent measurements and solid lines model data. Blue: O_3 only, red: O_3+He, grey: O_3+Ar and green: O_3+CO. Error bars give the total error with 1σ.

2.5 DISCUSSION

2.5.1 *Additional O_3 removal in CO + O_3 gas mixtures*

The results from the kinetic model convincingly show that the experimental setup should be adequate to separately quantify fractionation factors for O_3 photolysis and O_3 destruction using the reaction of O atoms with CO as a quencher. However, we observe a clear discrepancy between experimental and model results for $f(O_3)$ in the O_3 + CO experiments.

Analysis of the raw data shows that a significant loss of O_3 occurs immediately after mixing CO and O_3. The O_3 extracted from O_3 – CO mixtures (in all expansions) is always ~20% lower than when the same amount of O_3 is extracted either without a bath gas or in He/Ar mixtures. The initial loss of O_3 is attributed to fast and possible catalytic reactions with impurities in the CO reactant. We note that several investigations of the CO + O_3 system in the literature have reported similar problems of interfering reactions [*Arin and Warneck*, 1972; *Slanger et al.*, 1972]. Adding a carbonyl trap to purify the CO had no effect on the initial loss.

Whereas an initial, fast O_3 loss is undesired, our final results should principally not be affected (as long as the loss is rapid and the gas mixture sufficiently stable afterwards) since the amount and isotopic composition of the initial O_3 is determined independently for each single photolysis experiment.

The experiments without photolysis indeed demonstrate that only a much smaller loss of O_3 (2-3%/h) occurs during the period the gas stays in the discharge reactor between the second expansion (used for photolysis) and the third expansion (used to determine O_3(start)). This is faster than what is expected from thermal decomposition ($k_{td} = 1.65\times10^{-9}$ exp(-11435 K/T) $cm^3\ s^{-1}$ [M] ~ 0.3%/h, following *Steinfeld et al.* [1987] and *Baulch et al.* [1976]), which must be excluded as viable ozone sink anyway, because no loss is observed using Ar and He as a bath gas. A possible source for this additional loss might be decomposition on the metal tips of the electrodes in the discharge reactor, to which the gas mixtures are exposed up to 4 hours during the experiment.

Data is corrected for a) the initial loss of O_3 occurring at the moment of mixing O_3 and CO and b) for the loss of O_3 occurring during the measurements without photolysis during the standing time in the discharge reactor, however an additional loss of O_3 is observed in the O_3 + CO photolysis experiments. The experimental procedure in the O_3 + CO experiments is identical to the O_3 + He/Ar experiments and numerous tests showed that gas-handling errors couldn't cause the observed discrepancy. This indicates that an additional O_3 destruction reaction, which accounts for a loss of 20%, is occurring in the experiments employing CO. In principle, such an additional O_3 removal can occur either via loss on the reactor surfaces, or via an additional gas phase reaction. An important argument against surface reactions is the fact that the additional loss is not observed for O_3 only experiments and O_3 – He, –Ar mixtures, but occurs only when CO is used as bath gas. This suggests that additional gas phase reactions may occur in the presence of CO, and one possibility is photochemical recycling of HO_x species, involving catalytic reactions such as

$$CO + OH \rightarrow CO_2 + H \qquad k_8 = 1.5\times10^{-13}\ cm^3\ s^{-1} \qquad \text{(R2.8)}$$

$$H + O_3 \rightarrow OH + O_2 \qquad k_9 = 2.9\times10^{-11}\ cm^3\ s^{-1}. \qquad \text{(R2.9)}$$

Sources of OH may come from organic contaminations in the original CO, possible outgassing from the epoxy glue upon irradiation, or reaction of excited state $O(^1D)$ radicals, generated from possibly remaining UV light that penetrates the filter, with water levels in the reactor.

Simone [2014] showed that when $O(^1D)$ radicals are produced from O_3 photolysis, catalytic radical chemistry involving HO_x radicals can strongly affect experiments in photolysis reactors. In order to exclude OH from production of $O(^1D)$ via UV photolysis, we performed an experiment where two optical filters (GG455 and GG420) were used in series. The additional loss of O_3 remained the same, and therefore catalytic reaction cycles

initiated by $O(^1D)$ can be excluded as source for the extra O_3 removal. The most likely scenario is therefore a contribution of gas phase reactions involving unknown, likely organic, contaminations.

Since we were not able to analytically identify the source reaction of the 20% loss of O_3, we included in the kinetic modeling a reaction $O_3 + X$ and assign a range of possible fractionations to this reaction, as discussed in the following section (2.5.2). Technically, we implement this reaction in the Kintecus® code as an additional reaction pathway between O_3 and CO (R2.7). Since CO levels remain virtually constant during an experiment; this results in an additional pseudo first-order reaction for removal of O_3. The implemented rate coefficient for the total reaction R2.7 is then higher than upper limits derived from earlier results [*Arin and Warneck*, 1972], but it should be noted that the largest part of this is actually due to the parameterization of the reaction $O_3 + X$.

2.5.2 *Different model scenarios for additional O_3 removal*

To account for the additional loss of O_3 observed in our experiments we add an additional O_3 removal reaction R2.7 to the kinetic model. Since the source of O_3 loss could not be identified by analytical means, different scenarios needed to be considered to account for the supplemental loss of O_3. In Table 2.3 we illustrate three scenarios (S1 – S3). Depending on the isotope fractionation in the removal process, different fractionation values for the $O_3 + h\nu$ and $O_3 + O$ reaction channels are derived.

Table 2.3: Best fit for different model scenarios (S1- S3)[a]

	$\varepsilon_{O_3+h\nu}$ (‰)		ε_{O+O_3} (‰)		α (O_3 + X)		
	^{18}O	^{17}O	^{18}O	^{17}O	^{18}O	^{17}O	Notes
S1	−16.1 ±1.4	−8.05 ±0.7	−11.9 ±1.4	−5.95 ±0.7	1	1	O_3+CO (surface), O_3+H (gas phase)
S2	−13.4 ±1.4	−6.7 ±0.7	−14.6 ±1.4	−7.3 ±0.7	.9926	.9963	O_3+CO (gas phase) incompatible with previous work
S3	−9.4 ±1.4	−4.7 ±0.7	−18.6 ±1.4	−9.3 ±0.7	.9798	.9897	collisional controlled surface loss of O_3

[a]Errors are obtained as described in section 2.4.3.

In scenario S1, we assume that O_3 is removed without isotope fractionation ($\alpha = 1$). This scenario may correspond to heterogeneous reaction of $O_3 + CO$ on the reactor wall or the metal tips of the discharge electrodes, or to the catalytic O_3 removal by H (R2.9) in the gas phase. It has to be noted that surface reactions would occur independent of photolysis,

which is not in agreement with our observations, because a correction for the loss of O_3 in experiments without photolysis is already applied to the data. The catalytic pathway may therefore be a more realistic hypothesis. Since mass difference between H and O_3 are large, isotope effects related to differences in collisional frequencies are of minor importance. With values of 0.4‰ in ^{18}O and 0.2‰ in ^{17}O they are rather small and can therefore be neglected. The scenario leads to

$^{18}\varepsilon_{O_3+h\nu} = -16.1$ (±1.4)‰ and $^{17}\varepsilon_{O_3+h\nu} = -8.05$ (±0.7)‰ for photolysis and

$^{18}\varepsilon_{O_3+O} = -11.9$ (±1.4)‰ and $^{17}\varepsilon_{O_3+O} = -5.95$ (±0.7)‰ for chemical removal,

which corresponds to the highest possible fractionation values, in the photolysis and the lowest possible fractionations in the O + O_3 reaction, as derived by the model calculations.

Scenario S2 uses a calculated isotope effect for direct reaction of O_3 with CO in the gas phase. The corresponding isotope effect is equal to the collisional fractionation factors of about 0.9926 and 0.9963 for ^{18}O and ^{17}O (S2), which are obtained from

$$\alpha_{O_3+CO} = \sqrt{\frac{(m_{O_3} + m_{CO})/(m_{O_3} \times m_{CO})}{(m_{(^{48}O_3)} + m_{CO})/(m_{(^{48}O_3)} \times m_{CO})}} \tag{2.16}$$

In order to explain the observed rate of O_3 removal, this reaction would have to proceed with a rate coefficient of $k_{O_3+CO} = 6.5\times10^{-24}$ cm^3 s^{-1} to explain the observed additional loss of O_3. Although the rate coefficient is low, literature suggests an even lower rate coefficient with an upper limit of $\leq 4\times10^{-25}$ cm^3 s^{-1} [*Arin and Warneck*, 1972]. Therefore this scenario must be ruled out.

In a third scenario (S3), we again consider loss of ozone at the surface, but now assuming that the removal is controlled by the wall collision frequency, leading to fractionation factors as high as α = 0.9798 and 0.9897 for ^{18}O and ^{17}O, respectively. We note again that such a process should also happen in the dark and therefore be included in the correction value obtained from the measurements without photolysis, but we consider it conceptually to determine the range of possible fractionation values. Such a fractionation in the additional removal would result in fractionation values of

$^{18}\varepsilon_{O_3+h\nu} = -9.4$ (±1.4)‰ and $^{17}\varepsilon_{O_3+h\nu} = -4.7$ (±0.7)‰ for photolysis and

$^{18}\varepsilon_{O+O_3} = -18.6$ (±1.4)‰ and $^{17}\varepsilon_{O+O_3} = -9.3$ (±0.7)‰ for chemical removal.

These scenarios span the range of fractionation factors for the unidentified removal that we consider realistic under the experimental conditions. Despite thorough investigations the nature of the additional removal could not be identified. We therefore advocate the corresponding fractionation values in Table 2.3. Note that fractionation values in scenarios 2 and 3 are based on the simplistic assumption of hard sphere collisions, completely

neglecting isotope effects due to the energetic barrier that controls the speed of the reaction and other dynamic effects. Surface reactions cannot be ruled out completely, even though they are less compatible with our observations. We therefore might use scenario S3 as worst case to determine the uncertainty of our derived fractionation values. Based thereon, we derive lower values for the fractionation constants in the photolysis of about −9 and −4‰ for ^{18}O and ^{17}O. This solidly confirms that the fractionation in the predominant Chappuis band photolysis leads to a slight isotopic enrichment of ozone at about 1 to 2%.

2.5.3 *Isotope effects in the visible light photolysis of O_3*

In this study, we have investigated the isotope effect for O_3 photolysis in the Chappuis band (500>λ>700 nm), which dominates O_3 photolysis in the visible light region. The Chappuis band shows small vibronic structure on both sides of the absorption peak. The observed fractionation in the O_3 *only* experiments from photolysis and chemical removal together ($\varepsilon_{average}$ = −14‰) is very similar to the value of −15‰ that *Chakraborty and Bhattacharya* [2003] found in photolysis experiments using narrow-band light sources at 520 (± 2) nm and 630 (± 4) nm. In all photolysis experiments with pure O_3, photolysis is followed by destruction of another O atom via $O + O_3$. The comparison with the measurements by *Chakraborty and Bhattacharya* [2003] thus implies that the isotope fractionation in these two narrow wavelength regions is similar to the wavelength integrated photolysis fractionation in our study.

Theoretical calculations based on the measured absorption spectra of $^{16}O^{16}O^{16}O$ and $^{18}O^{18}O^{18}O$ postulated a strong wavelength dependency of the fractionation values in the Chappuis band, however. Based on calculations by *Liang et al.* [2006], fractionations can vary from −107‰ to +25‰ at individual wavelengths for $^{16}O^{16}O^{18}O$ and from −57‰ to +13‰ for $^{16}O^{16}O^{17}O$ (Figure 2.7). Since we are using a broadband light source, the isotope fractionation due to the vibronic structure should largely average out. When the calculated fractionation factors from *Liang et al.* [2006] are folded with the actinic flux spectrum of our photolysis lamp, we calculate slightly negative fractionations for visible light photolysis of symmetric and asymmetric O_3. For $^{16}O^{16}O^{17}O$ and $^{16}O^{16}O^{18}O$ fractionations are −3‰ and −6‰, for $^{16}O^{17}O^{16}O$ and $^{16}O^{18}O^{16}O$ fractionations are –5‰ and −10‰ respectively.

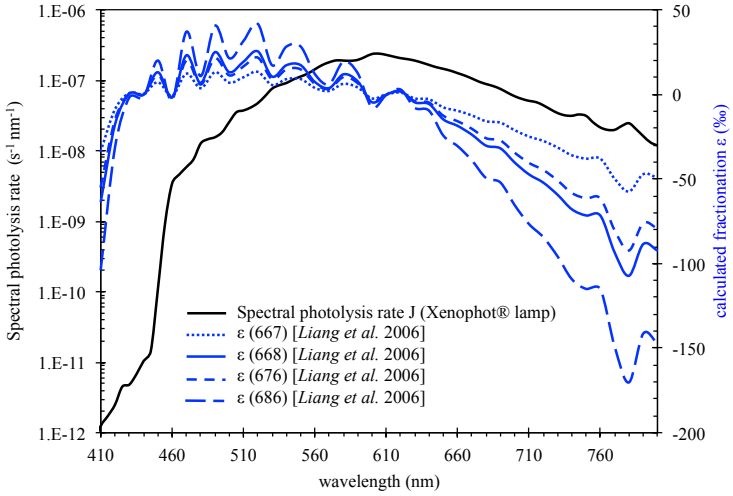

Figure 2.7. Spectral photolysis rate J (black line) of halogen photo optic Xenophot® lamp (with a band pass filter that cuts off radiation <455 nm) and wavelength dependent fractionations ε calculated by *Liang et al.* [2006] for visible light photolysis of O_3 ($^{16}O^{16}O^{17}O$, $^{16}O^{16}O^{18}O$, $^{16}O^{17}O^{16}O$, $^{16}O^{18}O^{16}O$). The calculated spectrally weighted fractionation, using the spectral fractionations from Liang (http://web.gps.caltech.edu/~mcl/ZPE/zpe.html) and our measured spectral photolysis rate (J) according to $(\Sigma_\lambda \varepsilon \times J)/(\Sigma_\lambda J)$ (λ= 410 to 800 nm) yields total fractionations of −3.2‰ and −6.0‰ for $^{16}O^{16}O^{17}O$ and $^{16}O^{16}O^{18}O$ respectively. For symmetric species total fractionations are −5.2‰ and −9.8‰ for $^{16}O^{17}O^{16}O$ and $^{16}O^{18}O^{16}O$.

The absolute discrepancy between our measurements and the theoretical calculations by *Liang et al.* [2006] is about 10‰ or more for $^{18}\varepsilon$. It is likely that this discrepancy is due to the simple zero point energy (ZPE) model, as it has been shown to suffer from several shortcomings in predicting fractionation effects in complex molecules as compared to more elaborate models [*Schmidt et al*. 2013]. While *Schmidt et al*. [2013] found a factor of three difference between their full wave packet calculations and the simple ZPE model in the UV photolysis of carbon dioxide, *Ndengué et al.* [2014] also obtained smaller fractionation factors for ozone photolysis compared to the results from *Liang et al.* [2006], as indicated by the prediction of larger atmospheric enrichments.

Cole and Boering [2006] analyzed the data from *Chakraborty and Bhattacharya* [2003] in more detail by applying kinetic modeling, similar to the model used in our study. Importantly, they also implemented fractionation effects in photolysis and O + O_3 separately. In the absence of information on the fractionation in the chemical removal they used the calculated fractionation for photolysis at the relevant wavelengths from *Liang et al.* [2004] and adjusted the fractionation in the O + O_3 reaction in order to fit the results, basically following our equation (2.10). Their base scenario uses a strong negative

fractionation in O_3 photolysis at 520 nm of ${}^{18}\varepsilon_{O_3+h\nu} = -24‰$ and ${}^{17}\varepsilon_{O_3+h\nu} = -12.5‰$ from *Liang* [2004]. In order to fit the observed isotopic composition from the experiments (${}^{18}\varepsilon_{obs} = -15‰$), they needed to postulate a negative fractionation in $O + O_3$ of ${}^{18}\varepsilon_{O+O_3} = -60‰$. As the fractionation in the chemical removal has to be the same when O_3 is photolysed at a different wavelength, but the calculated fractionation in photolysis at 630 nm is very different (${}^{18}\varepsilon_{O_3+h\nu} = +4.2‰$ and ${}^{17}\varepsilon_{O_3+h\nu} = +2.1‰$) it was not possible to fit the very similar experimental results at both wavelengths with these assumptions.

The results from our experiments imply that the fractionation in the chemical removal is much smaller than what had to be assumed by *Cole and Boering* [2006], which means that the assigned fractionation in visible photolysis (at 520 and 630 nm) from *Liang et al.* [2006] in their study was inadequate. *Cole and Boering* [2006] already discussed that in view of the strong vibronic structure of the O_3 absorption cross section in the Chappuis band, it would be desirable to calculate the fractionation at much higher spectral resolution in order to compare with narrow band light sources and this can indeed lead to large errors.

It is surprising that although the semi-empirical calculations predict a large wavelength dependency of the fractionation for photolysis in the Chappuis band [*Miller et al.*, 2005; *Liang et al.*, 2006], measurements at two different wavelengths from *Chakraborty and Bhattacharya* [2003] and our new broadband results yield very similar fractionation constants for visible light photolysis. It would be interesting to investigate experimentally whether this is a coincidence or whether the wavelength dependence is actually smaller than expected from the semi-empirical model calculations.

We note that *Morton et al.* [1990] briefly report on a set of photolysis experiments with visible light around the maximum of the Chappuis band at 590 nm. After 80% of dissociation the isotopic composition was within the experimental uncertainty of 6‰ equal to the initial O_3 and the authors state that any additional isotope effect for $O + O_3$ or $O_3 + h\nu$ in the visible light spectrum can be excluded. However, also in these experiments the isotope effect in the chemical removal must have been active, and this would imply that in their experimental setup the photolysis fractionation was actually negative in order to cancel out the enrichment expected from the chemical removal.

Furthermore, additional fractionations can occur in the dominating reaction $CO + O + M$ (R2.4), but this reaction does not directly involve O_3, whereas R2.2 and R2.3 do. Nevertheless, R2.4 can still affect O_3, but only via an effect on the O atom reservoir, which can then be transferred to O_3 again in the O_3 formation reaction (R2.2). *Pandey and Bhattacharya* [2006a, 2006b] reported a strong mass-independent fractionation in the reaction $CO + O + M$, but *Simone* [2014] showed that the reported enrichments are likely due to interferences from O_3 formation. Therefore, in our model we apply no fractionation effects for the CO_2 formation reaction.

2.5.4 *Application in the atmosphere*

In the atmosphere, O_3 is generally considered to be in photo-stationary equilibrium between formation and photolysis. The isotopic composition in equilibrium between O_3 formation and O_3 photolysis is the sum of the fractionations in those two processes. The effect of ${}^{18}\varepsilon =$ −9 to −16‰ in O_3 photolysis, reported in this study, is small, but still significant compared to the observed enrichments in $\delta^{18}O$ of ~ 90‰ in the troposphere [*Krankowsky et al.*, 1995; *Johnston and Thiemens*, 1997]. Despite the actinic flux spectrum of our light source used for photolysis being different from the actinic flux spectrum in the atmosphere, we expect that these values are somewhat representative for atmospheric ozone dissociation in the Chappuis band. This is due to the fact that we have essentially probed the peak region of that band and that our pure O_3 results are very similar to the relative short band measurements at 520 and 630 nm of *Chakraborty and Bhattacharya* [2003], which implies that isotope effects from ozone photolysis integrated over several nm in this wavelength region yield somewhat consistent values of about 1 to 2%.

In the middle atmosphere, the odd oxygen sink reaction O + O_3 is slow compared to photolysis and, therefore, the associated fractionation will likely be of minor importance for the isotopic composition of O_3 in this region. At the higher altitudes of the lower thermosphere (> 105 km), however, the odd oxygen sink reaction becomes a competitive removal channel for ozone [*Allen et al.,* 1984]. It will therefore well affect the ozone isotopic composition.

2.6 CONCLUSIONS AND OUTLOOK

An attempt to separately measure fractionation effects in O_3 photolysis in the Chappuis band and the O + O_3 reaction has been presented. By adding CO as bath gas we were able to effectively suppress the reaction pathway O + O_3 and therefore quantify isotope effects in visible light photolysis. Experiments with pure O_3 and O_3 in He or Ar as bath gas could successfully be reproduced with a kinetic model. However, in the presence of CO as bath gas, an additional unidentified removal channel of O_3 leads to a systematic uncertainty.

Under consideration of an additional O_3 removal reaction O_3+CO (R2.7) with different fractionation values, represented in scenarios S1-S3, we can quantify fractionations in O_3 photolysis and O_3 removal (O + O_3) to range between

$${}^{18}\varepsilon_{O_3+h\nu} = -16.1\ (\pm 1.4)‰,\ {}^{17}\varepsilon_{O_3+h\nu} = -8.05\ (\pm 0.7)‰$$

$${}^{18}\varepsilon_{O+O_3} = -11.9\ (\pm 1.4)‰,\ {}^{17}\varepsilon_{O+O_3} = -5.95\ (\pm 0.7)‰ \text{ and}$$

$${}^{18}\varepsilon_{O_3+h\nu} = -9.4\ (\pm 1.4)‰,\ {}^{17}\varepsilon_{O_3+h\nu} = -4.7\ (\pm 0.7)‰$$

$${}^{18}\varepsilon_{O+O_3} = -18.6\ (\pm 1.4)‰,\ {}^{17}\varepsilon_{O+O_3} = -9.3\ (\pm 0.7)‰.$$

With our findings we could quantify isotope effects in the O_3 photolysis in the Chappuis band and in the $O + O_3$ odd oxygen sink reaction, which provides valuable information for understanding isotope effects affecting ozone isotopic composition in the laboratory. These data also provide an important contribution to the modeling of atmospheric oxygen isotopes. Future photolysis studies employing the CO quencher technique should concentrate on a reduction of side reactions to further constrain individual fractionation factors.

For better understanding of the observed isotopic composition of stratospheric O_3, it would be of considerable interest to study the isotope effects due to O_3 photolysis in the UV spectrum. Furthermore, the determination of wavelength dependent fractionations and isotopologue-specific spectral absorption cross-sections of O_3 would provide an important contribution to the understanding of atmospheric O_3 and its isotopic composition.

3

WAVELENGTH DEPENDENT ISOTOPE FRACTIONATION IN VISIBLE LIGHT O_3 PHOTOLYSIS AND ATMOSPHERIC IMPLICATIONS

Abstract

The ^{17}O and ^{18}O isotope fractionation associated with photolysis of O_3 in the Chappuis band was determined using a broadband light source with cutoff filters at 455, 550, 620 nm and narrow band light sources at 530, 617 and 660 nm. The isotope effects follow a mass-dependent fractionation pattern ($\delta^{17}O/\delta^{18}O = 0.53$). Contrary to theoretical predictions, fractionations are negative for all wavelength ranges investigated and do not change sign at the absorption cross-section maximum. Observations differ from models by as much as 34‰ in $^{18}\varepsilon_{O_3+h\nu} = (^{18}J/^{16}J-1)$. The wavelength dependence is also weaker than predicted. Photo-induced fractionation is strongest when using a low wavelength cut-off at 620 nm with $^{18}\varepsilon_{O_3+h\nu} = -26.9(\pm1.4)$‰. With decreasing wavelength, fractionation values diminish to $^{18}\varepsilon_{O_3+h\nu} = -12.9(\pm1.3)$‰ at 530 nm. Results from an atmospheric model demonstrate that visible light photolysis is the most important tropospheric sink of O_3 and therefore must affect its isotopic composition.

This chapter is under review as:

Früchtl, M., C. Janssen, D. Taraborelli, S. Gromov, and T. Röckmann (2015), Wavelength dependent isotope fractionation in visible light O_3 photolysis and atmospheric implications, Geophysical Research Letters.

3.1 INTRODUCTION

Ozone (O_3) carries a strong enrichment (~ 100‰) in both heavy oxygen isotopes ^{17}O and ^{18}O compared to atmospheric O_2 [*Mauersberger*, 1981; *Krankowsky et al.*, 1995, 2007; *Johnson et al.*, 2000]. This enrichment shows a marked deviation from classical mass-dependent fractionation, where $\delta^{17}O \approx 0.52 \times \delta^{18}O$. Mass-independent isotope fractionation can be quantified by the ^{17}O excess,

$$\Delta^{17}O = \delta^{17}O - 0.52 \times \delta^{18}O \,. \tag{3.1}$$

The peculiar high enrichments in the heavy isotopes ^{17}O and ^{18}O originate from the O_3 formation reaction [*Krankowsky et al.*, 1995; *Johnson et al.*, 2000; *Mauersberger et al.*, 2001] and strongly depend on temperature and pressure [*Morton et al.*, 1990; *Thiemens and Jackson*, 1990; *Krankowsky et al.*, 2007]. In addition, atmospheric studies suggested a contribution of O_3 photolysis to the observed isotope enrichments in atmospheric O_3. At altitudes above 30 km atmospheric fractionations were higher than what is expected from the known isotope effects in O_3 formation [*Haverd et al.* 2005, *Krankowsky et al.,* 2007]. The observed additional enrichment was tentatively attributed to the process of O_3 photolysis.

A semi-analytical theory to calculate photolysis induced isotope effects in O_3 and other gases [*Miller and Yung,* 2000; *Miller et al.* 2005; *Liang et al.* 2006] predicts pronounced wavelength-dependent isotope effects during photolysis. In the Chappuis band (400-800 nm) calculated fractionations show significantly nanometer-scale variability superimposed on a general trend from positive fractionation on the short-wavelength side of the absorption maximum to strongly negative fractionation at the long-wavelength tail [*Liang et al.*, 2006]. *Ndengué et al.* [2010, 2012, 2014] performed improved calculations of isotope specific absorption cross-sections, using quantum mechanical MCTDH (Multiconfiguration Time-Dependent Hartree) wave packet propagation on ab-initio surfaces, but the cross sections are not provided which impedes direct comparison. For both types of calculation, model results show that the photolysis induced isotope effects contribute significantly to the isotopic composition of O_3 in the atmosphere [*Liang et al.* 2006, *Ndengué et al.,* 2014]. While *Ndengué et al.* [2014] claim a strict mass dependence for O_3 photo-dissociation, the results of the atmospheric model show a ^{17}O excess of 2.5 to 3.5‰ at altitudes up to 32 km. If significant, this would imply a non mass-dependent isotope fractionation from photolysis in the Huggins and/or Chappuis bands.

Due to the inherent approximations in the theoretical treatments, experimental studies are required to provide benchmark data. *Morton et al.* [1990] reported no significant change in O_3 when photolysed with visible light, whereas *Chakraborty and Bhattacharya* [2003] found a mass-dependent fractionation pattern ($\delta^{17}O/\delta^{18}O = 0.54$) for photolysis of

O_3 at 520 nm and 630 nm. The fractionation coefficients they obtained for both wavelengths showed similar values of ${}^{18}\varepsilon_{O_3+h\nu} = -13.7\pm2‰$ and ${}^{17}\varepsilon_{O_3+h\nu} = -7.25\pm0.1‰$. However, the calculations by *Liang et al.* [2006] yielded very different fractionations for photolysis at the two wavelengths, ${}^{18}\varepsilon_{O_3+h\nu} = +5.8‰$ at 520 nm and ${}^{18}\varepsilon_{O_3+h\nu} = -31‰$ at 630 nm (average values for the symmetric and asymmetric isotopomers).

A conceptual complication of the above photolysis experiments using pure O_3 samples is that the O atom that is produced during photolysis generally destroys another O_3 molecule in the reaction $O + O_3$. Thus, isotope effects in photolysis and chemical removal cannot be disentangled [*Brenninkmeijer et al.,* 2003]. In *Früchtl et al.* [2015a, chapter 2 of this thesis], we combined photolysis experiments of pure O_3 and O_3 mixed in a large excess of CO, which acts as O atom quencher, to separately quantify the fractionation in both removal processes. Photolysis experiments using a broadband light source with a 455 nm filter yielded ${}^{18}\varepsilon_{O_3+h\nu} = -16.1(\pm1.4)‰$ and ${}^{17}\varepsilon_{O_3+h\nu} = -8.05(\pm0.7)‰$, and ${}^{18}\varepsilon_{O+O_3} = -11.9(\pm1.4)‰$ and ${}^{17}\varepsilon_{O+O_3} = -5.95(\pm0.7)‰$. Notably, both fractionations are mass-dependent.

Following up on these results, in this chapter we examine the (low resolution) wavelength dependence of the isotope fractionation in the photolysis of O_3 by visible light using various light sources and cut-off filters.

3.2 METHODS

3.2.1 *Experimental procedure*

The experimental system has been described in detail in *Früchtl et al.* [2015a, see also chapter 2 of this thesis]. O_3 was produced by electric discharge from ~8.0 hPa of pure O_2 (99.9998%) in a spherical 1.0 L glass reactor with a cylindrical extension immersed in liquid nitrogen (LN_2). O_3 condensed at the reactor wall and the remaining O_2 was pumped away. Subsequently O_3 was brought to room temperature, and an aliquot was expanded to the cylindrical photolysis chamber (V = 630 cm^3) for photolysis. After photolysis, the leftover O_3 was separated from O_2 by pumping the mixture through a cryogenic trap cooled to the triple point temperature of N_2 (63 K). At this temperature O_3 condenses but O_2 produced during photolysis does not and can be pumped away. The collected O_3 was transferred to a sample bottle (V = 44 cm^3) containing molecular sieve (13X) immersed in LN_2 and subsequently converted to molecular O_2 by heating. The amount of O_2 originating from O_3 was then determined by measuring the pressure after transfer to a reference volume (V = 1.8 cm^3, containing molecular sieve). The isotopic composition was determined on a Dual Inlet IRMS (Thermo Finnigan Delta^{Plus} XL) with an uncertainty of 0.03‰ for $\delta^{18}O$ and 0.08‰ for $\delta^{17}O$ (n = 150).

Two sets of photolysis experiments were conducted. In a first set, a broadband light source (λ = 400 to 800 nm) with an emission peak at 605 nm was used (tungsten halogen lamp, Osram HLX 64633, described in *Früchtl et al.* [2015a, see also chapter 2 of this thesis]. To select different wavelength regions, we used different optical long pass glass color filters with cutoff wavelengths at 455±6, 550±6 or 620±5 nm (GG455, OG550, Schott; R-620, Hoya). For each experiment the corresponding filter was placed between the lamp and the photolytic chamber. In a second set, three narrow band light sources (high power LEDs) with emission peaks at 530, 617 and 660 nm and respective bandwidths (FWHM) of 33, 18 and 25 nm were used (Thorlabs M530L3, M617L3 and M660L3).

Each experiment consisted of measuring three aliquots from the same initial O_3 reservoir. The first aliquot expanded into the photolysis chamber was used as control measurement to correct for small O_3 losses that occur without photolysis. The second aliquot (expansion #2) was collected after 10 to 30 minutes of photolysis. The final aliquot (expansion #3) is the residual O_3 in the discharge reactor, which represents the original O_3 produced in the electric discharge.

In the following we refer to the amount of the photolysed sample (expansion #2, corrected for the control experiment) as $O_3(end)$ and the remaining O_3 from the discharge reactor (expansion #3) as $O_3(start)$. The remaining fraction $f(O_3)$ after a certain time t of photolysis is defined as $f(O_3) = O_3(\text{end})/O_3(\text{start})$. Isotope enrichments are reported as $\delta^x O = (N(^xO)/N(^{16}O))_{SA}/(N(^xO)/N(^{16}O))_{ST} - 1$, where x indicates heavy isotope mass numbers 18 or 17. δ quantifies the relative deviation of the ratio $N(^xO)/N(^{16}O)$ of isotope abundances (N) in a sample (SA) from the same ratio in a standard material (ST). Values are reported in per mill (‰). The isotopic composition of initial O_3 is chosen as standard.

3.2.2 *Photolysis rate and fractionations in O_3 photolysis*

The photolysis rate J is determined from the temporal evolution of O_3 removal (f) in the experiments

$$J = 0.5 \ln(f)/t \tag{3.2}$$

Measured photolysis rates range from $3.3(\pm0.06)\times10^{-4}$ s^{-1} (455 nm filter) to $0.9(\pm0.3)\times10^{-4}$ s^{-1} (530 nm LED) (Table 3.1). The spectral photolysis rate for each light source is shown in Figure 3.2a. Values are calculated by multiplying O_3 absorption cross sections [*Sander et al.*, 2011] with the spectral actinic flux under the assumption of unit quantum yield. The spectral actinic flux with different filters was obtained by multiplication of the actinic flux of the halogen lamp without filter (determined with a spectral photometer) with the filter internal transmittance published by the manufacturer. For LED light sources, the spectral actinic flux data provided by the manufacturer were used.

3.2.3 *Control measurements and error estimates*

The stability of the analytical system was characterized by *control* measurements without irradiation as described above. A loss of 4−7% of O_3 was observed in the control experiments, associated with changes of $\delta^{18}O < 0.1‰$ and $\delta^{17}O < 0.05‰$. For correction, average values from the control measurements were subtracted from the raw data of the photolysis experiments.

Uncertainty estimates for $\delta^{18}O$ and $\delta^{17}O$ include errors from control measurements ($\sigma_{control}$) and IRMS measurements ($\sigma_{O_3 end}$, $\sigma_{O_3 start}$) according to

$$\sigma = \sqrt{(\sigma_{O_3 end})^2 + (\sigma_{O_3 start})^2 + (\sigma_{control})^2}\,, \tag{3.3}$$

total errors are <0.2 ‰ for ^{17}O and ^{18}O.

Uncertainties in ln(*f*) were derived from experiments with pure CO_2 instead of O_3, because CO_2 is easy to trap and to transfer in vacuum systems with virtually no loss (>99.5% recovery). Considering a small non-linearity of the pressure sensor, errors in pressure reading and small changes in temperature, total relative uncertainties in ln(*f*) are between 2.6 and 2.8% [*Früchtl et al.,* 2015a, see chapter 2 of this thesis].

3.3 RESULTS

Figure 3.1 shows that, independent of the light source used, the remaining O_3 becomes isotopically enriched during the photolysis experiments, i.e., the heavy isotopologues are removed more slowly than $^{16}O_3$ for all wavelength ranges. The measured fractionations ε for ^{18}O vary between −12.4‰ and −19.4‰ and between −6.7‰ and −10.2‰ for ^{17}O (Figure 3.1a-d and Table 3.1). O_3 photolysis with the broadband lamp using a 550 nm or a 455 nm filter or the 617 nm LED, result in very similar fractionations (Table 3.1). For these experiments the peak emission is slightly above 600 nm. The fractionations become more negative towards longer wavelength (620 nm filter, 660 nm LED). At shorter wavelength (530 nm), the fractionations values are highest, but still clearly negative at $^{18}\varepsilon = -12.4‰$ and $^{17}\varepsilon = -6.7‰$.

As mentioned above, the observed fractionation in the photolysis experiments with pure O_3 does not only include O_3 photolysis (R3.1) but due to the photolytic production of O atoms, also the chemical O_3 removal via R3.2.

$$O_3 + h\nu \rightarrow O_2 + O \tag{R3.1}$$
$$O + O_3 \rightarrow 2O_2 \tag{R3.2}$$
$$O + O_2 + M \rightarrow O_3 + M \tag{R3.3}$$

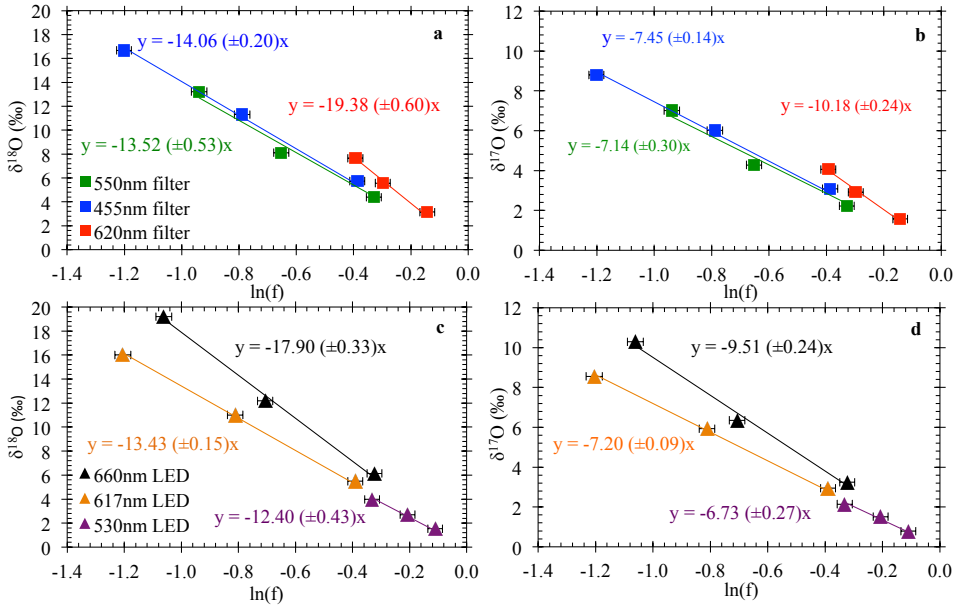

Figure 3.1a – 3.1d. Rayleigh fractionation plots for O_3 photolysis experiments of 10, 20 and 30 minutes (three points in each series). Top: photolysis with the halogen lamp and different filters. Bottom: photolysis with high power LEDs. $\delta^{17}O$ and $\delta^{18}O$ are given versus O_3(*start*). Errors in the slopes (ε_{total}) are based on least square fits forced through zero. Errors in ln(f) are between 0.026 and 0.028. Errors in δ values are < 0.2‰.

In our experiments the rates of O_3 photolysis (R3.1) and O + O_3 (R3.2) are very similar and reformation of O_3 via (R3.3) is negligible (<1%). Thus, the total fractionation (ε_{total}) is the average of the two fractionations in reactions R3.1 and R3.2

$$\varepsilon_{total} = (\varepsilon_{O_3+h\nu} + \varepsilon_{O+O_3}) / 2 \quad (3.4)$$

Using the previously determined fractionation values for (R3.2) of ${}^{18}\varepsilon_{O+O_3} = -11.9(\pm 1.4)‰$ and ${}^{17}\varepsilon_{O+O_3} = -5.95(\pm 0.7)‰$, the photolysis induced fractionations can be calculated from equation (3.4).

The resulting fractionations attributed to O_3 photolysis are shown in Table 3.1 and Figure 3.2b,c. For all the wavelength intervals investigated, photolysis of O_3 induces negative fractionations, with a trend to stronger isotopic fractionation at longer wavelengths. Measured fractionations range between −26.9‰ and −12.9‰ for ^{18}O and −14.4‰ and −7.5‰ for ^{17}O in experiments applying a 620 nm filter or the 530 nm LED respectively. Figure 3.2 also shows the wavelength dependent fractionations calculated by *Liang et al.* [2004, 2006]. By folding these fractionations with the photolysis spectra of our

light sources the predicted photo induced fractionations for our experimental conditions were calculated (Table 3.1, Figure 3.2b,c).

The theoretical predictions agree best with the experiments using the broadband lamp with 550 nm filter or 660 nm LED, with maximum differences of only 3.3‰ for $^{18}\varepsilon_{O_3+h\nu}$ and 1.8‰ for $^{17}\varepsilon_{O_3+h\nu}$. In qualitative agreement with calculations [*Liang et al.*, 2006] we observe a wavelength dependence and stronger fractionations at longer wavelengths. At shorter wavelengths, however, the observed wavelength dependence is much smaller than predicted and discrepancies become considerable (33.9‰ and 18.5‰ for $^{18}\varepsilon_{O_3+h\nu}$ and $^{17}\varepsilon_{O_3+h\nu}$ at 530 nm). Most importantly, the experimentally determined fractionations do not show change in sign towards shorter wavelengths, whereas the calculations predict a change from negative to positive values below 600 nm.

Table 3.1: Overview of measurement results compared to *Liang et al.* [2006].

	$J(s^{-1})$ ($\times 10^{-4}$)	$\varepsilon_{(total)}$ (‰)		$\varepsilon_{(O_3+h\nu)}$ (‰)		$\varepsilon_{(O_3+h\nu)\,Liang\,et\,al.}$ (‰)	
		^{18}O	^{17}O	^{18}O	^{17}O	^{18}O	^{17}O
455nm filter	3.34 (±0.06)	-14.1 (±0.2)	-7.5 (±0.1)	-16.2 (±1.1)	-8.9 (±0.6)	-9.6	-5.1
550nm filter	2.69 (±0.07)	-13.5 (±0.5)	-7.1 (±0.3)	-15.2 (±1.3)	-8.3 (±0.9)	-14.0	-7.4
620nm filter	1.18 (±0.08)	-19.4 (±0.6)	-10.2 (±0.2)	-26.9 (±1.4)	-14.4 (±1.0)	-34.0	-17.9
530nm LED	0.89 (±0.03)	-12.4 (±0.4)	-6.7 (±0.3)	-12.9 (±1.3)	-7.5 (±0.8)	20.9	10.9
617nm LED	3.33 (±0.07)	-13.4 (±0.2)	-7.2 (±0.1)	-15.0 (±1.1)	-8.4 (±0.6)	-1.5	-0.7
660nm LED	2.86 (±0.15)	-17.9 (±0.3)	-9.5 (±0.2)	-23.9 (±1.2)	-13.1 (±0.7)	-21.8	-11.4

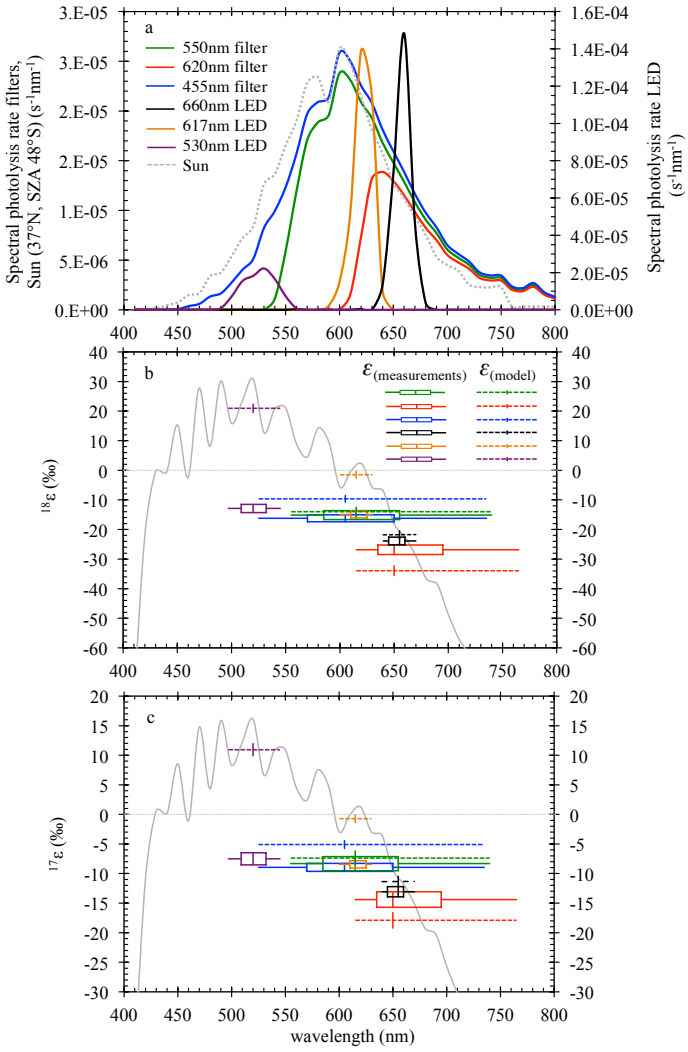

Figure 3.2. (a): Spectral photolysis rates for the different light sources used in the experiments. Green: 550 nm filter, Red: 620 nm filter, Blue: 455 nm filter, Orange: 617 nm LED, Black: 660 nm LED, Purple: 530 nm LED, Grey (dashed): Sun (37°N, SZA 48°S, from: http://rredc.nrel.gov/solar/spectra/am1.5/). Filter and LED data is scaled to the measured photolysis rate J of each light source (section 3.2.2) whereas the sun spectrum is scaled to $J_{455\text{nm filter}}$. b) and c): Isotope fractionations $^{18}\varepsilon$ and $^{17}\varepsilon$. Colors represent different filter and LEDs as defined in Figure 3.2a. The box width and solid horizontal lines indicate the wavelength intervals in which 50% and 90%, respectively, of the photons are emitted. Solid vertical lines indicate the medians. The height of the boxes marks the error for $^{18}\varepsilon_{O_3+h\nu}$ calculated as $\sigma_{O_3+h\nu} = \sqrt{(2\times\sigma_{\varepsilon(total)})^2 + (\sigma_{\varepsilon(O+O_3)})^2}$. The grey solid lines show the wavelength dependent fractionations as calculated by *Liang et al.* [2004, 2006]. The dashed lines show the fractionations expected from theoretical calculations by *Liang et al.* for our light sources.

The following Figure shows the three-isotope plot ($\delta^{17}O/\delta^{18}O$) for all photolysis experiments. There is no significant difference between the three-isotope slopes of individual experiments and a fit to all data follows a slope of 0.534 (±0.003), which is in agreement with previous results from *Chakraborty and Bhattacharya* [2003].

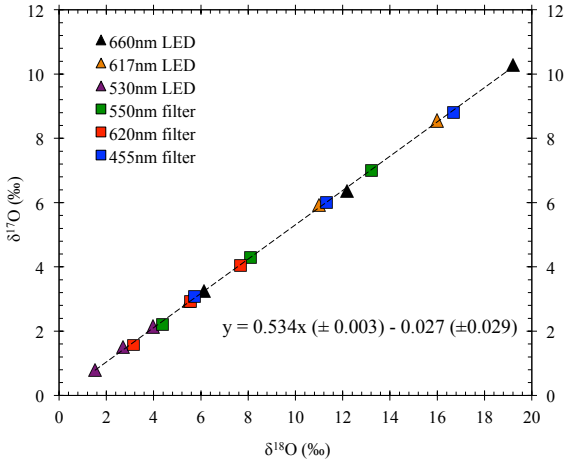

Figure 3.3. Three-isotope plot. Different symbols represent the different sets of experiments. The linear fit has a slope of 0.534±0.003 and a non-significant y-axis intercept.

3.4 DISCUSSION

A possible systematic uncertainty in the experimental determination of the photolysis-induced fractionation is due to the need to correct for the fractionation in the O + O_3 reaction. The correction depends on the results obtained in *Früchtl et al.* [2015a, see also chapter 2 of this thesis], where unexplained losses of O_3 might have introduced systematic errors in the determination of ε_{O+O_3}. Estimating the effects of these errors yielded lower limits of ${}^{18}\varepsilon_{O+O_3} = -18.6‰$ and ${}^{17}\varepsilon_{O+O_3} = -9.3‰$. According to equation 3.4, lower values assigned to ε_{O+O_3} would lead to correspondingly higher values for $\varepsilon_{O_3+h\nu}$. However even for the estimated lower limits for ε_{O+O_3}, the photolysis induced fractionations $\varepsilon_{O_3+h\nu}$ would remain negative over all of the wavelength ranges investigated with highest values of ${}^{18}\varepsilon_{O_3+h\nu} = -6.2‰$ and ${}^{17}\varepsilon_{O_3+h\nu} = -4.2‰$. Therefore the strong discrepancy between our measurements and the theoretical calculations by *Liang et al.* [2006], which predict positive fractionations for $\lambda < 600$ nm, cannot be attributed to erroneous assumptions in ε_{O+O_3}.

Isotope effects in O_3 photolysis depend on variations of the transition dipole moment (TDM) with isotopic substitution [*Schinke*, 1993]. Since the semi-empirical zero-point energy approach is based on the main isotopologue only, variations in TDM with isotopic substitution cannot be predicted accurately. For photolysis of N_2O, results from ab-initio calculations agree better with experimentally determined isotope fractionations than semi-empirical calculations [*Schmidt et al.,* 2011]. For CO_2, the ab-initio calculations [*Schmidt et al.,* 2013] reported three times stronger fractionations than predicted by the semi-empirical approach applied by *Liang et al.* [2004]. Furthermore, *Ndengué et al.* [2014] showed that the assumption by *Liang et al.* [2004] of a proportional relationship between changes in absorption cross sections under isotopic substitution and changes in zero point energy for both central and lateral substitution is not valid. This suggests that the discrepancies in the size and wavelength dependence between our observations and the theoretical calculations by *Liang et al.* [2004, 2006] are likely to arise from shortcomings in the semi analytical approach. The observed weak wavelength dependency of ε is experimentally supported by the results of *Chakraborty and Bhattacharya* [2003] who found similar fractionations for O_3 photolysis at 520 and 630 nm, although they could not take into account the $O + O_3$ reaction.

In order to assess the implications of our results for O_3 photolysis in the atmosphere, Figure 3.2a includes the spectral photolysis rate calculated using a typical solar actinic flux spectrum. This spectral photolysis rate is quite similar to that achieved with the broadband photolysis lamp using the 455 nm long pass filter, with the solar curve being slightly blue-shifted. The relatively weak wavelength dependence of the fractionation found in our experiments implicates that the overall fractionation under solar irradiation should be rather similar to the value obtained with the broadband lamp and the 455 nm filter. The blue-shift of the solar photolysis rate would result in a slightly larger contribution from the short-wave tail with lower fractionations and a smaller contribution from the long-wave tail with stronger fractionations. Since these tail regions are not well covered by our experiments, precise quantification is not possible at present, but we estimate that the total fractionation in the atmosphere may be a few per mill lower than what was found with the broadband lamp and the 455 nm filter.

Ozone is a highly reactive molecule and its isotopic composition in the atmosphere is determined by the dynamic balance between isotope fractionation in ozone formation and in its gross loss. In order to quantify the importance of Chappuis band photolysis as gross removal process, we analyzed the turnover of O_3 in the global model EMAC (ECHAM5/MESSy Atmospheric Chemistry, [*Jöckel et al.*, 2006, 2010]). EMAC is equipped with the comprehensive chemical mechanism accounting for all relevant gas-phase and photolytic O_3 reactions [*Taraborrelli et al.*, 2012], further revised and extended with monoterpenes/aromatics chemistry including ozonolysis [*Bloss et al.*, 2005; *Hens et al.*, 2014; *Nölscher et al.*, 2014; *Peeters et al.*, 2014]. The EMAC photolysis sub-model [*Sander et al.*, 2014] provides wavelength-resolved photolysis rates and their integrals for

the channels leading to $O(^3P)$ and $O(^1D)$ production. Photolysis in the Huggins band produces $O(^3P)$ and yields about 90% $O(^1D)$ and 10% $O(^3P)$ for the lower stratosphere and below. We diagnose that visible light photolysis in the Chappuis band accounts for more than 85% of the overall O_3 gross removal rate simulated by EMAC, from the free troposphere up to 50 hPa (Figure 3.4a). Only in the regions strongly affected by anthropogenic emissions the removal via non-photolytic sinks (predominantly in NO_x and HO_x chemistry) is of similar importance as Chappuis band photolysis near the surface (Figure 3.4b). Above 800 hPa, however, the photolytic sink clearly dominates (Figure 3.4b). We conclude that the fractionation in Chappuis band photolysis globally affects the isotopic composition of O_3 in the troposphere.

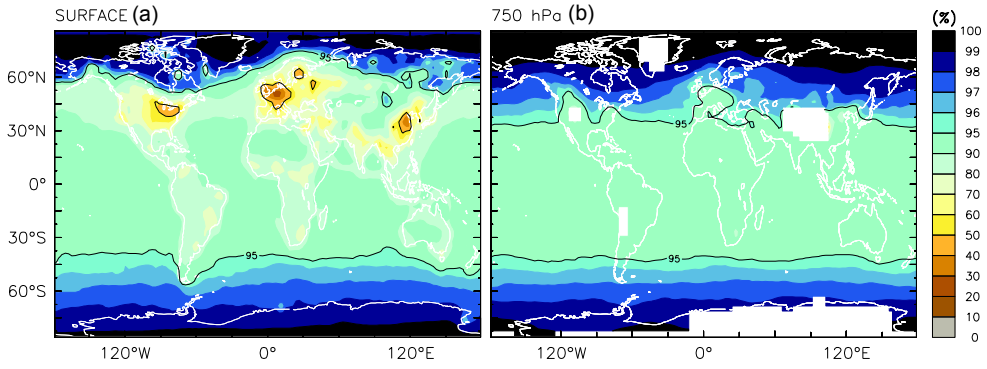

Figure 3.4. Fraction (in per cent) of the total O_3 sink attributed to photolysis leading to $O^3(P)$ production simulated by EMAC at the surface (a) and 750 hPa pressure (b) layers. Shown is a typical example from March 2001. White areas indicate regions with surface pressures lower than 750 hPa; superimposed contours refer to 50% and 95% levels, respectively.

The derived three-isotope slope of 0.534(±0.003) is at the upper end of the range that is usually considered as mass-dependent fractionation and the value is higher than the one used in the defining equation of $\Delta^{17}O$ (equation 3.1). For ${}^{18}\varepsilon_{O_3+h\nu}$ values of −15‰ in atmospheric Chappuis band photolysis and a difference of 0.014 in the three-isotope slope, the corresponding $\Delta^{17}O$ values would be 0.2 to 0.3‰. This is two orders of magnitude lower than $\Delta^{17}O$ of atmospheric O_3, which ranges between 25 and 40‰ [*Vicars and Savarino,* 2014; *Brenninkmeijer et al.,* 2003; *Krankowsky et al.,* 2007, *Johnston and Thiemens,* 1997]. Therefore, the contribution of visible light photolysis to the mass-independent isotope signature of atmospheric O_3 could be, at most, negligible.

Our results further indicate that previous experiments to determine the isotope fractionation in O_3 formation via photolytic recycling of O_3 in an O_2 bath gas using visible light [*Morton et al.*, 1990] may be biased by non-negligible isotope effects in O_3 photolysis.

Whereas the results from this study suggest shortcomings in the calculation of the overall wavelength dependence of photolysis induced O_3 fractionation in the Chappuis band, the wavelength resolution of the light sources employed is insufficient to examine smaller scale (few nm and sub-nm) variability that was also predicted by the calculations [*Miller et al.*, 2005; *Liang et al.*, 2006]. Laser light sources could help to investigate this further, but high power is required to realize sufficient removal of O_3 in laboratory experiments.

3.5 SUMMARY AND OUTLOOK

O_3 photolysis in the Chappuis band is associated with isotope effects that follow a pure mass-dependent fractionation pattern with a $\delta^{17}O/\delta^{18}O$ slope of 0.53, implying that its contribution to the ^{17}O excess in atmospheric O_3 is, at most, negligible. The observed fractionations vary with wavelength in the Chappuis band. The largest fractionations were observed for O_3 photolysis using the 620 nm filter, while the smallest fractionations were measured for photolysis with the LED at 530 nm. Altogether fractionations decreased with an increase in wavelength, as suggested in the calculations of *Liang et al.* [2006]. However for all experiments the photo induced isotope effects lead to an enrichment of the left over O_3, which is in contrast to the theoretical results. This discrepancy between our experiments and the calculations implies that atmospheric models underestimate the photolytically induced fractionation of tropospheric O_3. Since photolysis in the Chappuis band globally contributes to O_3 removal in the lower atmosphere, this is a significant effect, which needs to be considered in future atmospheric modeling.

4

TEMPERATURE DEPENDENCE OF ISOTOPE EFFECTS IN O_3 FORMATION AND VISIBLE LIGHT PHOTOLYSIS

Abstract

O_3 photolysis experiments using a high power LED with maximum emission in the Chappuis band at 617 nm, show that isotope fractionations during visible light photolysis of O_3 are independent of temperature. O_3 photolytic recycling experiments were carried out to investigate the isotope effects in O_3 formation at temperatures between 181 and 314 K. Whereas raw enrichments are similar to previously published values, taking the fractionation in the photolysis sink into account leads to significantly lower isotope enrichments attributable to O_3 formation. These enrichments in the formation process are then used to derive relative rate coefficients for isotope specific O_3 formation pathways that are consistent with our experimental results. Using previously measured and calculated rate coefficients for O_3 formation from a heavy atom and a light molecule (e.g. $^{18}O + {}^{16}O^{16}O$), we derived average relative rate coefficients for the O_3 formation channels in which a light atom reacts with a heavy molecule of 1.225 for ^{18}O containing species and 1.150 for ^{17}O respectively. When no temperature dependence is assumed for these channels, the temperature dependence for the other O_3 formation channels in which a light molecule reacts with a heavy atom are 0.001177 /K for formation of $^{16}O^{16}O^{18}O$ and 0.0009820 /K for formation of $^{16}O^{16}O^{17}O$. Detailed comparison of our enrichments to results by *Morton et al.* [1990] show small differences in the measured temperature dependence, which induces significant deviations for the ^{17}O excess in O_3 formation.

This chapter is in preparation for publication as:

Früchtl, M., C. Janssen, and T. Röckmann (2015), Temperature dependence of isotope effects in O_3 formation and visible light photolysis.

4.1 INTRODUCTION

Atmospheric ozone (O_3) has a very peculiar isotopic composition. The heavy isotope enrichment of about 100‰ versus atmospheric O_2, the substrate that it is formed from, is unusually large. Moreover, the enrichment is similar in both heavy isotopes (^{17}O and ^{18}O), which differs from what is expected for mass-dependent fractionation [*Mauersberger et al.,* 1981; *Krankowsky et al.,* 1995; *Johnson et al.,* 2000; *Brenninkmeijer et al.*, 2003; *Thiemens*, 2006]. The deviation from the classical theory of mass-dependent fractionation can be quantified as $\Delta^{17}O = \delta^{17}O - 0.52 \times \delta^{18}O$ [*Clayton et al.,* 1973; *Thiemens and Heidenreich,* 1983]. The oxygen isotope anomaly of O_3 is an important tracer for chemical processes in the atmosphere, because the isotopic signature can be transferred to other atmospheric components in chemical reactions involving O_3.

Numerous laboratory and atmospheric studies investigated the isotope anomaly of O_3. *Morton et al.* [1990] successfully identified the O_3 formation reaction as the main source for the unusually high enrichments and proved that no excited states were involved. It was shown that the enrichments in O_3 formation strongly vary with temperature and pressure of the gas in which O_3 is formed. At pressures above ~130 hPa the enrichments in O_3 decrease from the low-pressure plateau and they nearly disappear at pressures of 20 atm. With increasing temperature, the enrichments in O_3 increase and the temperature dependency is slightly stronger for ^{18}O- than for ^{17}O- substituted O_3. Above 200 K, enrichments measured for $^{50}O_3$ ($^{18}O^{16}O^{16}O$ and $^{16}O^{18}O^{16}O$) are higher than those in $^{49}O_3$ ($^{17}O^{16}O^{16}O$ and $^{16}O^{17}O^{16}O$), but there is a cross-over at about 200 K and at lower temperatures the enrichments of $^{49}O_3$ are higher [*Morton et al.,* 1990; *Krankowsky et al.,* 2007].

As an important contribution to understanding the anomalous isotopic composition of O_3, rate coefficients in the individual isotopic reaction channels of O_3 formation were investigated. Laboratory experiments showed that the rate coefficients for O_3 formation exhibit strong differences when O_3 is formed from different isotopic reactant species. Rate coefficients for reactions where isotopically heavy O atoms (e.g. ^{18}O) combine with isotopically light O_2 molecules ($^{16}O^{16}O$) are actually lower than the rate coefficient for formation of the most abundant O_3 molecule ($^{16}O^{16}O^{16}O$). However, when isotopically light O atoms combine with isotopically heavy O_2 molecules to form asymmetric O_3 molecules (e.g. $^{16}O + {}^{16}O^{18}O \rightarrow {}^{16}O^{16}O^{18}O$) the rate coefficients are almost 50% higher than for the normal reaction channel. In addition, when the same reactants form the symmetric product $^{16}O^{18}O^{16}O$, the rate coefficient is similar to the one of $^{16}O^{16}O^{16}O$ [*Mauersberger et al.,* 1999]. The combination of the isotope effects in all isotopic reaction channels then results in the strong enrichments for isotopically substituted O_3 isotopologues. Based on these findings and the measured fractionation effects determined for O_3 formation from photolysis recycling experiments [*Morton et al.,* 1990], further rate coefficients for other isotopic combinations in $O + O_2$ were measured and calculated in consecutive studies. The temperature dependence of the relative rate coefficients was also determined and it was

shown, that the relatively "slow" isotopic O_3 formation channels, in which a light molecule ($^{16}O^{16}O$) reacts with a heavy atom (^{18}O), show a pronounced temperature dependency and decrease with decreasing temperature, whereas the temperature dependence for the other rate coefficients is small [*Janssen et al.,* 1999, 2001, 2003; *Anderson et al.*, 1997; *Mauersberger et al.,* 1999].

These measurements provided important input for the theoretical investigation of the isotope enrichments observed in O_3. Marcus and coworkers [*Gao and Marcus*, 2001, 2002; *Gao et al.*, 2002; *Hathorn and Marcus*, 1999, 2000] could reproduce the observed relative rate coefficients of individual isotopic formation channels in the framework of a modified RRKM theory treatment. The two parameters that are essential (and have to be adjusted) in the modified theory are 1) a mass-dependent parameter that links the relative rate coefficient to the zero point energy (ZPE) difference of the isotopic exchange reaction that is related to a certain O_3 formation channel (Figure 1.9) and 2) a parameter that slows down the rate coefficients for symmetric O_3 molecules (where the ZPE change in the associated exchange channel is 0) by roughly 15%. This is realized by restricting the number of vibrational and rotational states that are accessible for O_3 formation of symmetric relative to asymmetric molecules.

Babikov et al. [2003a,b] investigated the isotope specific rate coefficients for O_3 formation with quantum mechanical calculations on a fully developed potential energy surface (PES). They demonstrated that the mass-independent effect in O_3 originates from the energy transfer mechanism when O_3 metastable states are formed and stabilized. The accessibility of these metastable states for O_3 formation is determined by differences in zero point energy between the isotopically substituted or non-substituted O_2 molecules.

Although it is known that the O_3 formation reaction is the most important source of the observed isotope enrichments in tropospheric and stratospheric ozone, atmospheric observations indicated an additional contribution of O_3 destruction reactions [*Krankowsky et al.,* 2007; *Haverd et al.,* 2005; *Ndengué et al.,* 2014]. Under stratospheric conditions additional fractionation effects might occur from UV photolysis of O_3, while in the troposphere visible light O_3 photolysis is more relevant. Besides photolysis, other reactions, such as the reaction of O_3 with NO_2 might have an impact on the isotopic composition of tropospheric O_3 [*Johnston and Thiemens*, 1997; *Brenninkmeijer et al.,* 2003; *Savarino et al.,* 2008; *Berhanu et al.* 2012].

Isotope effects in O_3 photolysis were investigated in previous studies [*Bhattacharya and Thiemens*, 1988; *Thiemens and Jackson,* 1988; *Morton et al.,* 1990; *Chakraborty and Bhattacharya,* 2003], but only in the experiments published by *Früchtl et al.* [2015a, see also chapter 2 of this thesis], it was possible to distinguish fractionation effects associated with O_3 photolysis from isotope effects in the odd oxygen sink reaction $O + O_3$ by using CO as O atom quencher. Both O_3 destruction reactions led to an isotopic enrichment of the left-over O_3 and the fractionations are mass-dependent.

Here we determined the temperature dependence of the isotope fractionation in visible light photolysis of O_3. We then use photolytic recycling experiments of O_3 to investigate the temperature dependent isotope effects of both formation and visible light photolysis between 181 and 314 K. Using a kinetic model, we derive a consistent set of isotope specific relative rate coefficients that are in agreement with our observations.

4.2 MATERIALS AND METHODS

4.2.1 *Ozone photolysis and photochemical recycling*

During photolysis experiments with pure O_3 using visible light, the isotope effects in the removal reactions (photolysis and $O + O_3$) can be studied relatively independently of O_3 formation, because O_3 formation requires the presence of O_2 molecules. O_2 is absent in the beginning of an experiment and is only formed in the course of the experiment, and the interference from the re-formation of O_3 increases with increasing removal of O_3.

When O_3 is photolysed in the presence of a large excess of O_2, however, the O atoms produced during O_3 photolysis react with O_2 to produce new O_3. In photolysis recycling experiments the excess of O_2 is sufficiently large that the net removal of O_3 is avoided by suppressing the $O + O_3$ reaction. Irrespective of the initial O_3 isotopic composition, after long irradiation times, the isotopic composition of the reformed O_3 approaches an isotopic equilibrium that does not change anymore with an increase in photolysis time. The isotopic composition of the O_3 molecules is then exclusively determined by the isotopic composition of the surrounding O_2 bath gas and by the isotope fractionation in the formation and photolytic destruction of O_3. The speed of the isotope exchange reaction is driven by the O_3 photolysis rate, but the speed of the net O_3 destruction is driven by the much slower rate of conversion by $O + O_3$.

In the work described below we carried out both types of experiments, i.e. photolysis experiments and photochemical recycling experiments.

4.2.2 *Experimental setup*

For our experiments we used the same experimental setup as described in detail in *Früchtl et al.* [2015a,b, see chapter 2 and 3 of this thesis], but in order to determine the temperature dependence, the photochemical reactor was replaced by a new cylindrical reactor (l = 58 cm, d = 4 cm, $V \approx 730$ cm^2) where the temperature during photolysis can be precisely controlled.

The reactor is fully made out of Suprasil glass and has three cylindrical walls. The central volume holds the gas mixtures to be analyzed (referred to as photolysis reactor), the middle volume contains the circulating cooling liquid and the outer volume is evacuated in order to avoid water to condensate on the reactor walls at low temperatures. To prevent

heat loss and condensation on the front and terminal windows, two additional evacuated chambers are attached to the front and the back of the reactor.

Temperature was controlled by connecting the photolysis reactor to a cryostat (Huber unistat 405 or Huber unistat 390 for temperatures > 233.15 K and > 183.15 K, respectively), containing a thermofluid (SilOil, type: M90.055.03) that was constantly flushed through the volume around the photolysis reactor. The set temperature of the cryostat was independently validated by measuring the temperature of the thermo fluid at the in- and outlet of the photolysis reactor with two thermocouples. The deviation was always less than 3.5 K. In the following, the indicated temperatures correspond to the temperature directly measured in the thermofluid. Aluminum foil was wrapped around the photolysis reactor and a flat surface mirror (reflection > 95%) was placed at the opposite side of the reactor to increase the photolysis rate in our experimental setting. To avoid condensation of water on the outside of the photolysis reactor and possible associated changes in the optical conditions, the reactor was packed in thermoplastic foil.

O_3 was generated using an electric discharge from ~12 hPa of pure O_2. During O_3 generation, O_3 was collected at liquid nitrogen temperatures. Leftover oxygen was pumped away until a pressure of $\sim 4\times10^{-2}$ hPa, before O_3 was brought to room temperature. For the photochemical recycling experiments, O_3 was mixed with pure O_2 in a ratio O_3:O_2 = 1:100. Either the pure O_3 or the O_3 – O_2 mixture was then expanded to the photolysis reactor. Photolysis experiments were carried out using a 617 nm power LED (Thorlabs, M617L3, FWHM = 18 nm) that was installed directly in front of the cylindrical photolysis chamber. After photolysis, O_3 was separated from present O_2 by pumping the mixture through a cryogenic trap that was cooled to 63 K. At the triple point of N_2, O_3 condenses whereas O_2 does not and was in most cases pumped away. The collected O_3 was then transferred to a sample bottle containing molecular sieve (Sigma Aldrich 13X, 1.6mm) exposed to liquid nitrogen. For isotope analysis, O_3 was converted to O_2 by heating and the isotopic composition was measured with a Thermo Finnigan Delta^{Plus}XL IRMS in Dual Inlet mode versus our laboratory O_2 standard (99.9998% purity). Internal uncertainties (1σ, n = 150) of the Dual Inlet IRMS are 0.03‰ and 0.08‰ in $\delta^{18}O$ and $\delta^{17}O$ respectively.

For two sets of experiments at 293.95 and 251.45 K, the remaining O_2 was collected in an additional sample bottle containing a porous polymer adsorbent (HayeSep®D, Sigma Aldrich, 100-120 mesh) immersed in liquid nitrogen. The procedure was tested using pure O_2 and non-photolyzed O_2 – O_3 mixtures. After collection, the isotopic composition of O_2 after a photolysis experiment was determined with the IRMS.

In order to determine the isotopic composition of the starting O_3, the remaining O_3 in the discharge was sampled for two sets of experiments without photolysis and measured at the IRMS. Since the generation of O_3 using the electric discharge followed the same procedure for every experiment, we use the average measured isotopic composition for O_3 at the start of the experiment, $\delta^{18}O$ = 23(±1.3) ‰ and $\delta^{17}O$ = 26.5(±1.9) ‰.

4.2.3 *Measurement procedure*

As explained in section 4.2.1, two different sets of experiments were conducted to investigate the isotope effects in 1) the removal of pure O_3 during photolysis and 2) photochemical recycling of O_3 in an excess of O_2. The goal of the photolysis experiments was to determine the temperature dependence of the previously established fractionation in O_3 photolysis with a well-characterized LED light source that we had used in earlier experiments [*Früchtl et al*., 2015b, chapter 3 of this thesis].

Pure O_3 was expanded to the photolysis reactor resulting in a total pressure of ≈ 6 hPa. There the O_3 was photolysed for 10, 20 or 30 minutes at temperatures ranging from 230.85 to 313.95 K.

For the photochemical recycling experiments, O_2 – O_3 mixtures were expanded to the photolysis reactor. The photolysis rate was determined from the pressure increase in the reaction vessel during a typical O_3 photolysis experiment [*Früchtl et al.,* 2015a,b, chapter 2 and 3 of this thesis]. This was done for each temperature investigated since the rate coefficients involved are temperature dependent and in particular at low temperatures some formation of ice on the reactor windows could not be avoided, which lowered the amount of photons entering the reactor and therefore increased the photolysis e-folding time. In order to establish isotopic equilibrium between the O_2 bath gas and the O_3, the experiments were carried out for approximately 4 photolysis e-folding times, based on these measurements, corresponding to between 6 and 20 hours of irradiation depending on the experimental conditions. Comparison with the time evolution of the isotopic enrichment in the model, later indicated that the photolysis rates determined this way were overestimated by about 25%, and a corresponding correction was applied. The photochemical model was used to correct for the remaining small disequilibrium (see next section).

4.2.4 *From raw data to equilibrium enrichments*

In order to derive the effect of the O_3 formation reactions only (δ_{O_2+O+M}) we removed the effect of photolysis from the enrichments measured ($\delta_{measured}$) in the photolytic recycling experiments:

$$\left(\delta_{O+O_2+M}+1\right)=\left(\delta_{measured}+1\right)/\left(\delta_{h\nu}+1\right) \tag{4.1}$$

where $\delta_{h\nu} = -\varepsilon_{h\nu}$ in photochemical equilibrium and $^{18}\varepsilon_{h\nu} = -15‰$ and $^{17}\varepsilon_{h\nu} = -8.4$ ‰, respectively.

In addition, the evaluation of the photolysis recycling data with the kinetic model reveals that even after 800 minutes of photolysis the isotopic equilibrium between O_2 and

O_3 is not fully established. Evaluation of the temporal evolution in the model allows the straightforward application of a corresponding correction ($\Delta\delta_{eq}$) that is derived as the difference of the model results in equilibrium and at the time of measurement. In addition, the model also calculates the isotopic composition of the O_2 reservoir. Although the change in its isotopic composition is small because of the large reservoir size, it is larger than the precision of our isotope measurements and is taken into account in the final data evaluation (δ_{O_2}). Summed up, we define the equilibrium enrichment (δ_{eq}) as

$$\left(1+\delta_{eq}\right)=\frac{\left(1+\delta_{O+O_2+M}\right)\times\left(1+\delta_{\Delta eq}\right)}{\left(1+\delta_{O_2}\right)} \tag{4.2}$$

The respective data are also included in Table 4.1.

4.2.5 *Photochemical model*

The reaction kinetics of the pure O_3 photolysis and photolytic recycling experiments were simulated with the kinetic modeling software Kintecus® [*Ianni*, 2003]. The key reactions and the corresponding (temperature dependent) rate coefficients are shown below. For these reactions all possible isotopic combinations were considered. A complete list of the reactions including all possible isotopic substitutions and the corresponding isotope effects applied in the model is given in *Früchtl et al.* [2015a, chapter 2 of this thesis], see also Appendix table A1.

$O_3 + h\nu \rightarrow O(^3P) + O_2$,	J_{O_3}	(R4.1)
$O(^3P) + O_2 + M \rightarrow O_3 + M$,	$k_2 = 6.0\times10^{-34}\,(300\text{ K}/T)^{-2.4}\,\text{cm}^6\,\text{s}^{-1}$	(R4.2)
$O(^3P) + O_3 \rightarrow O_2 + O_2$,	$k_3 = 8.0\times10^{-12}\exp(-2060\text{ K}/T)\,\text{cm}^3\text{s}^{-1}$	(R4.3)
$Q + OO \leftrightarrow QO + O$,	$k_{4a} = 3.4\times10^{-12}(300\text{ K/T})^{1.1}\,\text{cm}^3\text{s}^{-1}$	(R4.4a)
$O + QQ \leftrightarrow OQ + Q$,	$k_{4b} = 2.7\times10^{-12}(300\text{ K/T})^{0.9}\,\text{cm}^3\text{s}^{-1}$	(R4.4b)

Here Q stands for ^{18}O, and similar exchange reactions occur for ^{17}O, in the following denoted with P. As described above, the rate coefficient for O_3 photolysis (R4.1) was experimentally determined and corrected for an overestimation of 25%. Values for J_{O_3} applied for simulations at different temperatures varied between 1.66×10^{-4} and $4.61\times10^{-5}\text{s}^{-1}$ for temperatures of 313.95 and 181.35 K respectively. Rate coefficient values for R4.2 and R4.3 are taken from *Sander et al.* [2011]. Values for k_{4a} and k_{4b} are adopted from *Fleurat-Lessard et al.* [2003].

An important anchor for the evaluation of the isotope effects is the fractionation in reaction O + O_3 (R4.3), which was determined by *Früchtl et al.* [2015a, chapter 2 of this

thesis]. If this value is known, the fractionation in photolysis ε_{hv} can be determined from the photolysis experiments with relatively little interference of the formation reactions. Once ε_{hv} is determined, the photolysis recycling measurements can be used to obtain the fractionation effects in the formation channels (R4.2).

In the base scenario of the kinetic model, fractionation effects from previous studies were included. Isotope effects in the individual isotopic reaction channels (also referred to as relative rate coefficients) for O_3 formation (R4.2) are adopted from *Janssen et al.* [1999] and *Mauersberger et al.* [1999] or derived from the empirical zero point energy relationship described in *Janssen et al.* [2001] and *Babikov et al.* [2003]. The pressure and temperature dependencies of the kinetic isotope effect in O_3 formation are included in the kinetic model following the calculations from *Wiegel et al.* [2013] and *Tuzson et al.* [2005]. As in [*Wiegel et al.*, 2013], the pressure dependent isotope effect was derived from the O_3 formation kinetic isotope effect at low pressure and the pressure dependence of the O_3 isotopic enrichments. The temperature dependency in the base scenario is derived from previous experimental measurements of the isotope effects in formation of ozone isotopomers containing one heavy isotope ^{18}O [*Wiegel et al.*, 2013; *Tuzson et al.,* 2005]. A more detailed description is given in section 4.2.6. Fractionation coefficients applied for the isotopic exchange reaction (R4.4a, R4.4b) are based on *Janssen and Tuzson* [2010]. For photolysis with the 617 nm LED we use the values of −15‰ and −8.4‰ for $^{18}\varepsilon_{hv}$ and $^{17}\varepsilon_{hv}$ respectively as determined by *Früchtl et al.* [2015b, chapter 3 of this thesis].

Initial number densities of O_3 for the different temperatures 313.95, 293.95, 273.05, 251.45, 230.85, 200.35 and 181.35 K were 1.57×10^{16}, 1.10×10^{16}, 1.65×10^{16}, 1.10×10^{16}, 1.57×10^{16}, 1.6×10^{16}, 1.58×10^{16} cm^{-3}, respectively.

4.2.6 *Relative rate coefficients for individual isotopic O_3 formation channels and their temperature dependence*

For quantitative evaluation of the relative rate coefficients in O_3 formation, we remove the established fractionation in photolysis ε_{hv} from the measured isotope enrichments such that the pure enrichment in the formation reactions can be evaluated with the kinetic model where the fractionation in photolysis is then of course also neglected.

When O_3 and O_2 are in photochemical isotope equilibrium, the isotopologue enrichments ($^i\delta$) are directly linked to the relative rate coefficients of isotope specific ozone formation channels and the isotope equilibrium constant (K_{eq}) of the isotope exchange reactions R4.4a and R4.4b [*Anderson et al.,* 1997].

$$1+{}^{i}\delta = \frac{2}{3}\left(\frac{1}{K_{eq}}\frac{k_{y+OO}}{k_{O+OO}}+\frac{k_{O+Oy}}{k_{O+OO}}\right) \tag{4.3}$$

${}^{i}\delta$ denotes the measured enrichment of $^{49}O_3$ or $^{50}O_3$ relative to the O_2 bath gas in our photolytic recycling experiments. The subscript y in the rate coefficients denotes a heavy atom ^{17}O or ^{18}O. Note that k_{O+Oy} is the average of two individual rate coefficients leading to symmetric and asymmetric molecules, respectively, which cannot be distinguished with our measurements. If they need to be distinguished in the following, the order of isotopes in the O_2 molecule indicates the channel, i.e., k_{O+OQ} is the channel for formation of OOQ and k_{O+QO} is the channel for formation of OQO.

Since k_{y+OO} / k_{O+OO} has been directly measured [*Janssen et al.,* 1999; *Mauersberger et al.,* 1999], equation 4.3 can be applied to derive rate coefficient ratios for the sum of the reaction channels forming symmetric and asymmetric O_3 molecules.

Assuming the same temperature dependency for k_{O+yO} / k_{O+OO} and k_{O+Oy} / k_{O+OO} and based on experimental data for k_{Q+OO} / k_{O+OO} from *Janssen et al.* [2003], *Wiegel et al.* [2013] derived the following temperature dependent isotope effects for the different O_3 formation channels, which are included in our base model:

$$\frac{k_{O+OQ}}{k_{O+OO}}(T) = 1.45 + 0.0000207 \times (T-300\ \mathrm{K}) \tag{4.4}$$

$$\frac{k_{O+QO}}{k_{O+OO}}(T) = 1.08 + 0.0000207 \times (T-300\ \mathrm{K}) \tag{4.5}$$

$$\frac{k_{Q+OO}}{k_{O+OO}}(T) = 0.92 + 0.00103 \times (T-300\ \mathrm{K}) \tag{4.6}$$

$$\frac{k_{O+OP}}{k_{O+OO}}(T) = 1.35 + 0.0000207 \times (T-300\ \mathrm{K}) \tag{4.7}$$

$$\frac{k_{O+PO}}{k_{O+OO}}(T) = 0.99 + 0.0000207 \times (T-300\ \mathrm{K}) \tag{4.8}$$

$$\frac{k_{P+OO}}{k_{O+OO}}(T) = 1.03 + 0.000782 \times (T-300\ \mathrm{K}) \tag{4.9}$$

Note that the temperature dependence for the ^{17}O - containing isotopomers (4.9) is not based on measurements, unlike for ^{18}O. *Wiegel et al.* [2013] derived eq. 4.9, for example, by assuming that the other rate coefficients involving ^{17}O (4.7, 4.8) have the same temperature dependency as 4.4 and 4.5 for ^{18}O.

In this study, we use our new high-precision data on the temperature dependent isotope enrichments to derive improved relative rate coefficients using the same approach.

4.3 RESULTS AND DISCUSSION

4.3.1 *Temperature dependence of isotope effects in visible light O_3 photolysis*

Figure 4.1 shows the measured and modeled $\delta^{17}O$ and $\delta^{18}O$ values of the leftover O_3 as a function of the remaining fraction of O_3. As found in previous studies [*Früchtl et al.,* 2015a,b, chapter 2 and 3 of this thesis], the remaining O_3 becomes successively enriched in the course of a photolysis experiment. The enrichment is approximately linear for the room temperature experiments, but is clearly non-linear at 230.85 K. At lower temperatures, the reaction rate of O_3 formation (R4.2) increases whereas the O_3 removal rate via $O + O_3$ (R4.3) decreases. Thus, the interference from O_3 formation reactions in these O_3 removal experiments becomes relatively more important at lower temperatures. As newly formed O_3 carries a strong isotope enrichment, this leads to higher isotopic enrichments of the remaining O_3 at lower temperatures after same degree of photolysis. For example at 230.85 K the isotope enrichments increase to $\delta^{18}O$ = 22‰ and $\delta^{17}O$ = 13‰ after 30 minutes of photolysis whereas at 306.15 K, after same time of photolysis, we find isotope enrichments of $\delta^{18}O$ = 16‰ and $\delta^{17}O$ = 9‰.

The base model with the fractionation effects in O_3 formation, photolysis and chemical removal included, actually reproduces the experimental data very well. The temperature dependence of the isotope enrichment in the remaining O_3 arises only from the increasing importance of O_3 formation. The good agreement between model results and experimental data (Figure 4.1) shows that the assumption of a temperature-independent fractionation in O_3 photolysis is valid within the experimental errors. Thus, for the remainder of the experiments we consider that photolysis with the 617 nm LED induces a temperature-independent fractionation of $^{18}\varepsilon_{hv} = -15‰$ and $^{18}\varepsilon_{hv} = -8.4‰$.

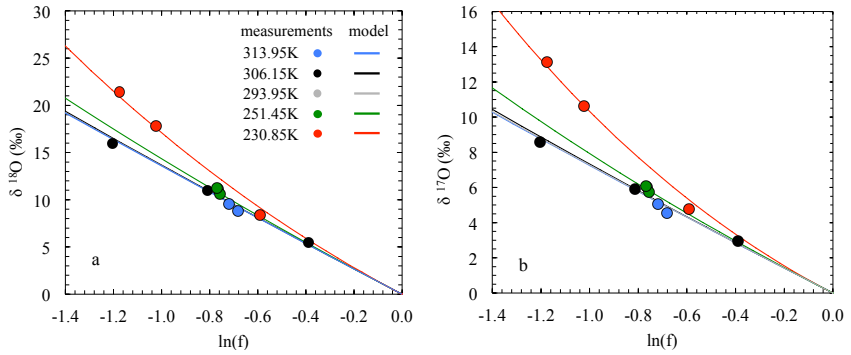

Figure 4.1. Experimental and modeled evolution of O_3 isotopic composition as a function of the remaining fraction of O_3 for photolysis experiments using the visible light LED with an emission maximum at 617 nm (^{18}O (a) and ^{17}O (b)). Symbols: experimental data, solid lines: model predictions. Different colors represent different temperatures. Blue: 313.95K, black: 306.15 K, grey: 293.95 K, green: 251.45 K and red: 230.85 K.

4.3.2 *Photolytic recycling and isotope effects in O_3 formation*

4.3.2.1 Temperature dependence

Table 4.1 and Figure 4.2 show the results of the isotope enrichments ($\delta_{measured}$) of O_3 determined after about 4 photolysis e-folding times from the experiments as a function of temperature. Figure 4.2 also includes previous data from *Morton et al.* [1990], which were obtained with a similar setup and have been used as reference enrichments for many experimental and theoretical studies in the literature to date.

The results are generally in good agreement, although the temperature dependence of the observed enrichments is slightly different. For the interpretation, however, it is important that the data from *Morton et al.* [1990] have always been interpreted as pure formation signatures, whereas in our experiments the contribution of photolysis is clearly established (see 4.3.1).

To illustrate the discrepancy, we show in Figure 4.3 (left panels) the temporal evolution of the isotopic composition of O_3 as derived from the kinetic model calculations using the base model, which is set up to reproduce the enrichments from *Morton et al.* [1990], with the experimental data. The predicted enrichments are significantly higher than measured. The largest part of the discrepancy can be attributed to the fact that the base model includes the effect of photolysis established for our photolysis light source (4.3.1). When this effect is excluded, the modeled enrichments are in much better agreement with the measurements (Figure 4.3 right panels). This discrepancy indicates that the previously neglected isotope signal from photolysis has wrongly been attributed to O_3 formation. To resolve this discrepancy it is necessary to adjust the underlying rate coefficients for O_3 formation (see below).

Table 4.1: Overview of experimental photolytic recycling data.

Temperature	Photolysis time	$\delta_{measured}$ (‰)		δ_{O_2+O+M} (‰)		δ_{eq} (‰)		
(K)	(min)	^{17}O	^{18}O	^{17}O	^{18}O	^{17}O	^{18}O	$\Delta^{17}O$
313.95	384	104.8	117.1	95.6	100.6	99.8	106.2	44.6
293.95	360	100.6	110.5	91.4	94.1	93.5	97.9	42.6
273.05	360	92.6	99.9	83.5	83.6	86.0	87.6	40.4
251.45	354	85.7	91.1	76.7	74.9	78.8	78.6	39.7
230.85	480	78.5	82.2	69.5	66.2	71.9	69.7	35.6
200.35	774	62.9	64.7	54.1	49.0	55.9	51.6	29.1
181.35	1224	54.9	54.6	46.1	39.0	47.4	41.1	26.0
181.35	1224	54.8	54.6	46.0	39.1	47.4	41.1	26.0
181.35	1800	54.6	54.5	45.8	39.0	47.1	41.0	25.8

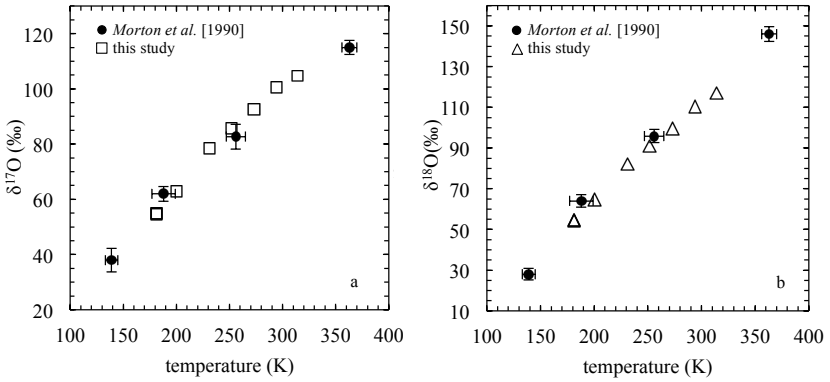

Figure 4.2. Isotope enrichments of O_3 determined after photolysis as a function of temperature. Open symbols: Experimental data of this work, filled symbols: Data from *Morton et al.* [1990], used as reevaluated in *Brenninkmeijer et al.* [2003].

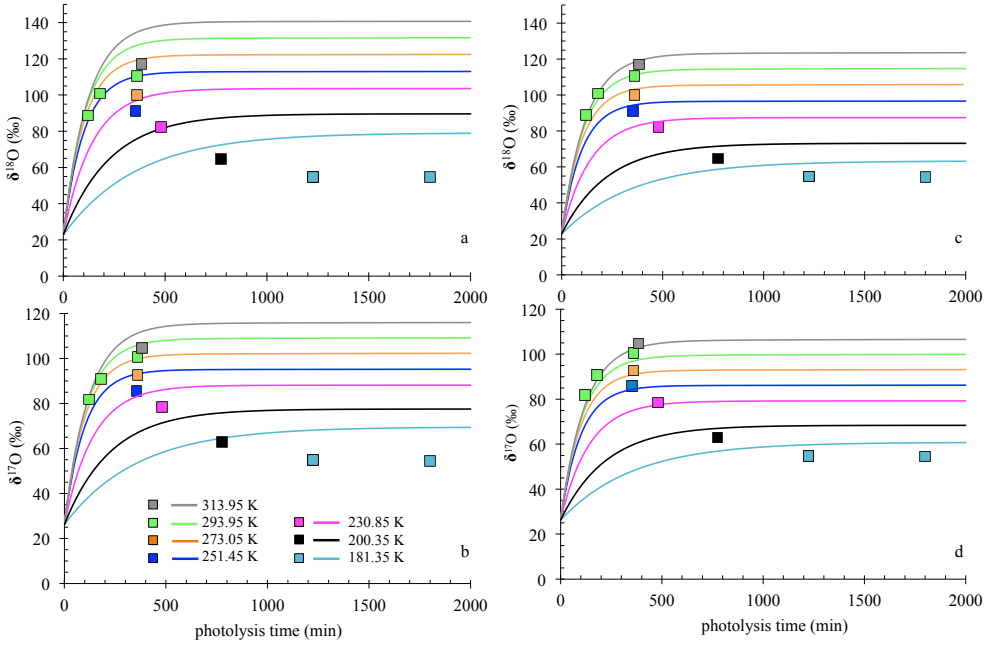

Figure 4.3. Temporal evolution of the isotopic composition of O_3 after photolytic recycling at different temperatures. Symbols: measurements, solid lines: model simulations. Different colors represent different temperature conditions. Grey: 313.95 K, Green: 293.95 K, Orange: 273.05 K, Dark blue: 251.45 K, Magenta: 230.85 K, Black: 200.35 K and light blue: 181.35 K. The photolytic recycling experiments were simulated under the assumption of $^{18}\varepsilon_{hv} = -15‰$ and $^{17}\varepsilon_{hv} = -8.4$ ‰ (a, b) and $^{18}\varepsilon_{hv} = 0‰$ and $^{17}\varepsilon_{hv} = 0‰$ (c, d).

4.3.2.2 Pressure dependence

In order to demonstrate general consistency between our dataset and the data from *Morton et al.* [1990], a few measurements were also carried out to investigate the pressure dependence of the isotope enrichment in photolytic recycling experiments. Figure 4.4 shows that – similar to the temperature dependence – the experimental results are generally in good agreement with the measurements of *Morton et al.* [1990].

The results of the experiments at different pressures are only shown for completeness but will not be investigated in detail.

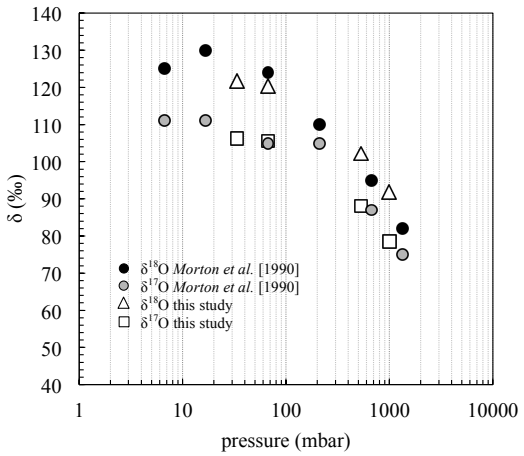

Figure 4.4. Dependence of $\delta^{17}O$ and $\delta^{18}O$ on pressure of this study at room temperature (filled symbols) and data by *Morton et al.* [1990] at 321 K (presented in *Brenninkmeijer et al*. [2003] (open symbols). Data of this study is corrected for temperature effects.

4.3.2.3 Relative rate coefficients for isotopic O_3 formation channels and the effect on modeled enrichments

The equilibrium enrichments derived from the new high precision measurements and related kinetic modeling can be used to adjust the relative rate coefficients in O_3 formation based on equation 4.3. The relative rate coefficient k_{Q+OO} / k_{O+OO} and its temperature dependence were measured by *Janssen et al.* [2003] and parameterized by *Wiegel et al*. [2013] as given in equation 4.6. We adopt the value of this relative rate coefficient at 300 K, k_{Q+OO} / k_{O+OO} = 0.92, as anchor point for the reevaluation of the ^{18}O-related rate coefficients. The temperature dependence in the other two relative rate coefficients leading to $^{50}O_3$ (O + QO and O + OQ) was determined to be very small and not significantly different from zero [*Janssen et al.,* 2003; *Wiegel et al.,* 2013]. Therefore, we first set this

temperature dependence to 0 and attribute the entire temperature dependence in the observed enrichment for ^{18}O-substituted O_3 to the Q + OO channel. The resulting values for the Q + OO channel and the average of the O + QO and O + OQ channels are shown in Figure 4.5.

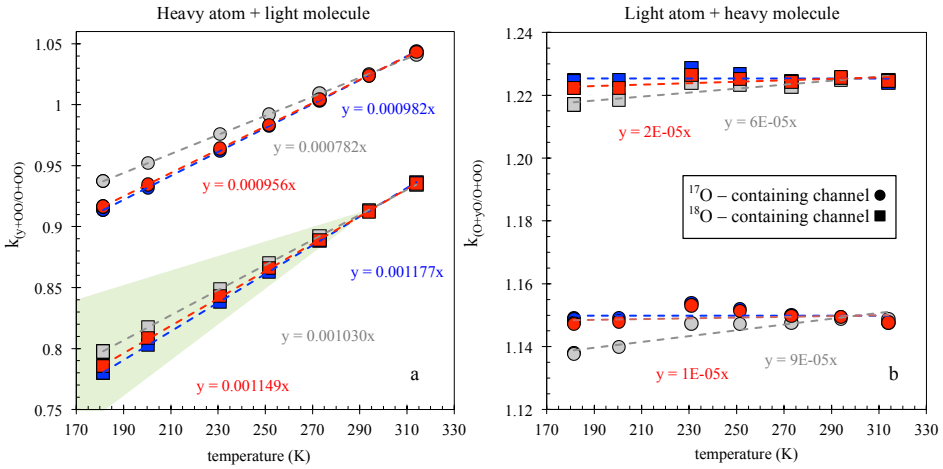

Figure 4.5. The dependence of rate coefficient ratios in O_3 formation on temperature. (a) O_3 formation channels of which a heavy atom (^{17}O or ^{18}O) reacts with a light molecule ($^{16}O^{16}O$) and (b) O_3 formation channels in which a light atom (^{16}O) reacts with a heavy molecule ($^{17}O^{16}O$, $^{18}O^{16}O$). Squares: reaction channels containing ^{18}O species, Circles: reaction channels containing ^{17}O species. Grey color: A temperature gradient of 0.000781 / K and 0.001030 / K is applied for k_{P+OO} and k_{Q+OO}, respectively [*Janssen et al.,* 2003; *Wiegel et al.*, 2013]. Blue color: No temperature gradient is assumed for channels in which a light atom reacts with a heavy molecule which leads to a temperature gradient of 0.001177 / K for k_{P+OO} and 0.000982 / K for k_{Q+OO}. Red color: Temperature effects for $0.5 \times (k_{O+OQ} + k_{O+QO}) / k_{O+OO}$ and $0.5 \times (k_{O+OP} + k_{O+PO}) / k_{O+OO}$ are adopted from *Wiegel et al.* [2013], which leads to a temperature dependence of 0.000956 / K for k_{P+OO} and 0.001149 for k_{Q+OO}. The grey shaded area marks the error range (±0.00042) given by *Janssen et al.* [2003].

The figure also shows results when the small temperature dependence of the other rate coefficients as derived by *Wiegel et al.* [2013] is included.

Similarly for ^{17}O-substituted O_3, we adopt the value of relative rate coefficient at 300 K, $K_{P+OO} / k_{O+OO} = 1.03$, as anchor point for the reevaluation of other rate coefficients. When the temperature dependence of the other relative rate coefficients involving ^{17}O atoms is set to 0, equation 4.3 can be solved again and the results are presented in Figure 4.5.

For this case, i.e. when we assume no temperature dependence for reaction channels in which a heavy molecule reacts with a light atom, the fit to the measurements yields a temperature dependence of 0.001177 / K for k_{Q+OO} / k_{O+OO} and 0.000982 / K for k_{P+OO} / k_{O+OO}. This is within the errors of the previously derived temperature dependencies (see shaded area in Figure 4.5) [*Janssen et al*., 2003]. In this case, the average rate coefficient values for the other isotopic channels are $0.5 \times (k_{O+OQ} + k_{O+QO}) / k_{O+OO} = 1.225$ and $0.5 \times (k_{O+OP} + k_{O+PO}) / k_{O+OO} = 1.150$ (Figure 4.5). These values are lower than the values from previous studies because the rate of the O_3 formation channels is directly linked to the isotope enrichments (4.3) which in our study are partly attributed to fractionation effects in O_3 photolysis.

Assuming a temperature dependence in the rate coefficient ratios k_{Q+OO} / k_{O+OO} and k_{P+OO} / k_{O+OO} of 0.001030 / K and 0.000782 / K [*Janssen et al.,* 2003; *Wiegel et al.,* 2013] means that a minor part of the temperature dependence must be attributed to the other channels. This leads to a slightly different average rate coefficient ratio of $0.5 \times (k_{O+OQ} + k_{O+QO}) / k_{O+OO} = 1.221$ and $0.5 \times (k_{O+OP} + k_{O+PO}) / k_{O+OO} = 1.144$ (Figure 4.5).

It is well established that the relative rate coefficients for the two formation channels differ and that the channels leading to asymmetric species are particularly fast with rate coefficient ratios of $k_{O+OQ} / k_{O+OO} = 1.45$ and $k_{O+OP} / k_{O+OO} = 1.35$ (for P = ^{17}O) [*Janssen et al.* 2001; Figure 1.9]. In comparison, relative rate coefficients for reaction channels leading to symmetric molecules are much slower. A value of $k_{O+QO} / k_{O+OO} = 1.08$, determined in *Janssen et al.* [1999] has been used in most of the existing literature. However, Tuzson [2005] remeasured this value and also published a measurement of the corresponding ^{17}O reaction. He finds $k_{O+QO} / k_{O+OO} = 1.02$ and $k_{O+PO} / k_{O+OO} = 0.99$ [*Tuzson*, 2005]. Nevertheless, the important quantity for our isotope model calculations is the average of the relative rate coefficients of the two channels, whereas changes in the distribution do not matter. This has been tested in additional model runs (not shown).

The analysis of our data shows that the lower isotope enrichments attributed to the contribution of photolysis in the photolytical recycling experiments can almost exclusively be explained by a lowering of the relative rate constant for the formation of symmetric O_3 k_{O+QO} compared to the value of 1.08 from *Janssen et al.* [1999]. This value always appeared as an outlier in the plot of relative rate coefficients versus exchange in ZPE in the isotope exchange process (see Figure 1.9). The new measurement of $k_{O+OQ} / k_{O+OO} = 1.225$ is therefore compatible with the large rate coefficient ratio of 1.45 for the symmetric channel, and a value very close to 1, in agreement with the determination by *Tuzson* [2005].

With the adjusted rate coefficient ratios, the model reproduces the measurements very well (Figure 4.6). The small remaining differences are due to experimental scatter and the fact that the rate coefficient ratios are assumed to have linear temperature dependence in the slow rate coefficients ratio for k_{y+OO} / k_{O+OO} and no temperature dependence in k_{O+yO} / k_{O+OO}.

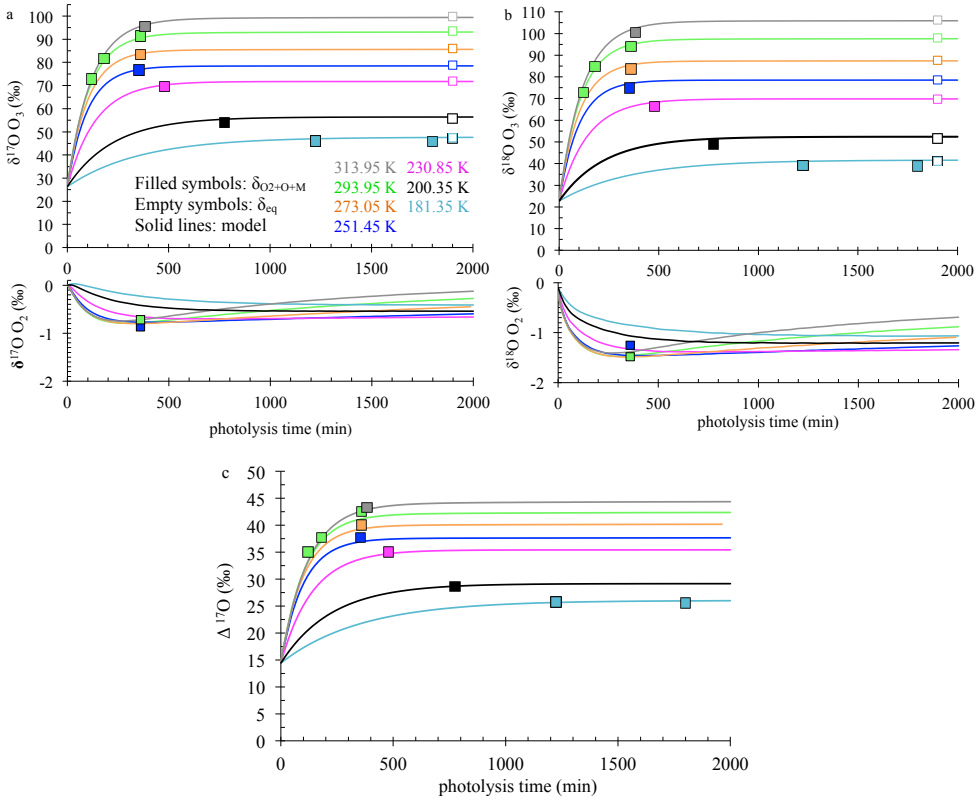

Figure 4.6. Temporal evolution of (a) $\delta^{18}O$ (O_3 and O_2), (b) $\delta^{17}O$ (O_3 and O_2) and (c) $\Delta^{17}O$ at various temperatures. The photolysis fractionation has been removed from the measured data (filled symbols) and the photolysis fractionation was set to 0 in the model, so the results present isotope effects from the formation reactions only. Open symbols on the right hand end of the figure show $\delta_{eq.}$ Different colors represent different temperatures. (a) and (b) also contain results of two independent measurements of the remaining O_2 after photolysis with a systematic deviation of 0.5‰. Grey: 313.95 K, Green: 293.95 K, Orange: 273.05 K, Dark Blue: 251.45 K, Magenta: 230.85 K, Black: 200.35 K and Light Blue: 181.35 K. Rate coefficient ratios in O_3 formation are adjusted to fit δ_{eq} assuming a linear temperature dependence in the slow rate coefficient ratio of the heavy atom with the light molecule and no temperature dependence in the other channels.

4.3.3 *Temperature dependence of isotope effects in O_3 formation – comparison with Morton et al. [1990]*

25 years after the original photolytic recycling experiments by *Morton et al.* [1990] we revisited these experiments with a high precision experimental setup. The isotope measurements have a precision of 0.1‰ and 0.05‰ for $\delta^{17}O$ and $\delta^{18}O$, respectively, and

are thus at least an order of magnitude more precise than the data from *Morton et al.* [1990]. The most important improvement compared to the data from *Morton et al.* [1990] is that we have clearly established a significant contribution of photolysis to the observed isotope enrichments, and this has to be taken into account in the data analysis.

When the fractionation in photolysis is removed from the data, the enrichments that we now attribute to formation are significantly lower than those of *Morton et al.* [1990] (Figure 4.7)

In addition, the temperature dependence is slightly different. The differences between the two datasets actually become clearly apparent when the ^{17}O excess is calculated according to $\Delta^{17}O = \delta^{17}O - 0.52 \times \delta^{18}O$ (Figure 4.7c). $\Delta^{17}O$ values obtained from our measurements show a much stronger temperature dependence than those of *Morton et al.* [1990]. We note that this discrepancy is not due to the attribution of part of the enrichment to photolysis. Since this is a mass-dependent effect, taking the photolysis fractionation into account has no effect on the $\Delta^{17}O$ values. The reason why apparently small differences in $\delta^{17}O$ and $\delta^{18}O$ lead to significant differences in $\Delta^{17}O$ for measurements above 230 K arises from the fact, that (before correction for photolysis) fractionations in ^{17}O are slightly higher compared to *Morton et al.* [1990] while fractionations in ^{18}O are lower (Figure 4.7a,b). For measurements at temperatures below 230 K, both $\delta^{17}O$ and $\delta^{18}O$ are lower than those measured by *Morton et al.* [1990] which leads to smaller values in $\Delta^{17}O$ that are more in line with the results from *Morton et al.* [1990].

The discrepancy between the $\Delta^{17}O$ values found in our study and the results reported in *Morton et al.* [1990] is intriguing, since such a difference would imply the existence of additional mass-independent fractionation processes in this simple photochemical system that involves only few species and reactions. The experimental approaches of the two studies are very similar and it is hard to attribute the differences to differences in the experimental setup. The two experimental series were carried out with different light sources. However, *Früchtl et al.* [2015b, chapter 3 of this thesis] showed that the wavelength dependence of the fractionation in photolysis is relatively weak and in fact the photolysis fractionation with the LED used in the present study was found to be very similar to the fractionation with a broadband photolysis lamp of the same type as used in the experiments of *Morton et al.* [1990]. In addition, the fractionation in visible light photolysis and in the chemical removal of O_3 have both been established to be mass-dependent [*Früchtl et al.,* 2015a,b, chapter 2 and 3 of this thesis]. They therefore will not affect $\Delta^{17}O$. We thus conclude that differences in the removal reactions cannot be the cause of the different $\Delta^{17}O$ values.

The most likely explanation for the difference may be the errors in the isotope measurements reported in *Morton et al.* [1990]. These measurements were not carried out with an isotope ratio mass spectrometer, but with a small Mattauch-Herzog type mass spectrometer, where background corrections of 0.5% and 2.5% for ^{17}O and ^{18}O

measurements, respectively, were required. Another possible artifact, especially in small spectrometers, is the presence of water molecules in the ion source that via ion molecule reactions can lead to the formation of HO_2^+ ions which could possibly affect the measurement of the m/z = 33 signal. The original data of *Morton et al.* [1990] also show a considerable scatter, which is even larger than the reevaluated data from *Brenninkmeijer et al.* [2003] that are shown in Figure 4.2.

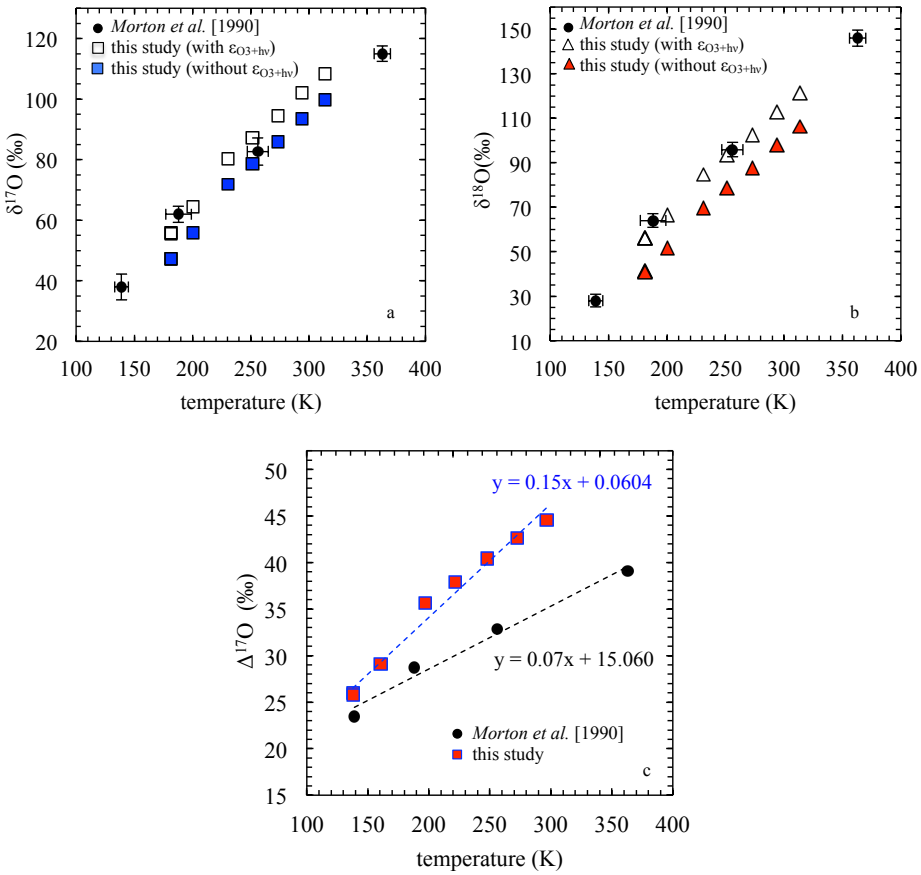

Figure 4.7. Dependence of (a) $\delta^{17}O_{eq}$ and (b) $\delta^{18}O_{eq}$ in O_3 on temperature. Symbols represent δ_{eq} of this study with isotope effects in O_3 photolysis (empty symbols) and without isotope effects in O_3 photolysis (filled symbols). Black circles: Data based on *Morton et al.* [1990] as presented in *Brenninkmeijer et al.* [2003]. (c) Represents the temperature dependence of $\Delta^{17}O$ for measurements of this study (filled squares) and *Morton et al.* [1990] (black circles).

4.4 CONCLUSION AND OUTLOOK

Photolysis experiments of O_3 with visible light carried out at temperatures between 181 and 314 K showed that the fractionations in O_3 photolysis are independent of temperature. We used this information in the evaluation of photolytic recycling experiments, in which O_3 is photolysed in a large excess of O_2, to determine the temperature dependent isotope effect originating from O_3 formation. The total enrichments observed in the experiments are similar to the generally accepted values from the literature, but when the effect of photolysis is removed, the isotope enrichments arising from only the O_3 formation reactions are lower than assumed previously.

Based on measurements and calculations of relative rate coefficients for individual isotopic O_3 formation channels by *Janssen et al.* [2003], *Mauersberger et al.* [1999], *Tuzson* [2005] and *Wiegel et al.* [2013], a consistent set of relative rate coefficients for the single-substituted O_3 isotopologues were derived that fits the new high precision enrichment data.

Assuming no temperature dependence in the reaction channel where a light atom reacts with a heavy molecule, we found temperature gradients of 0.001177/K in k_{Q+OO}/k_{O+OO} and 0.000982/K in k_{P+OO}/k_{O+OO}. This led to average rate coefficient values for the other isotopic channels of 1.225 in k_{O+QO}/k_{O+OO} and 1.150 in k_{O+OP}/k_{O+OO}.

The symmetric and asymmetric O_3 formation channels cannot be resolved by mass spectrometric measurements on O_2 produced from O_3, so only the average values are constrained by our measurements. When the measured "fast" rate coefficient ratios for formation of asymmetric molecules, k_{Q+OO}/k_{O+OO} and k_{P+OO}/k_{O+OO}, are considered at their published values, the rate coefficient ratio for the symmetric channel k_{O+QO}/k_{O+OO} must be very close to 1, thus lower than assumed previously (Figure 1.9) but in agreement with a recent redetermination of this rate coefficient by *Tuzson* [2005]. The lower overall enrichments attributed to the effect of photolysis are thus in agreement with the re-determined rate coefficient ratios.

The improvements of the new photolytic recycling experiments presented here compared to *Morton et al.* [1990] who performed similar experiments 25 years ago are 1) a much more precise dataset on equilibrium isotope enrichments and 2) a re-interpretation of these enrichments including a significant effect form photolysis. Although the raw data look relatively consistent, the temperature dependencies for both ^{17}O- and ^{18}O-substituted O_3 are slightly different, which leads to considerable differences in $\Delta^{17}O$ especially at relatively high temperatures.

5

SUMMARY AND OUTLOOK

5.1 GENERAL SCOPE AND APPROACH

Since the discovery of an anomalous isotopic enrichment in atmospheric O_3 [*Mauersberger et al.* 1981, 1983; *Heidenreich and Thiemens,* 1983], an intense scientific effort has been made both experimentally and theoretically to determine the origin of the peculiar isotopic composition in O_3. Although the O_3 formation reaction has been identified as a source for the O_3 anomaly, as shown in chapter 1 of this thesis, atmospheric measurements [*Krankowsky et al.*, 2007; *Haverd et al.,* 2005] pointed towards an additional fractionation effect arising from O_3 photolysis at altitudes above 25 km. However, only few laboratory studies exist that investigate isotope fractionations in photo dissociation of O_3 [*Bhattacharya and Thiemens,* 1988; *Morton et al., 1990*; *Chakraborty and Bhattacharya* 2003] and none of them was able to successfully quantify isotope fractionations in O_3 photolysis without the interference from accompanying reactions.

This thesis provided new experimental data on the quantification of isotope effects in O_3 photolysis, as well as the O_3 removal reaction $O + O_3$. In the stratosphere O_3 photolysis occurs largely in the Hartley band at UV wavelengths ($\lambda < 320$ nm). UV photolysis leads to electronically excited oxygen molecules and atoms (R1.3a), which initiate additional O_3 destruction reactions and fuel HO_x catalytic loss cycles of O_3. To exclude the excited state chemistry, the work in this thesis was focused on photolysis in the Chappuis bands at wavelengths between 400 and 800 nm, which enabled us to investigate the fractionation effects in only O_3 photolysis and the associated reaction $O + O_3$ as well as O_3 formation.

5.2 TOOLS

A new experimental system for the investigation of isotope effects in O_3 destruction reactions was developed, in which the gas mixtures are in contact exclusively with glass or Teflon surfaces. The setup is described in detail in chapter 2.2.1. In this system, O_3 was either photolysed purely or in presence of different bath gases such as He, Ar or CO. To reach one of the main goals of this thesis, photolysis of O_3 in presence of a large excess of

CO led to the suppression of the O_3 removal reaction $O + O_3$ and the O_3 formation reaction (see below).

In order to allow quantitative evaluation of the experimental data, a reaction kinetic model was developed, which involved explicit representation of all different isotope reaction channels for the involved chemical reactions (chapter 2.3). The seven chemical reactions (R2.1-R2.7) are represented by 240 (Table 2.1) isotope specific reaction pathways. It is necessary to include isotope channels containing multiple substituted molecules in both the reactants and the reaction products when isotope effects are investigated on the per mill scale.

5.3 MAIN FINDINGS

Using these analytical tools, experiments were carried out to answer the following scientific questions that were stated in the introduction:

(i) What is the oxygen isotope fractionation associated with photolysis of O_3 in the Chappuis band?
What is the isotope fractionation associated with removal of O_3 via reaction with O atoms? (Chapter 2)

In laboratory O_3 photolysis experiments with a broadband photolysis lamp, the remaining O_3 gets isotopically enriched, which means that the heavy O_3 isotopologues are removed more slowly than $^{16}O^{16}O^{16}O$. The isotope fractionation in photolysis was separated from the fractionation in the chemical removal via $O + O_3$ by using CO as O atom quencher. It turns out that the two removal pathways induce rather similar isotope fractionation. For visible light photolysis we find $^{18}\varepsilon = -16.1(\pm1.4)‰$ and $^{17}\varepsilon = -8.05(\pm0.7)‰$, for O_3 decomposition via $O + O_3$ we find $^{18}\varepsilon = -11.9‰$ and $^{17}\varepsilon = -5.95‰$. Notably, the results can be modeled well within the experimental errors by assuming that both fractionation processes are mass-dependent. The fractionation effects are small, but significant compared to the total enrichments of 90‰ measured for atmospheric O_3 [*Krankowsky et al*., 1995; *Johnston and Thiemens,* 1997]. While the chemical O_3 decomposition is of minor importance compared to O_3 photolysis in the lower and middle atmosphere, in the thermosphere $O + O_3$ is an important O_3 removal channel. Therefore in this region, isotope fractionation in the reaction $O + O_3$ is important for the isotopic composition of atmospheric O_3.

(ii) What is the wavelength dependence of fractionation effects in visible light photolysis of O_3? (Chapter 3)

The isotope fractionation associated with photolysis of O_3 in the Chappuis band is wavelength dependent. In contrast to theoretical calculations, O_3 that remains after

photolysis becomes enriched in the heavy isotopes at all wavelengths investigated, and on both sides of the absorption spectrum maximum. This means that when O_3 is photolysed using selected portions of the Chappuis band, $^{16}O^{16}O^{16}O$ is always photolyzed faster than the heavier isotopologues. Isotope fractionations decrease from $^{18}\varepsilon = -12.9‰$ during photolysis using a 530 nm LED to $^{18}\varepsilon = -26.9‰$ when using a broadband photolysis lamp and a long-pass filter with a cut-off at 620 nm. The wavelength dependence is much weaker than what is expected from theoretical predictions [*Liang et al.,* 2006]. In the past, the photo-induced isotope effects, which have been included in previous model calculations based on these theoretical predictions, have therefore been underestimated. Results from the global atmospheric model EMAC further demonstrate that Chappuis band photolysis is the most important sink of tropospheric O_3. It is therefore important to take the fractionation effects in photolysis into account for interpretation of tropospheric data.

(iii) What is the fractionation effect arising from the O_3 formation reaction only, when separated from effects in O_3 photolysis and the O_3 decomposition $O + O_3$? What is the temperature dependence of fractionation effects in O_3 formation? What is the effect of photolysis fractionations on the calculation of the isotope specific relative rate coefficients for O_3 formation? (Chapter 4)

Isotope fractionation effects in visible photolysis of O_3 do not depend on temperature. In previous studies, fractionation effects assigned to the O_3 formation reaction were overestimated, because the additional isotope effects in O_3 photolysis were not quantified and not considered in the evaluation. When fractionation effects in O_3 photolysis are taken into account the isotope enrichments that originate from the formation effects have to be corrected downward. At a pressure of 65 hPa, the resulting equilibrium enrichments of O_3 versus O_2 are $\delta^{18}O = 106.2‰$ and $\delta^{17}O = 99.8‰$ at 313 K, and $\delta^{18}O = 41‰$ and $\delta^{17}O = 47.3‰$ at 181 K. Using previously measured and calculated rate coefficient values of some isotope specific O_3 formation channels and their temperature dependence we derived relative rate coefficients of $0.5\times(k_{O+OQ}+k_{O+QO}) / k_{O+OO} = 1.225$ and $0.5\times(k_{O+OP}+k_{O+PO}) / k_{O+OO} = 1.150$. Compared to previous studies [*Morton et al*., 1990] we observe slight differences in the temperature dependence of the measured isotope enrichments, which lead to distinct differences in the ^{17}O excess between our measurement results and the previously reported values.

The results obtained in the framework of this thesis provide a significant contribution to atmospheric isotope research and add to advance the investigation and the understanding of mass-independent fractionation in O_3.

5.4 FUTURE RESEARCH

It was shown, that isotope effects in O_3 photolysis in the Chappuis band contribute to the total enrichments observed in laboratory as well at atmospheric O_3 and therefore need to be considered in future theoretical and experimental research when investigating the isotope anomaly in O_3.

The most important weakness of the work presented in this thesis is the unexplained O_3 removal of 20% in photolysis experiments with CO-O_3 gas mixtures, which could not be analytically identified. In order to quantify the effect of the unexplained removal on the final results presented in chapter 2, possible isotope effects due to the unidentified reaction O_3 + X were included in the kinetic model. Although we are confident that the associated errors have been thoroughly assessed, it would be desirable to discover a way to exclude this interference. Further investigations of the reaction CO + O_3 would be helpful, particularly because an unidentified interference of chemical reactions when CO is mixed with O_3 has already been reported earlier [*Arin and Warneck,* 1972; *Slanger et al*., 1992].

The high-precision experimental setup presented in this thesis could be used to study other isotope transfer and fractionation mechanisms. As one important example, isotope fractionation effects in CO_2 formation from the reaction CO + O (R2.4.) are still unidentified. *Pandey and Bhattacharya* [2006a,b] reported a strong mass-independent fractionation effect while *Simone* [2014] states that this effect might originate from interference of O_3 formation. This reaction was actually already carried out in the experiments described in chapter 2, however the focus was on the O_3 removal and not on the reaction product CO_2. The available data may already provide some information, but this could not be accomplished in the framework of this thesis.

As a further interesting aspect, the CO + O reaction has been suggested as a possible cause of the observed clumped isotope anomaly of stratospheric CO_2 [*Yeung et al.,* 2009]. In order to characterize the clumped isotope composition of the product CO_2 isotopically, larger amounts would have to be produced, which should also be in principle possible.

It would be of considerable interest to extend the available measurements for visible light photolysis to include also photolysis in the UV part of the spectrum. While visible light O_3 photolysis is significant in the lower troposphere, at altitudes > 20 km, UV photolysis contributes with 95% to the total O_3 photolysis at altitudes > 45 km [*Ndengué et al.* 2014], which makes isotope effects in UV photolysis an important quantity for stratospheric O_3 observations and atmospheric modeling. In the past, very few studies focused on the investigation of isotope effects in UV photolysis of O_3 and as shown in chapter 1 of this thesis, conclusive results are still missing [*Bhattacharya and Thiemens*, 1988; *Chakraborty and Bhattacharya,* 2003; *Cole and Boering* 2006]. The experimental setup used in this research, can be applied to investigate isotope effects in UV photolysis. However, the disentanglement of fractionation effects in O_3 photolysis and chemical removal reactions is more difficult in this case because formation of $O(^1D)$ and

electronically excited oxygen molecules $O_2(^1\Delta)$ lead to catalytic O_3 destruction cycles as mentioned before. Therefore the quantification of isotope effects in UV photolysis is a challenging task.

In order to validate fractionation factors predicted by model calculations [*Liang et al.*, 2004, 2006; *Miller et al.,* 2005; *Ndengué et al.,* 2012, 2014], it is desirable to put further effort into the determination of fractionations at higher spectral resolution. Since the O_3 absorption cross sections show diffuse structures in the Huggins band and to a smaller degree also in the Chappuis band, comparisons of model predictions with broadband light sources are difficult and it would be valuable to be able to experimentally determine the small-scale variability of the fractionation. Furthermore, an experimental study applying narrow band laser light sources at wavelength were maximum and minimum fractionations are predicted by semi-empirical calculations, e.g. at 780 and 520 nm, might be a useful aspect of a measurement-model comparison study on wavelength dependency of visible light photolysis. In particular the long-wavelength end of the Chappuis band is not well covered by the measurements in this thesis.

Another important aspect for the isotopic composition of tropospheric O_3 is the isotope fractionation in the reaction $NO + O_3$. As shown in chapter 1.3.2 ozone chemistry in the troposphere is mainly driven by reaction cycles involving NO_x species. In the polluted troposphere, O_3 decomposition via reaction $NO + O_3$ can dominate O_3 cycling and therefore an isotope effect associated with this reaction would contribute significantly to the isotopic composition of ambient O_3. The conduction of O_3 photolysis in visible light in presence of NO, instead of CO, therefore would give valuable information about the contribution of potential additional isotope effects originating from the reaction $NO + O_3$. Since fractionations in $O + O_3$ and O_3 formation were quantified in this study, fractionation in $NO + O_3$ can be derived.

APPENDIX

Table A1. List of all reactions and rate coefficients applied in the kinetic model

	Number of reaction	Reaction	Rate coefficient
O_3 photolysis	1	OOO → O+OO	$k_1 = 3.4 \times 10^{-4}\ s^{-1}$
	2	OOQ → O+OQ	$k_1 \times 0.5 \times \alpha$ [a]
	3	OOQ → Q+OO	$k_1 \times 0.5 \times \alpha$ [a]
	4	OQO → O+OQ	$k_1 \times 0.5 \times \alpha$ [a]
	5	OOP → O+OP	$k_1 \times 0.5 \times \alpha$ [a]
	6	OOP → P+OO	$k_1 \times 0.5 \times \alpha$ [a]
	7	OPO → O+OP	$k_1 \times 0.5 \times \alpha$ [a]
	8	OPP → O+PP	$k_1 \times 0.5$
	9	OPP → P+OP	$k_1 \times 0.5$
	10	POP → P+OP	k_1
	11	OQQ → O+QQ	$k_1 \times 0.5$
	12	OQQ → Q+OQ	$k_1 \times 0.5$
	13	QOQ → Q+OQ	k_1
	14	POQ → Q+OP	$k_1 \times 0.5$
	15	POQ → P+OQ	$k_1 \times 0.5$
	16	OPQ → O+PQ	$k_1 \times 0.5$
	17	OPQ → Q+OP	$k_1 \times 0.5$
	18	OQP → O+PQ	$k_1 \times 0.5$
	19	OQP→ P+OQ	$k_1 \times 0.5$
	20	PQQ → P+QQ	$k_1 \times 0.5$
	21	PQQ→ Q+PQ	$k_1 \times 0.5$
	22	QPQ → Q+PQ	k_1
	23	PPQ → P+PQ	k1 x 0.5
	24	PPQ → Q+PP	$k_1 \times 0.5$
	25	PQP → P+PQ	k_1
	26	PPP → P+PP	k_1
	27	QQQ → Q+QQ	k_1
O_3 formation	1	O+OO+M → OOO+M	k_{2a} [b]

M = O_2, Ar, He, CO	2	O+OQ+M → OOQ+M	k_{2a} x 0.5 x α^{b}
	3	O+OQ+M → OQO+M	k_{2a} x 0.5 x α^{b}
	4	Q+OO+M → OOQ+M	k_{2a} x α^{b}
	5	O+OP+M → OOP+M	k_{2a} x 0.5 x α^{b}
	6	O+OP+M → OPO+M	k_{2a} x 0.5 x α^{b}
	7	P+OO+M → OOP+M	k_{2a} x 1.03
	8	O+PP+M → OPP+M	k_{2a} x 1.23
	9	O+QQ+M → OQQ+M	k_{2a} x 1.5
	10	O+PQ+M → OPQ+M	k_{2a} x 0.5 x 1.5
	11	O+PQ+M → OQP+M	k_{2a} x 0.5 x 1.3
	12	P+OP+M → POP+M	k_{2a} x 0.5 x 1.03
	13	P+OP+M → OPP+M	k_{2a} x 0.5 x 1.03
	14	P+OQ+M → POQ+M	k_{2a} x 0.5 x 1.3
	15	P+OQ+M → OQP+M	k_{2a} x 0.5 x 1.03
	16	Q+OQ+M → QOQ+M	k_{2a} x 0.5 x 1.04
	17	Q+OQ+M → OQQ+M	k_{2a} x 0.5 x 0.92
	18	Q+OP+M → POQ+M	k_{2a} x 0.5 x 1.03
	19	Q+OP+M → OPQ+M	k_{2a} x 0.5 x 0.92
	20	P+QQ+M → PQQ+M	k_{2a} x 1.31
	21	Q+PQ+M → QPQ+M	k_{2a} x 0.5 x 1.03
	22	Q+PQ+M → PQQ+M	k_{2a} x 0.5 x 1.03
	23	P+PQ+M → PPQ+M	k_{2a} x 0.5 x 1.3
	24	P+PQ+M → PQP+M	k_{2a} x 0.5 x 1.03
	25	Q+PP+M → PPQ+M	k_{2a} x 1.03
	26	P+PP+M → PPP+M	k_{2a} x 1.02
	27	Q+QQ+M → QQQ+M	k_{2a} x 1.03
O_3 formation M = O_3	1	O+OO+OOO → OOO+OOO	$k_{2b} = 1.3 \times 10^{-33}$ $cm^6 s^{-1}$
	2	O+OQ+OOO → OOQ+OOO	k_{2b} x 0.5 x 1.45224
	3	O+OQ+OOO → OQO+OOO	k_{2b} x 0.5 x 1.07985
	4	Q+OO+OOO → OOQ+OOO	k_{2b} x 0.92
	5	O+OP+OOO → OOP+OOO	k_{2b} x 0.5 x 1.35297
	6	O+OP+OOO → OPO+OOO	k_{2b} x 0.5 x 0.98993
	7	P+OO+OOO → OOP+OOO	k_{2b} x 1.03
	8	O+PP+OOO → OPP+OOO	k_{2b} x 1.23
	9	O+QQ+OOO → OQQ+OOO	k_{2b} x 1.5
	10	O+PQ+OOO → OPQ+OOO	k_{2b} x 0.5 x 1.5

	11	O+PQ+OOO → OQP+OOO	k_{2b} x 0.5 x 1.3
	12	P+OP+OOO → POP+OOO	k_{2b} x 0.5 x 1.03
	13	P+OP+OOO → OPP+OOO	k_{2b} x 0.5 x 1.03
	14	P+OQ+OOO → POQ+OOO	k_{2b} x 0.5 x 1.3
	15	P+OQ+OOO → OQP+OOO	k_{2b} x 0.5 x 1.03
	16	Q+OQ+OOO → QOQ+OOO	k_{2b} x 0.5 x 1.04
	17	Q+OQ+OOO → OQQ+OOO	k_{2b} x 0.5 x 0.92
	18	Q+OP+OOO → POQ+OOO	k_{2b} x 0.5 x 1.03
	19	Q+OP+OOO → OPQ+OOO	k_{2b} x 0.5 x 0.92
	20	P+QQ+OOO → PQQ+OOO	k_{2b} x 1.31
	21	Q+PQ+OOO → QPQ+OOO	k_{2b} x 0.5 x 1.03
	22	Q+PQ+OOO → PQQ+OOO	k_{2b} x 0.5 x 1.03
	23	P+PQ+OOO → PPQ+OOO	k_{2b} x 0.5 x 1.3
	24	P+PQ+OOO → PQP+OOO	k_{2b} x 0.5 x 1.03
	25	Q+PP+OOO → PPQ+OOO	k_{2b} x 1.03
	26	P+PP+OOO → PPP+OOO	k_{2b} x 1.02
	27	Q+QQ+OOO → QQQ+OOO	k_{2b} x 1.03
	to 270	continues in same manner for all isotopic substitutions	
O_3 decomposition	1	OOO+O → OO+OO	k_3=9.54x10^{-15} cm^{3}s^{-1}
	2	OOO+Q → OO+OQ	k_3 x α^c
	3	OOO+P → OO+OP	k_3 x α^c
	4	OOQ+O → OO+OQ	k_3 x α^c
	5	OQO+O → OQ+OO	k_3 x α^c
	6	OOP+O → OO+OP	k_3 x α^c
	7	OPO+O → OP+OO	k_3 x α^c
	8	OPP+O → OP+OP	k_3 x 0.5
	9	OPP+O → PP+OO	k_3 x 0.5
	10	POP+O → OP+OP	k_3
	11	OQQ+O → OQ+OQ	k_3 x 0.5
	12	OQQ+O → QQ+OO	k_3 x 0.5
	13	QOQ+O → OQ+OQ	k_3
	14	POQ+O → OP+OQ	k_3
	15	OPQ+O → OO+PQ	k_3 x 0.5
	16	OPQ+O → OP+OQ	k_3 x 0.5
	17	OQP+O → PQ+OO	k_3 x 0.5
	18	OQP+O → OP+OQ	k_3 x 0.5

19	OOQ+P → PQ+OO	k_3 x 0.5
20	OOQ+P → OQ+OP	k_3 x 0.5
21	OQO+P → OQ+OP	k_3
22	OOQ+Q → QQ+OO	k_3 x 0.5
23	OOQ+Q → OQ+OQ	k_3 x 0.5
24	OPO+Q → OQ+OP	k_3
25	OOP+P → PP+OO	k_3 x 0.5
26	OOP+P → OP+OP	k_3 x 0.5
27	OPO+P → OP+OP	k_3
28	OOP+Q → OQ+OP	k_3 x 0.5
29	OOP+Q → PQ+OO	k_3 x 0.5
30	OQP+P → PP+OQ	k_3 x 0.5
31	OQP+P → PQ+OP	k_3 x 0.5
32	OQP+Q → PQ+OQ	k_3
33	PQQ+Q → PQ+QQ	k_3
34	PQQ+P → PQ+PQ	k_3 x 0.5
35	PQQ+P → PP+QQ	k_3 x 0.5
36	QPQ+Q → PQ+QQ	k_3
37	QPQ+P → PQ+PQ	k_3
38	PPQ+Q → PP+QQ	k_3 x 0.5
39	PPQ+Q → PQ+PQ	k_3 x 0.5
40	PPQ+P → PP+PQ	k_3
41	PPP+P → PP+PP	k_3
42	PPP+Q → PP+PQ	k_3
43	QQQ+Q → QQ+QQ	k_3
44	QQQ+P → PQ+QQ	k_3
45	OPP+P → OP+PP	k_3
46	OPP+Q → OQ+PP	k_3 x 0.5
47	OPP+Q → PQ+OP	k_3 x 0.5
48	POP+P → OP+PP	k_3
49	POP+Q → OP+PQ	k_3
50	OQQ+P → OP+QQ	k_3 x 0.5
51	OQQ+P → OQ+PQ	k_3 x 0.5
52	OQQ+Q → OQ+QQ	k_3
53	QOQ+P → PQ+OQ	k_3
54	QOQ+Q → QQ+OQ	k_3

	55	POQ+P → PP+OQ	k_3 x 0.5
	56	POQ+P → OP+PQ	k_3 x 0.5
	57	POQ+Q → PQ+OQ	k_3 x 0.5
	58	POQ+Q → QQ+OP	k_3 x 0.5
	59	OPQ+P → OP+PQ	k_3
	60	OPQ+Q → OP+QQ	k_3 x 0.5
	61	OPQ+Q → OQ+PQ	k_3 x 0.5
	62	OQO+Q → OQ+OQ	k_3
	63	QQQ+O → OQ+QQ	k_3
	64	QPQ+O → PQ+OQ	k_3
	65	PPQ+O → PP+OQ	k_3 x 0.5
	66	PPQ+O → PQ+OP	k_3 x 0.5
	67	PQP+O → PQ+OP	k_3
	68	PPP+O → OP+PP	k_3
	69	PQP+Q → PQ+PQ	k_3
	70	PQQ+O → QQ+OP	k_3 x 0.5
	71	PQQ+O → OQ+PQ	k_3 x 0.5
	72	PQP+P → PQ+PP	k_3
CO_2 formation	1	O+CO+M → COO+M	$k_4 = 2.56 \times 10^{-36} cm^6 s^{-1}$
	2	Q+CO+M → COQ+M	k_4
	3	O+CQ+M → COQ+M	k_4
	4	P+CO+M → COP+M	k_4
	5	O+CP+M → COP+M	k_4
	6	P+CP+M → CPP+M	k_4
	7	P+CQ+M → CPQ+M	k_4
	8	Q+CP+M → CPQ+M	k_4
	9	Q+CQ+M → CQQ+M	k_4
isotopic exchange	1	Q+OO → O+OQ	$k_{5a} = 3.33 \times 10^{-12} cm^3 s^{-1}$
$O + O_2$	2	O+OQ → Q+OO	k_{5a} x 0.5x 0.92751
	3	P+OO → O+OP	k_{5a}
	4	O+OP → P+OO	k_{5a} x 0.5 x 0.96104
	5	Q+OQ → O+QQ	k_{5a} x 0.5
	6	P+OP → O+PP	k_{5a} x 0.5
	7	O+QQ → Q+OQ	$k_{5b} = 2.65 \times 10^{-12}$
	8	O+PP → P+OP	k_{5a}
	9	Q+OP → P+OQ	k_{5a} x 0.5

	10	Q+OP → O+PQ	k_{5a} x 0.5
	11	P+OQ → Q+OP	k_{5a} x 0.5
	12	P+OQ → O+PQ	k_{5a} x 0.5
	13	O+PQ → P+OQ	k_{5a} x 0.5
	14	O+PQ → Q+OP	k_{5a} x 0.5
	15	P+PQ → Q+PP	k_{5a} x 0.5
	16	P+QQ → Q+PQ	k_{5a}
	17	Q+PQ → P+QQ	k_{5a} x 0.5
	18	Q+PP → P+PQ	k_{5a}
isotopic exchange	1	Q+CO → O+CQ	k_6=2.20 x 10^{-15}cm^{3}s^{-1}
O + CO	2	O+CQ → Q+CO	k_6 x 0.906
	3	P+CO → O+CP	k_6
	4	O+CP → P+CO	k_6 x 0.9518
	5	Q+CP → P+CQ	k_6
	6	P+CQ → Q+CP	k_6
O_3 + CO	1	OOO+CO → COO+OO	k_7=6.5 x 10^{-24}cm^{3}s^{-1}
	2	OOQ+CO → COO+OQ	k_7 x 0.5
	3	OOQ+CO → COQ+OO	k_7 x 0.5
	4	OQO+CO → COO+OQ	k_7
	5	OOP+CO → COO+OP	k_7 x 0.5
	6	OOP+CO → COP+OO	k_7 x 0.5
	7	OPO+CO → COO+OP	k_7
	8	OPP+CO → COO+PP	k_7 x 0.5
	9	OPP+CO → COP+OP	k_7 x 0.5
	10	POP+CO → COP+OP	k_7
	11	OQQ+CO → COO+QQ	k_7 x 0.5
	12	OQQ+CO → COQ+OQ	k_7 x 0.5
	13	QOQ+CO → COQ+OQ	k_7
	14	POQ+CO → COP+OQ	k_7 x 0.5
	15	POQ+CO → COQ+OP	k_7 x 0.5
	16	OPQ+CO → COO+PQ	k_7 x 0.5
	17	OPQ+CO → COQ+OP	k_7 x 0.5
	18	OQP+CO → COO+PQ	k_7 x 0.5
	19	OQP+CO → COP+OQ	k_7 x 0.5
	20	PQQ+CO → COP+QQ	k_7 x 0.5
	21	PQQ+CO → COQ+PQ	k_7 x 0.5

22	QPQ+CO → COQ+PQ	k_7
23	PPQ+CO → COP+PQ	k_7 x 0.5
24	PPQ+CO → COQ+PP	k_7 x 0.5
25	PQP+CO → COP+PQ	k_7
26	PPP+CO → COP+PP	k_7
27	QQQ+CO → COQ+QQ	k_7
28	OOO+CP → COP+OO	k_7
29	OOQ+CP → COP+OQ	k_7 x 0.5
30	OOQ+CP → CPQ+OO	k_7 x 0.5
31	OQO+CP → COP+OQ	k_7
32	OOP+CP → COP+OP	k_7 x 0.5
33	OOP+CP → CPP+OO	k_7 x 0.5
34	OPO+CP → COP+OP	k_7
35	OPP+CP → COP+PP	k_7 x 0.5
36	OPP+CP → CPP+OP	k_7 x 0.5
37	POP+CP → CPP+OP	k_7
38	OQQ+CP → COP+QQ	k_7 x 0.5
39	OQQ+CP → CPQ+OQ	k_7 x 0.5
40	QOQ+CP → CPQ+OQ	k_7
41	POQ+CP → COP+PQ	k_7 x 0.5
42	POQ+CP → CPQ+OP	k_7 x 0.5
43	OPQ+CP → COP+PQ	k_7 x 0.5
44	OPQ+CP → CPQ+OP	k_7 x 0.5
45	OQP+CP → COP+PQ	k_7 x 0.5
46	OQP+CP → CPP+OQ	k_7 x 0.5
47	PQQ+CP → CPP+QQ	k_7 x 0.5
48	PQQ+CP → CPQ+PQ	k_7 x 0.5
49	QPQ+CP → CPQ+PQ	k_7
50	PPQ+CP → CPP+PQ	k_7 x 0.5
51	PPQ+CP → CPQ+PP	k_7 x 0.5
52	PQP+CP → CPP+PQ	k_7
53	PPP+CP → CPP+PP	k_7
54	QQQ+CP → CPQ+QQ	k_7
55	OOO+CQ → COQ+OO	k_7
56	OOQ+CQ → COQ+OQ	k_7 x 0.5
57	OOQ+CQ → CQQ+OO	k_7 x 0.5

58	OQO+CQ → COQ+OQ	k_7
59	OOP+CQ → COQ+OP	k_7 x 0.5
60	OOP+CQ → CPQ+OO	k_7 x 0.5
61	OPO+CQ → COQ+OP	k_7
62	OPP+CQ → COQ+PP	k_7 x 0.5
63	OPP+CQ → CPQ+OP	k_7 x 0.5
64	POP+CQ → CPQ+OP	k_7
65	OQQ+CQ → COQ+QQ	k_7 x 0.5
66	OQQ+CQ → CQQ+OQ	k_7 x 0.5
67	QOQ+CQ → CQQ+OQ	k_7
68	POQ+CQ → COQ+PQ	k_7 x 0.5
69	POQ+CQ → CQQ+OP	k_7 x 0.5
70	OPQ+CQ → COQ+PQ	k_7 x 0.5
71	OPQ+CQ → CQQ+OP	k_7 x 0.5
72	OQP+CQ → COQ+PQ	k_7 x 0.5
73	OQP+CQ → >COQ+PQ	k_7 x 0.5
74	PQQ+CQ → CPQ+QQ	k_7 x 0.5
75	PQQ+CQ → CQQ+PQ	k_7 x 0.5
76	QPQ+CQ → CQQ+PQ	k_7
77	PPQ+CQ → CPQ+PQ	k_7 x 0.5
78	PPQ+CQ → CQQ+PP	k_7 x 0.5
79	PQP+CQ → CPQ+PQ	k_7
80	PPP+CQ → CPQ+PP	k_7
81	QQQ+CQ → CQQ+QQ	k_7

[a] Fractionation factors for O_3 photolysis were adjusted following mass-dependent fractionation rules.
[b] Isotope effects and rate coefficients in O_3 formation varied for different bath gases (M). Rate coefficients were adjusted to temperature and pressure dependence. Table A2 gives an overview of rate and fractionation factors used for different collision partners M.
[c] Fractionation factors for O_3 decomposition were adjusted following mass-dependent fractionation rules.

Table A2. Ozone formation rate coefficients (in cm^6s^{-1}) and isotope effects for different collision partners M = O_2, He, CO or Ar.

Reaction	M = O_2	M = He	M = CO	M = Ar
O+OO+M → OOO+M	**k_{2a} = 5.72 x 10^{-34}**	**k_{2a} = 3.43 x 10^{-34}**	**k_{2a} = 6.06 x 10^{-34}**	**k_{2a} = 4.23 x 10^{-34}**
O+OQ+M → OOQ+M	k_{2a} x 0.5 x 1.45224	k_{2a} x 0.5 x 1.3646	k_{2a} x 0.5 x 1.36074	k_{2a} x 0.5 x 1.35934
O+OQ+M → OQO+M	k_{2a} x 0.5 x 1.07985	k_{2a} x 0.5 x 1.07197	k_{2a} x 0.5 x 1.07162	k_{2a} x 0.5 x 1.07150
Q+OO+M → OOQ+M	k_{2a} x 0.92	k_{2a} x 0.92	k_{2a} x 0.92	k_{2a} x 0.92
O+OP+M → OOP+M	k_{2a} x 0.5 x 1.35297	k_{2a} x 0.5 x 1.28296	k_{2a} x 0.5 x 1.27990	k_{2a} x 0.5 x 1.27879
O+OP+M → OPO+M	k_{2a} x 0.5 x 0.98993	k_{2a} x 0.5 x 0.98657	k_{2a} x 0.5 x 0.98643	k_{2a} x 0.5 x 0.98637
P+OO+M → OOP+M	k_{2a} x 1.03	k_{2a} x 1.03	k_{2a} x 1.03	k_{2a} x 1.03

BIBLIOGRAPHY

Allen, M., J. I. Lunine, and Y. L. Yung (1984), The vertical distribution of ozone in the mesosphere and lower thermosphere. *J. Geophys. Res.-Atmospheres*, 89, pp. 4841–4872.

Anderson, S. M., D. Hülsebusch, and K. Mauersberger (1997), Surprising rate coefficients for four isotopic variants of $O+O_2+M$, *J. Chem. Phys.*, 107(14), pp. 5385–5392.

Andrews, D. G. (2010), An introduction to atmospheric Physics, 2nd Edition, Cambridge University Press, 248 pp.

Arin, L. M., and P. Warneck (1972), Reaction of ozone with carbon monoxide, *J. Phys. Chem.*, 76(11), pp. 1514–1516.

Babikov, D., B.K. Kendrick, R.B. Walker, R. Schinke, and R.T. Pack (2003a), Quantum origin of an anomlaous isotope effect in ozone formation, *Chem. Phys. Lett.,* 372, pp. 686–691.

Babikov, D., B. K. Kendrick, R. B. Walker, R. T. Pack, P. Fleurat-Lessard, and R. Schinke (2003b), Formation of ozone: Metastable states and anomalous isotope effect, *J. Chem. Phys.*, 119(5), pp. 2577–2589.

Bains-Sahota, S. K., and M. H. Thiemens (1987), Mass-independent oxygen isotopic fractionation in a microwave plasma, *J. Phys. Chem.*, 91(16), p. 4370–4374.

Batthacharya, S.K., and M.H. Thiemens (1988), Isotope fractionation in ozone decomposition, *Geophys. Res. Lett.*, 15(1), pp. 9–12.

Baulch, D. L., D. D. Drysdale, J. Duxbury, and S. J. Grant (1976), Homogeneous gas phase reactions of the O_2-O_3 systems, the CO-O_2-H_2 system, and of Sulphur-containing species. In: Volume 3 of evaluated kinetic data for high temperature reactions, 118, Butterworth, London, 593 pp.

Berhanu, T. A., J. Savarino, S.K. Bhattacharya, and W.C. Vicars (2012), ^{17}O excess transfer during the $NO_2 + O_3 \rightarrow NO_3 + O_2$ reaction, *J. Chem. Phys.*, 136(044311), pp. 1-8.

Bloss, C., V. Wagner, M. E. Jenkin, R. Volkamer, W. J. Bloss, J. D. Lee, D. R. Heard, K. Wirtz, M. Martin-Reviejo, G. Rea, J. C. Wenger, and M. J. Pilling (2005), Development of a detailed chemical mechanism (MCMv3.1) for the atmospheric oxidation of aromatic hydrocarbons, *Atmos. Chem. Phys.*, 5(3), pp. 641–664.

Bransden, B. H., and C. J. Joachain (2003), Physics of atoms and molecules, 2nd Edition, Pearson Education Limited, Essex, 1114 pp.

Brenninkmeijer, C. A. M., C. Janssen, J. Kaiser, T. Röckmann, T. S. Rhee, and S. S. Assonov (2003), Isotope effects in the chemistry of atmospheric trace compounds, *Chem. Rev.*, 103(12), pp. 5125–5162.

Brenninkmeijer C. A. M (2009), Applications of stable isotope analysis to atmospheric trace gas budgets, *Eur. Phys. J. Conferences 1*, pp. 137–148.

Burrows, J. P., A. Richter, A. Dehn, B. Deters, S. Himmelmann, S. Voigt, and J. Orphal (1999), Atmospheric remote-sensing reference data from Gome-2. Temperature-dependent absorption cross sections of O_3 in the 231-794 nm range, *J. Quant. Spectros. Radiat. Transfer*, 61(4), pp. 509–517.

Chakraborty, S., and S. K. Bhattacharya (2003), Oxygen isotopic fractionation during UV and visible light photodissociation of ozone, *J. Chem. Phys.*, 118(5), pp. 2164–2172.

Chapman, S. (1930), On ozone and atomic oxygen in the upper atmosphere, *Philos. Mag.*, 10(64), pp. 369–383.

Chehade, W., B. Gür, P. Spietz, V. Gorshelev, A. Serdyuchenko, J. P. Burrows, and M. Weber (2013), Temperature dependent ozone absorption cross section spectra measured with GOME-2 FM3 spectrometer and first application in satellite retrievals, *Atmos.Meas.Tech.*, 6, pp.1623–1632.

Clayton, R. N., L. Grossman, and T. K. Mayeda (1973), A component of primitive nuclear composition in carbonaceous meteorites, *Science*, 182(4111), pp. 485–488.

Cole, A. S., and K. A. Boering (2006), Mass-dependent and non-mass-dependent isotope effects in ozone photolysis: resolving theory and experiments, *J. Chem. Phys.*, 125(18), pp. 184301–184314.

Chubachi, S. (1985), A special ozone observation at Syowa Station, Antarctica from February 1982 to January 1983, *Ozone Symposium*, Greece 1984.

DeMore, W. B. (1972), Pressure dependence and mechanism of the reaction of atomic oxygen and carbon monoxide, *J. Phys. Chem.*, 76(24), pp. 3527–3532.

Dessler, A. (2000), Chemistry and Physics of stratospheric ozone, Academic Press, San Diego, 214 pp.

EEA European Environemtal Agency (2014), Exceedance of air quality limit values in urban areas (CSI 004) – Assessment published Nov 2014, http://www.eea.europa.eu/data-and-maps/indicators/exceedance-of-air-quality-limit-3/assessment. (July 2015)

European Union (2015), Air quaility standards, http://ec.europa.eu/environment/air/quality/standards.htm. (July 2015)

Farman, J. C., B. G. Gardiner, and J. D. Shanklin (1985), Large losses of total ozone in Antarctica reveal seasonal Cl_x/No_x interaction, *Nature*, 315(6016), pp. 207–210.

Faure, G., and T. M. Mensing (2005), Isotopes, principles and applications, Wiley, New Jersey, 897 pp.

Feilberg, K. L., A. A. Wiegel, and K. A. Boering (2013), Probing the unusual isotope effects in ozone formation: Bath gas and pressure dependence of the non-mass-dependent isotope enrichments in ozone, *Chem. Phys. Lett.*, 556, pp. 1–8.

Fischer, J., R. R. Gamache, A. Goldman, L. S. Rothman, and A. Perrin (2003), Total internal partition sums for molecular species in the 2000 edition of the HITRAN database, *J. Quant. Spectrosc. Radiat. Transf.*, 82(1–4), pp. 401–412.

Fleurat-Lessard, P., S. Y. Grebenshchikov, R. Schinke, C. Janssen, and D. Krankowsky (2003), Isotope dependence of the $O+O_2$ exchange reaction: Experiment and theory, *J. Chem. Phys.*, 119(9), pp. 4700–4712.

Früchtl, M., C. Janssen, T. Röckmann (2015a), Experimental study on isotope fractionation effects in visible photolysis of O_3 and in the $O+O_3$ odd oxygen sink reaction, J. *Geophys. Res. Atmos.,* 120, pp. 1–19.

Früchtl, M., C. Janssen, D. Taraborelli, S. Gromov, and T. Röckmann (2015b) - submitted, Wavelength dependent isotope fractionation in visible light O_3 photolysis and atmospheric implications, *Geophys. Res. Lett*.

Gao, Y. Q., and R. A. Marcus (2002), On the theory of the strange and unconventional isotopic effects in ozone formation, *J. Chem. Phys.*, 116(1), pp. 137–154.

Gao, Y. Q., and R. A. Marcus (2001), Strange and unconventional isotope effects in ozone formation, *Science*, 293(5528), pp. 259–263.

Gao, Y. Q. , W.-C. Chen, R.A. Marcus (2002), A theoretical study of ozone isotope effects using a modified ab initio potential energy surface, *J.Chem. Phys.*, 117 (4), pp. 1526–1543.

Günther, J., B. Erbacher, D. Krankowsky, and K. Mauersberger (1999): Pressure dependence of two relative ozone formation rate coefficients, *Chem. Phys. Lett.*, 306, pp. 209–113.

Günther, J., D. Krankowsky, and K. Mauersberger (2000): Third-body dependence of rate coefficients for ozone formation in ^{16}O-^{18}O mixtures, *Chem. Phys. Lett.*, 324, pp. 31–36.

Hathorn, B. C., R. A. Marcus (1999), An intramolecular theory of the mass-independent isotope effects for ozone. I, *J. Chem. Phys.*, 111(4087).

Hathorn, B. C., R. A. Marcus (2000), An intramolecular theory of the mass-independent isotope effects for ozone. II. Numerical implementation at low pressures using a loose transition state, *J. Chem. Phys.*, 113(9497).

Haynes, W. M. (2012), CRC Handbook of Chemistry and Physics, 93rd Edition, Taylor & Francis, Boca Raton, 2664 pp.

Haverd, V., G. C. Toon, and D. W. T. Griffith (2005), Evidence for altitude-dependent photolysis-induced ^{18}O isotopic fractionation in stratospheric ozone, *Geophys. Res. Lett.*, 32, L22808(1–4).

Hegglin, M. I., D. W. Fahey, M. McFarland, S. A. Montzka, and E. R. Nash (2015), Twenty questions and answers about the ozone layer: 2014 update, scientific assessment of ozone depletion: 2014, 84 pp., *World Meteorological Organization*, Geneva, Switzerland. International Union of Pure and Applied Chemistry (2014), Compendium of chemical terminology Gold Book, Version 2.3.3, 1622 pp.

Heidenreich, J. E. I., and M. H. Thiemens (1983), A non-mass-dependent isotope effect in the production of ozone from molecular oxygen, *J. Chem. Phys.*, 78(2), pp. 892–895.

Hens, K., A. Novelli, M. Martinez, J. Auld, R. Axinte, B. Bohn, H. Fischer, P. Keronen, D. Kubistin, A. C. Nölscher, R. Oswald, P. Paasonen, T. Petäjä, E. Regelin, R. Sander, V. Sinha, M. Sipilä, D. Taraborelli, C. Tatum Ernest, J. Williams, J. Leloieveld, and H. Harder (2014), Observation and modelling of HO_x radicals in a boreal forest, *Atmos. Chem. Phys.*, *14*(16), pp. 8723–8747,

Hippler, H., R. Rahn, and J. Troe (1990), Temperature and pressure dependence of ozone formation rates in the range 1–1000 bar and 90–370 K, *J. Chem. Phys.*, 93(9), pp. 6560–6569.

Ianni, J. C. (2003), A Comparison of the Bader-Deuflhard and the Cash-Karp Runge-Kutta Integrators for the GRI-MECH 3.0 Model Based on the Chemical Kinetics Code Kintecus, in Computational Fluid and Solid Mechanics 2003, edited by K. J. Bathe, Elsevier Science Ltd., Oxford, UK, pp. 1368–1372.

Jacob, D. J. (1999), Introduction to Atmospheric Chemistry, Princeton University Press, Princeton, 267 pp.

Jaffe, S., and F. S. Klein (1966), Isotopic exchange reactions of atomic oxygen produced by the photolysis of NO_2 at 3660 A*, *Trans. Faraday Soc.*, 62, pp. 3135–3141.

Janssen, C., J. Guenther, D. Krankowsky, and K. Mauersberger (1999), Relative formation rates of $^{50}O_3$ and $^{52}O_3$ in ^{16}O –^{18}O mixtures, *J. Chem. Phys.*, 111(16), pp. 7179–7182.

Janssen, C., J. Guenther, K. Mauersberger, and D. Krankowsky (2001), Kinetic origin of the ozone isotope effect: A critical analysis of enrichments and rate coefficients, *Phys. Chem. Chem. Phys.*, 3, pp. 4718–4721.

Janssen, C., J. Guenther, D. Krankowsky, and K. Mauersberger (2003), Temperature dependence of ozone rate coefficients and isotopologue fractionation in ^{16}O – ^{18}O oxygen mixtures, *Chem. Phys. Lett.*, 367, pp. 34–38.

Janssen, C., and B. Tuzson (2010), Isotope evidence for ozone formation on surfaces, *J. Phys. Chem.*, 114(36), pp. 9709–9719.

Johnson, D. G., K. W. Jucks, W. A. Traub, and K. V. Chance (2000), Isotopic composition of stratospheric ozone, *J. Geophys. Res.*, 105(D7), pp. 9025–9031.

Johnston, J. C., and M. H. Thiemens (1997), The isotopic composition of tropospheric ozone in three environments, *J. Geophys. Res.*, 102(D21), pp. 395–425,

Jöckel, P. et al. (2006), The atmospheric chemistry general circulation model ECHAM5/MESSy1: consistent simulation of ozone from the surface to the mesosphere, *Atmos. Chem. Phys.*, 6, pp. 5067−5104.

Jöckel, P., A. Kerkweg, A. Pozzer, R. Sander, H. Tost, H. Riede, A. Baumgaertner, S. Gromov, and B. Kern (2010), Development cycle 2 of the Modular Earth Submodel System (MESSy2), *Geosci. Model Dev.*, *3*(2), pp. 717−752.

Kaye , J.A., and D.F. Strobel (1983), Enhancement of heavy ozone in the earth's atmosphere?, *J. Geophys. Res.*, 88(C13), pp. 8847–8452.

Krankowsky, D., F. Bartecki, G. G. Klees, K. Mauersberger, and K. Schellenbach (1995), Measurement of heavy isotope enrichment in tropospheric ozone, *Geophys. Res. Lett.*, 22(13), pp. 1713–1716.

Krankowsky, D., and K. Mauersberger (1996): Heavy ozone—a difficult puzzle to solve, *Science*, 274(5291), pp. 1324–1325.

Krankowsky D., P. Lämmerzahl, and K. Mauersberger (2000), Isotopic measurements of stratospheric ozone, *Geophys. Res. Lett*., 27(17), pp. 2593–2595.

Krankowsky, D., P. Lämmerzahl, K. Mauersberger, C. Janssen, B. Tuzson, and T. Röckmann (2007), Stratospheric ozone isotope fractionations derived from collected samples, *J. Geophys. Res.*, 112, D08301(1–7).

Kuhn, N., and T. M. Klapötke (2014), Allgemeine und anorganische Chemie: Eine Einführung, Springer-Verlag Berlin Heidelberg, pp. 247.

Liang, M.-C., G. A. Blake, and Y. L. Yung (2004), A semianalytic model for photo-induced isotopic fractionation in simple molecules, *J. Geophys. Res.*, 109, D10308(1–12).

Liang, M.-C., F. W. Irion, J. D. Weibel, C. E. Miller, G. A. Blake, and Y. L. Yung (2006), Isotopic composition of stratospheric ozone, *J. Geophys. Res.*, 111, D02302(1–11).

London, J. (1980): Radiative energy sources and sinks in the stratosphere and mesosphere, Proceedings of the NATO Advanced Institute on atmopsheric ozone, A.C. Aikin, ed., U.S. Dept. of Transportation, FAA-EE-80-20, FAA, Washington, D.C., US, 1980.

Maeburn, G. M., D. Perner, J. LeCalvé, and M. Bourène (1968), A pulsed-radiolysis study of atomic oxygen reactions in the gas phase, *J. Phys. Chem.*, 107(4), pp. 3920–3925.

Mauersberger, K. (1981), Measurement of heavy ozone in the stratosphere, *Geophys. Res. Lett.*, *8*(8), pp. 935–937.

Mauersberger, K. (1987), Ozone isotope measurements in the stratosphere, *Geophys. Res. Lett*, 14(1), pp. 80–83.

Mauersberger, K., J. Morton, B. Schueler, and J. Stehr (1993), Multi-Isotope study of ozone: Implications for the heavy ozone anomaly, *Geophys. Res. Lett.*, 20(11), pp. 1031–1034.

Mauersberger, K., B. Erbacher, D. Krankowsky, J. Guenther, and R. Nickel (1999), Ozone isotope enrichment: Isotopomer-specific rate coefficients, *Science,* 283(5400), pp. 370–372.

Mauersberger, K., P. Lämmerzahl, and D. Krankowsky (2001), Stratospheric ozone isotope enrichments-revisited, *Geophys. Res. Lett.*, 28(16), pp. 3155–3158.

Mauersberger, K., D. Krankowsky, and C. Janssen (2003), Oxygen isotope processes and transfer reactions, *Space Science Reviews*, 106, pp. 265–279.

Miller, C. E., and Y. L. Yung (2000), Photo-induced isotope fractionation, *J. Geophys. Res.*, 105(D23), 29, pp. 29039–29051.

Miller, C.E., R.M. Onorato, M.-C. Liang, and Y.L. Yung (2005), Extraordinary isotopic fractionation in ozone photolysis, *Geophys. Res. Lett.*, 32, L14814(1–4).

Morton, J., J. Barnes, B. Schueler, and K. Mauersberger (1990), Laboratory studies of heavy ozone, *J. Geophys. Res.*, 95(D1), pp. 901–907.

Myhre, G., D. Shindell, F.-M. Bréon, W. Collins, J. Fuglestvedt, J. Huang, D. Koch, J.-F. Lamarque, D. Lee, B. Mendoza, T. Nakajima, A. Robock, G. Stephens, T. Takemura and H. Zhang (2013), Anthropogenic and Natural Radiative Forcing. In: Climate Change 2013: The Physical Science Basis. Contribution of Working Group I to the Fifth Assessment Report of the Intergovernmental Panel on Climate Change [Stocker, T. F., D. Qin, G.-K. Plattner, M. Tignor, S. K. Allen, J. Boschung, A. Nauels, Y. Xia, V. Bex and P. M. Midgley (eds.)]. Cambridge University Press, Cambridge, United Kingdom and New York, NY, USA, pp. 659–740.

Ndengué, S. A., F. Gatti, R. Schinke, H.-D. Meyer, and R. Jost (2010), Absorption cross section of ozone isotopologues calculated with the multiconfiguration, *J. Phys. Chem.*, 114, pp. 9855–9863.

Ndengué, S. A., R. Schinke, F. Gatti, H. D. Meyer, and R. Jost (2012), Ozone photodissociation: Isotopic and electronic branching ratios for symmetric and asymmetric isotopologues, *J. Phys. Chem. A*, 116(50), pp. 12271–12279.

Ndengué, S., S. Madronich, F. Gatti, H.-D. Meyer, O. Motapon, and R. Jost (2014), Ozone photolysis: strong isotopologue/isotopomer selectivity in the stratosphere, *J. Geophys. Res. Atmos.*, 119, pp. 4286–4302.

Nölscher, A. C., T. Butler, J. Auld, P. Veres, A. Muñoz, D. Taraborrelli, L. Vereecken, J. Lelieveld, and J. Williams (2014), Using total OH reactivity to assess isoprene photooxidation via measurement and model, *Atmos. Environ.*, 89, pp. 453–463.

Pack, A., and D. Herwartz (2014), The triple oxygen composition of the earth mantle and understanding $\Delta^{17}O$ variations in terrestrial rocks and minerals, *Earth and Planetary Science Letters*, 390, pp. 138–145.

Pandey, A., and S. K. Bhattacharya (2006a), Anomalous oxygen isotope enrichment in CO_2 produced from O+CO: estimates based on experimental results and model predictions, *J. Chem. Phys.*, 124, 234301(1–13).

Pandey, A., and S. K. Bhattacharya (2006b), Erratum: "Anomalous oxygen isotope enrichment in CO_2 produced from O+CO: Estimates based on experimental results and model predictions" [J. Chem. Phys. 124, 234301 (2006)], *J. Chem. Phys.*, 125(14), 149903(1–2).

Peeters, J., J.-F. Müller, T. Stavrakou, and V. S. Nguyen (2014), Hydroxyl radical recycling in isoprene oxidation driven by hydrogen bonding and hydrogen tunneling: The Upgraded LIM1 Mechanism, *J. Phys. Chem. A*, *118*(38), pp. 8625–8643.

Pyle, J., and T. Shepherd (2005), Ozone and Climate: A review of Interconnections. In: Safeguarding the ozone layer and the global climate system: Issues related to hydrofluorocarbons and perfluorocarbon, Cambridge University Press, 478 pp.

Richet, P., Y. Bottinga, and M. Javoy (1977), A Review of hydrogen, carbon, nitrogen, oxygen, sulphur, and chlorine stable isotope fractionation among gaseous molecules, *Ann.Rev.Earth Planet. Sci.*, 5(196), pp. 65–110.

Rothman, L. S. et al. (2013), The HITRAN2012 molecular spectroscopic database, *J. Quant. Spectrosc. Radiat. Transf.*, 130, pp. 4–50.

Rubin, M. B. (2001), The history of ozone. The Schönbein Period, 1839-1868, *Bull. Hist. Chem.*, 26(1), pp. 40–56.

Sander, S. P., , J. Abbatt, J.R. Barker, J. B. Burkholder, R. R. Friedl, D. M. Golden, R. E. Huie, C. E. Kolb, M. J. Kurylo, G. K. Moortgat, V. L. Orkin, and P. H. Wine (2011), Chemical Kinetics and Photochemical Data for Use in Atmospheric Studies Evaluation Number 17 NASA Panel for Data Evaluation No. 17, JPL Publication 10–6, Jet Propulsion Laboratory, Pasadena, http://jpldataeval.jpl.nasa.gov.

Sander, R., P. Jöckel, O. Kirner, A. T. Kunert, J. Landgraf, and A. Pozzer (2014), The photolysis module JVAL-14, compatible with the MESSy standard, and the JVal PreProcessor (JVPP), *Geosci. Model Dev.*, *7*(6), pp. 2653–2662.

Savarino, J.; S.K. Bhattacharya, S. Morin, M. Baroni, and J.-F. Doussin (2008): The $NO+O_3$ reaction: A triple oxygen isotope prespective on the reaction dynamics and atmospheric implications for the transfer of the ozone isotope anomly, *J. Chem. Phys.*, 128(194303), pp. 1–12.

Schueler, B., J. Morton, and K. Mauersberger (1990), Measurements of isotopic abundances in collected stratospheric ozone samples, *Geophys. Res. Lett.,* 17(9), pp. 1295–1298.

Schinke, R. (1993), Photodisccoiation dynamics, Cambridge monographs on atomic, molecular and chemical physics 1, Cambridge Univeristy Press, Cambridge, pp. 412.

Schmidt, J. A., M. S. Johnson, and R. Schinke (2013), Carbon dioxide photolysis from 150 to 210nm: Singlet and triplet channel dynamics, UV-spectrum, and isotope effects, *PNAS*, 110(44), pp. 17691–17696.

Schmidt, J. A., M. S. Johnson, ,and R. Schinke (2011), Isotope effects in N_2O photolysis from first principles, *Atmos. Chem. Phys.*, 11, pp. 8965-8975.

Schoeberl, M. R., A. R. Douglas, J. C. Gille, J.A. Gleason, W. R. Grose, C. H. Jackman, S. T. Massie, M. P. McCormick, A. J. Miller, P. A. Newman, L. R. Poole, R. B. Rood, G. J. Rottman, R. S. Stolarski, and J. W. Waters (1999), Ozone and stratospheric chemistry, In: Eos Science Plan, Sterling Spangler, 397 pp.

Seinfeld, J. H., and S. N. Pandis (2006), Atmospheric Chemistry and Physics, John Wiley & Sons, New Jersey, 1203 pp.

Simonaitis, R., and J. Heicklen (1972), Kinetics and mechanism of the reaction of $O(^3P)$ with carbon monoxide, *J. Chem. Phys.*, 56(5), pp. 2004–2011.

Simone, D. (2014), The production and characterisation of high purity ozone and experimental and modelling studies of anomalous oxygen isotope effects in the formation of carbon dioxide from irradiated mixtures of carbon monoxide and ozone or oxygen, PhD Thesis, L'Université Pierre et Marie Currie, 146 p.

Slanger, T., B. J. Wood, and G. Black (1972), Kinetics of $O(^3P)$ + CO+M recombination, *J. Chem. Phys.*, 57(1), pp. 233–238.

Steinfeld, J. M., S. M. Adler-Golden, and J. W. Gallagher (1987), Critical survey of data on the spectroscopy and kinetics of ozone in the mesosphere and thermosphere, *J. Phys. Chem. Ref. Data*, 16(4), pp. 911–951.

Stevenson, D. S., F. J. Dentener, M. G. Schultz, K. Ellingsen, T. P. C. van Noije, O. Wild, G. Zeng, M. Amnn, C. S. Atherton, N. Bell, et al. (2000), Multimodel ensemble simulations of present-day and near-future tropospheric ozone, *J. Geophys. Res.*, 111(D8), pp. 1–23.

Stuhl, F., and H. Niki (1971), Measurements of rate constants for termolecular reactions of $O(^3P)$ with NO, O_2, CO, N_2, and CO_2 using a pulsed vacuum-UV photolysis-chemiluminescent method, *J. Chem. Phys.*, 55(8), pp. 3943–3953.

Taraborrelli, D., M. G. Lawrence, J. N. Crowley, T. J. Dillon, S. Gromov, C. B. M. Grosz, L. Vereecken, and J. Lelieveld (2012), Hydroxyl radical buffered by isoprene oxidation over tropical forests, *Nat. Geosci.*, *5*(3), pp. 190−193.

Thiemens, M. H., and J. E. Heidenreich (1983), The mass-independent fractionation of oxygen- a novel isotope effect and its possible cosmochemical implications, *Science*, 219(4588), pp. 1073–1075.

Thiemens, M. H., and T. Jackson (1988), New experimental evidence for the mechanism for production of isotopically heavy O_3, *Geophys. Res. Lett*, 15(7), pp. 639–642.

Thiemens, M. H., and T. Jackson (1990), Pressure dependency for heavy isotope enhancement in ozone formation, *Geophys. Res. Lett*, 17(6), pp. 717–719.

Thiemens, M. H. (2006), History and applications of mass-independent isotope effects, *Annu. Rev. Earth Planet Sciences*, 34, pp. 217–262.

Thiemens, M. H. (2013), Introduction to chemistry and applications in nature of mass indendent isotope effects special feature, *PNAS*, 110(44), pp. 17631–17637.

Tuzson, B. (2005), Symmetry specific study of ozone isotopomer formation, PhD Thesis, Rupertus Carola University of Heidelberg, 127p.

Urey, H. C. (1947), The thermodynamic properties of isotopic substances, *J. Chem. Soc.*, pp. 562–581.

Vicars, W. C., S. K. Batthacharya, J. Erbland, and J. Savarino (2012), Measurements of the ^{17}O-exeess (Δ^{17}O) of tropospheric ozone using a nitrite-coated filter, *Rapid. Comm. Mass Spectrom*., 26(10), pp. 1219–1231.

Vicars, W. C., and J. Savarino (2014), Quantitative constraints on the ^{17}O-excess (Δ^{17}O) siganture of surface ozone: Ambient measurements from 50°N to 50°S using the nitrite-coated filter technique, Geochemica et Cosmochimica Acta, 135, pp. 270–287.

Weston, R.E. (2012), When is an isotope effect non-mass dependent? *Journal of Nuclear Science and Technology*, 43(4), pp. 295–299.

Wiegel, A. A., A. S. Cole, K. J. Hoag, E. L. Atlas, S. M. Schauffler, and K. A. Boering (2013), Unexpected variations in the triple oxygen isotope composition of stratospheric carbon dioxide, *PNAS*, 110(44), pp. 17680–17685.

WHO (World Health Organization) (2000), Air quality guidelines for Europe, 2nd Edition, WHO Regional Publications, European Series, 91, 273 pp.

WMO (World Meteorolgical Organization) (2014), Assessment for decision makers: Scientific assessment of ozone depletion: 2014, Global Ozone Research and Monitoring Project – Report no. 56, Geneva, Switzerland, 88 pp.

Yeung, L.Y., H. P. Affek, K. J. Hoag, W. Guo, A. A. Wiegel, E. L. Atlas, S. M. Schauffler, M. Okumura, K. A. Boering, and J. M. Eiler (2009), Large and unexpected enrichment in stratospheric ^{16}O^{13}C^{18}O and its meridional variation, *PNAS*, 106(28), pp. 11497–11501.

Young, E.D., A. Galy, and H. Nagahara (2002), Kinetic and equilibruim mass-dependent isotope fractionation laws in nature and their geochemical and cosmochemical significance, *Geochemica et Cosmochimia Acta*, 66(6), pp. 1095–1104.

Young, P. J., A. T. Archibald, K.W. Bowman, J.-F. Lamarque, V. Naik, D. S. Stevenson, S. Tilmes, A. Voulgarakis, O. Wild, D. Bergmann, P. Cameron-Smith, I. Cionni, W. J. Collins S. B. Dalsøren. R. M. Doherty, V. Eyring, et al. (2013), Pre-industrial to end 21st century projections of tropospheric ozone from the atmospheric chemistry and climate model intercomparison project (ACCMIP), *Atmos. Chem. Phys.,* 13, pp. 2063–2090.

ACKNOWLEDGEMENTS

I would like to express my great appreciation to my supervisors Prof. Thomas Röckmann and Dr. Christof Janssen for many valuable discussions and suggestions during the development of this research. With immense knowledge and interest in the subject they guided me into new directions and always gave me helpful input and insightful comments. They are great scientists and it has been a privilege to work with them.

I would like to thank all members of the INTRAMIF project for the motivating and inspiring atmosphere at many conferences, summer schools and workshops we attended together. It was a pleasure to work in this project.

Further I want to thank the glassblowing team for their support, especially Matthijs Krijnen, who realized all my wishes in the shortest time possible. Many thanks also to Huib van Weelden for the calibration of the lamps and filters.

I wish to thank all my current and former colleagues from the Atmospheric Physics and Chemistry Group for the inspiring group meetings, working discussions and enjoyable celebrations. A very special thank you should be given to Carina van der Veen, Henk Snellen and Michel Bolder for the valuable technical support on this project. I also want to thank Bastiaan Jonkheid for his help and very useful comments on my research as well as Magdalena Hofmann for her interest in my work and her incredible support during the last months. I would also like to extend my thanks to Dorota Mrozek for many memorable and inspiring moments at conferences and lab visits we attended together, such as in Paris.

I want to express my gratitude to Qingyi Feng for being supportive and optimistic at all times as well as for nice evenings in many different restaurants.

Special thanks should also be given to Jacco, Rianne, Henriette, Barbara and Ramona for the considerable time we spent together talking about everything but science.

Last but not least I would like to express my deepest gratefulness to my partner Duco for his patience, constant support, encouragement and love that I received from him especially during the last years.

Danken möchte ich auch meiner Schwester Stefanie für ihre herzlichen Aufmunterungen und meinem Bruder Andreas für seine Hilfsbereitschaft.

Ganz besonderer Dank gilt natürlich meinen lieben Eltern. Ohne ihre Unterstützung, ihr Verständnis und ihren Glauben an mich, wäre ich heute nicht an diesem Punkt angelangt. Ohne euch wäre diese Doktorarbeit nicht möglich gewesen.

CURRICULUM VITAE

Marion Früchtl was born on December 25, 1983 in Schongau, Germany. She grew up with one older brother and a younger sister in a small village in Bavaria.

In 2004, after she obtained her high school diploma, Marion enrolled at the University of Augsburg to study Geography. She received the pre-degree in physical geography and economical geography with the minor subjects communication sciences and sociology in 2006. During her studies Marion developed a growing interest in environmental sciences and therefore specialized in the field of climatology and environmental management.

In 2008 her curiosity about climate change related topics brought her to Sweden, where she followed the master level course "Greenhouse gases and the carbon cycle" at the University of Lund. During her stay in Sweden, Marion deepened her knowledge in climate research as well as in the application of different measurement techniques. Under the supervision of Prof. Torben Christensen she conducted field measurements to investigate the impacts of increased carbon dioxide concentrations on polar ecosystems and performed laboratory measurements following up novel findings relating to methane emissions from terrestrial plants under aerobic conditions

From February to April 2010, as a member of the atmospheric physics and chemistry group guided by Prof. Thomas Röckmann at Utrecht University, Marion continued her research in the framework of her diploma thesis with the title "New experimental data on aerobic methane release from living plants – The influence of UV irradiation and physical injury".

In September 2010, after Marion received her diploma degree in physical geography she returned to Utrecht to pursue a PhD degree under the supervision of Prof. Thomas Röckmann at the Institute for Marine and Atmospheric Research Utrecht (IMAU). As part of the Marie Curie Initial Training network INTRAMIF (Initial Training Network on Mass-independent Fractionation) her PhD project focused on isotope effects in ozone photolysis with visible light and the chemical destruction of ozone. The results are presented in this thesis.